A Study on Automatic Welding System of Fixed Aluminum Pipes Using Vision Sensors

July 2009

Baskoro, Ario Sunar

A Study on Automatic Welding System of Fixed Aluminum Pipes Using Vision Sensors

July 2009

A thesis submitted in partial fulfilment of the requirements for the degree of
Doctor of Philosophy in Engineering

Keio University

Graduate School of Science and Technology
School of Integrated Design Engineering

Baskoro, Ario Sunar

Table of Contents

List of Figures

List of Tables

θ	: rotation angle (deg)
v	: welding speed (cm/min)
I	: welding current (A)
q	: shielding gas (l/min)
l	: back shielding gas (l/min)
f	: pulse current frequency (Hz)
W	: image parameter of width (pixels)
L	: image parameter of length (pixels)
A	: image parameter of area (pixels)
g_{avg}	: brightness average
p_{avg}	: percentage of brightness average
$f(i)$	: frequency of brightness at i
p_{top}	: percentage of top brightness
p_{btm}	: percentage of bottom brightness
$g_v'(i,j)$	: differential values of brightness along vertical axis
$g_h'(i,j)$	: differential values of brightness along horizontal axis
$g(i,j)$	: brightness value of a pixel at (i,j)
y_{top}	: maximum position
y_{btm}	: minimum position
L_{lmax}	: left edge position
L_{rmax}	: right edge position
L_{lmax}	: left edge position at maximum width
L_{rmax}	: right edge position at maximum width
Δv	: change of welding speed (cm/min)
B	: estimated back bead width (mm)
w_r	: reference back bead width (mm)
w_n	: back bead width at the concerned time step n (mm)
e	: error
Δe	: change of error
s	: welding distance (mm)

t_{cont}	: control time (s)
v_{min}	: minimum welding speed (cm/min)
v_{max}	: minimum welding speed (cm/min)
A,B,C	: parameters of the hyperboloidal mirror shape
D	: distance between lens to a center point of the camera (mm)
p(u, v)	: image coordinate
P(X,Y,Z)	: a real-world three-dimensional position
p_{out}	: percentage of outer brightness
p_{in}	: percentage of inner brightness
Δp_{out}	: difference percentage of outer brightness
Δp_{in}	: difference percentage of inner brightness
g_{out}	: outer brightness
g_{in}	: inner brightness
$v_{m,n}$	: particle velocity
ω	: inertia weight
$p_{m,n}$	: particle variables
r_1, r_2	: independent uniform random numbers
Γ_1, Γ_2	: learning factors
$p_{m,n}^{local\,best}$	: best local solution
$p_{m,n}^{global\,best}$	: best global solution
w_c	: computed width (mm)
w_t	: corresponding target of width (mm)
f	: fitness function cost

Acknowledgments

Abstract

Arc welding processes of aluminum alloys are important in the automotive and maritime sectors, and have potential for high strength aerospace alloys due to lighter and cheaper structures. One of the arc welding processes is Tungsten Inert Gas (TIG) welding that is widely used in the industries for welding of aluminum alloys. Since the arc welding process is nonlinear and multivariable-coupled because it involves many uncertainty parameters, it is very difficult to obtain a practical and useful controllable model of an arc welding process through classical modeling approaches. Therefore, intelligent control systems are necessary to be developed for modeling and controlling the welding process.

In this study, automatic welding system for horizontally fixed aluminum pipe of 6063S-T5 using a vision sensor is proposed. The welding of aluminum pipe is conducted by monitoring the backside image of molten pool and controlling the welding speed using Neural Network and Fuzzy Inference Systems. Furthermore, an omnidirectional camera, which can observe the entire area around the camera, is adopted for monitoring the molten pool. Finally, the optimization of image processing algorithm to search the edge detection range for detecting the edge of molten pool is conducted using Particle Swarm Optimization (PSO) and Genetic Algorithm (GA).

Chapter 1 describes the background, literature review, original contributions and the outline of this work.

Chapter 2 describes the welding penetration control of fixed aluminum pipes by monitoring the backside image of molten pool using vision sensor. Generally, the edge detection of the molten pool is difficult in aluminum welding, because the contrast of the image is much lower compared to steel welding. Accordingly, a new image processing algorithm to obtain the edge detection range for detecting the edge of the molten pool is proposed. Neural Network model for welding speed control is constructed to perform the welding process automatically.

Chapter 3 describes the automatic welding process of aluminum pipe by monitoring the backside image of the molten pool using Fuzzy Inference System. At first, a simulation system of the welding control using Fuzzy Inference System is constructed to confirm the validity of the control algorithm. Then a series of welding control experiments is conducted to evaluate the performance of the fuzzy controller.

Chapter 4 describes the welding penetration control of aluminum pipe using an omnidirectional camera. A new image processing algorithm is constructed to process the omnidirectional image and to recognize the edge of the molten pool. Back bead width data as the result of detection are delivered into the Fuzzy Inference System to control welding speed.

Chapter 5 describes Particle Swarm Optimization (PSO) and Genetic Algorithm (GA) to optimize the image processing algorithm for searching the edge detection range of the molten pool. Finally, the welding control experiments are conducted using the Fuzzy Inference System which controls the welding speed using the input data of the detected back bead width, and the effectiveness of the system is confirmed.

Chapter 6 summarizes the results of this thesis and discusses future research.

Chapter 1

Introduction

1.1 Background

Recently, arc welding process of aluminum alloys is important in the automotive and maritime sectors, and has potential for high strength aerospace alloys due to lighter and cheaper structures. Aluminum alloys have been used in various industrial sectors because of such a desirable mechanical or metallurgical property as light weight, excellent corrosion resistance, high strength, high toughness, extreme temperature capability, versatility of extruding and recycling capabilities. One of the arc welding process is Tungsten Inert Gas (TIG) welding that is widely used in the industries for welding aluminum alloys because of optimum weld quality, minimum distortion, it can be done in all positions, the good visibility because the gas around the arc is transparent and weld pool is clean.

Arc welding process is nonlinear and multivariable-coupled because it involves many uncertainties, such as, influences of metallurgy, heat transfer, chemical reaction, arc physics, and magnetization [1]. Therefore, it is very difficult to obtain a practical and useful controllable model of an arc welding process through classical modeling approaches. The weld bead width is difficult to be controlled due to the non-linearity and uncertainties of the process. Accordingly, intelligent control systems has been developed for modeling and controlling the welding process, as they derive the control performance based on human experience, knowledge, and logic techniques, instead of mathematical process models. Neural networks [2-7] and fuzzy techniques [8-12] have been studied for arc welding processes. Another difficulty in controlling an arc welding process is how to detect weld pool geometrical features, such as weld bead width and penetration, either from the topside of weld pool or back side, conveniently and in real-time. Various efforts have been made to sense weld pool sizes in real-time from the topside, such as ultrasonic detection, non-transfer plasma charge sensor, infrared sensing, pool image processing, and radiographic sensing to produce weld quality control [13-16]. In order to achieve better control of weld quality, it is important to use advanced real-time control methodologies.

There have been many studies on welding process of stainless steel [9] [17] and aluminum pipes [18-21] by rotating the pipe and welding torch was kept static. The experiment using the image sensing to control the TIG weld width for aluminum alloy plate was conducted with the algorithm of image processing and pattern recognition of molten pool's edge [22]. The visual sensing system was analyzed from the point of the view of light intensity and recovers the shape and height of the weld pool by SFS (shape from shading) algorithm from the welding pool image [23]. In fact, experimental studies of welding of aluminum pipes have been conducted [18-21], unfortunately, the welding process was conducted in rotated pipe.

However, compared to plate welding, welding of aluminum pipes is more difficult due to the characteristics of the welding process and aluminum properties. If the constant welding conditions are maintained over the full joint length, the bead width becomes wider as the circumferential welding of small diameter pipes progresses. In order to avoid these errors and to obtain the uniform weld bead over the entire circumference of the pipe, the welding conditions should be controlled as the welding proceeds. The precise control of bead width has been very difficult by constant welding conditions. The automation of bead width control requires the ability to adjust speed of welding torch or control welding arc current. Therefore, appropriate control model algorithm should be used in automatic welding process.

Another difficulty in welding of aluminum pipes compared with stainless steel pipe is that the image of aluminum molten pool has very low brightness due to the low melting point. Therefore, new technique in detecting molten pool edge is necessary. Since the input of control system using vision sensors is the good parameter value of detected molten pool, the robust image processing algorithm is very important to be constructed.

1.2 Objectives

In order to study the automatic welding system of fixed aluminum pipes in TIG welding using vision sensors, the objectives of this thesis focused on:

1. Automatic welding control of fixed aluminum pipes using neural network.
2. Welding penetration control using fuzzy inference system.
3. New monitoring system of backside image of molten pool using omnidirectional camera.

4. Improvement of image processing algorithm optimization of backside image of molten pool using Genetic Algorithm (GA) and Particle Swarm Optimization (PSO).

1.3 Literature Review

1.3.1 TIG Welding

The Tungsten Inert Gas (TIG) welding, or also know as Gas Tungsten Inert Gas Welding (GTAW) uses a permanent, nonconsumable tungsten electrode to create an arc to a workpiece. The electrode is shielded by an inert gas, such as argon or helium or mixture of the two to prevent electrode degradataion. TIG welding process can be performed with or without filler (autogeneously). The schematic of TIG welding process is presented in Fig. 1.1. In TIG welding, the current from the power supply is passed to the tungsten electrode of a torch through a contact tube to heat and melt the material. A welding power supply produces energy, which is conducted across the arc through a column between the electrode and the workpiece of highly ionized gas and metal vapors known as plasma. A shielding gas that flows through the gas nozzle protects the weld pool and the electrode. The key purpose of the shielding gas in TIG welding is to protect the hot and molten parts of the workpiece, the filler metal and the electrode from the deleterious influence of the surrounding air that can affect oxidation process. The shielding gas also affects the characteristics of the arc and the appearance of the weld [24-27].
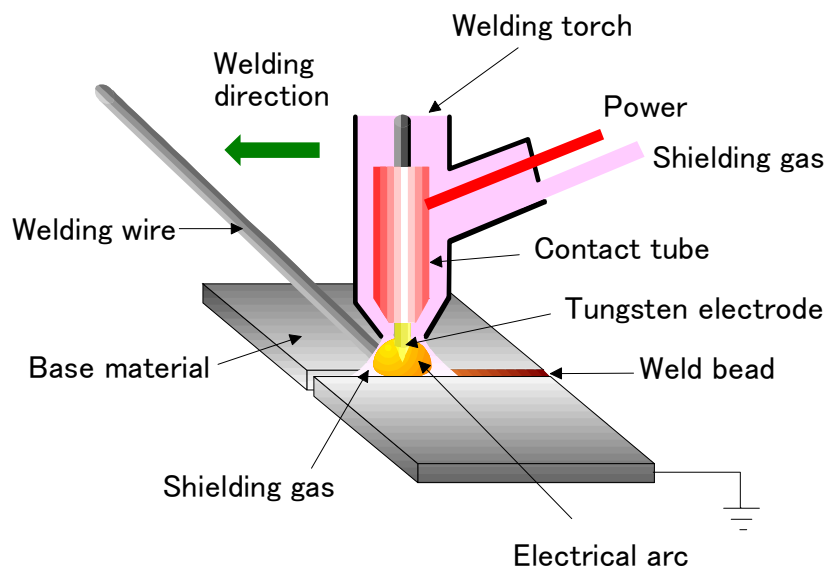
Fig. 1.1 Schematic of TIG welding process

Typical applications for TIG welding are welding of pipes, pressure vessels and heat exchangers. Since TIG welding can be used to weld thin metals and small objects, the method is also used in the electronic industry. In addition, TIG is often used to make root or first pass welds for piping of various sizes. In maintenance and repair work, the process is commonly used to repair tools and dies, especially components made of aluminum and magnesium. Because the welding products are highly resistant to corrosion and cracking over long time periods, TIG welding procedure is used for critical welding operations like sealing spent nuclear fuel canisters before burial. Some advantages of TIG welding which are very high weld quality, absence of slag and very little spatter. The method is extremely versatile, since most weldable materials can be welded, moreover many welding positions and joint configurations can be used [24-27].

(a) Notation of welding process   (b) Direct Current Electrode Negative (DCEN)

(c) Direct Current Electrode Positive (DCEP)   (d) Alternating Current (AC)
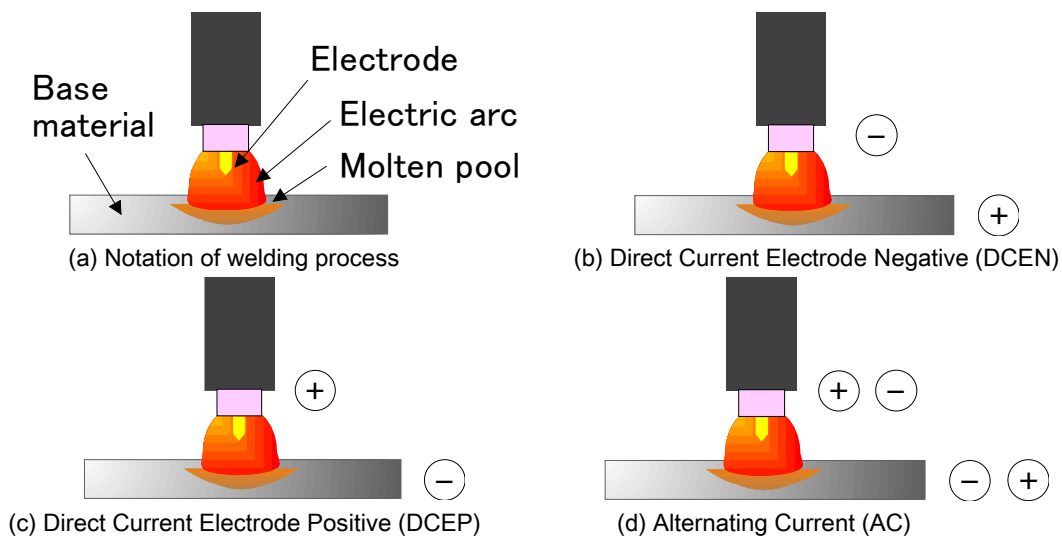
Fig. 1.2 Schematic of welding polarity

TIG process can be operated in several different current modes, including Direct Current (DC), with the Electrode Negative (EN) or Positive (EP), or Alternating Current (AC). These different current result in different arc and weld characteristics [24]. Figure 1.2 (a) shows the schematic of welding polarity. In TIG welding process using DC arc, the tungsten electrode has a negative polarity. The electrode thus becomes the cathode and the workpiece becomes the anode. The polarity is called Straight Polarity or Direct Current Electrode Negative (DCEN) as shown in Fig. 1.2 (b). In DCEN, electrons are emitted from the tungsten electrode and accelerated to very high speeds and kinetic energies while traveling through the arc. These high-energy electrons collide with the

workpiece, give up their kinetic energy and generate heat in the workpiece. These results in deep penetrating, narrow welds, but with higher workpiece heat input. About two-thirds of the net heat available from the arc after losses from various sources enters the workpiece [24].

On the contrary, the Reverse Polarity, or Direct Current Electrode Positive (DCEP) is the reverse of DCEN as presented in Fig. 1.2 (c). DCEP is used for welding certain thin section and low melting point materials. In this polarity, the heating effect of the electrons is on the tungsten electrode rather than on the workpiece. Therefore, large water-cooled electrode holders are required, shallow welds are produced and workpiece heat input can be kept low. This operation is good for welding thin sections or heat-sensitive metals and alloys such as aluminum or magnesium [24].

Alternating current (AC) that shown in Fig. 1.2 (d). The AC mode tends to result in some of the characteristics of both of the DC modes, during the corresponding half cycles, but with some bias toward the straight polarity half-cycle due to the greater inertia and greater resistance of large positive ions. During this half cycle, DCEP is used for the removing an oxide film from the surface of weld pool or workpiece. The oxide film promotes emission during the half-cycle (AC) when the workpiece is negative polarity. As the oxide is depleted, the emission moves to a new location that has a high enough oxide content to sustain the discharge of electrons. Because the arc root or cathode spot where the emission occurs is highly mobile in AC or DCEP, as a result, the arc is much less stable than in DCEN [24].

1.3.2 Pipe Welding

Circumferential butt-welded pipes are frequently used in power stations, offshore structures, and process industries. The schematic of circumferential TIG welding of pipe is shown in Fig. 1.3. It is common that the pipe is maintained fixed during the welding process, although the rotated pipe also can be performed. During the welding process, the welding torch moves along the surface of pipe circumferentially, from 0° to 360°. The weld bead profiles that are produced from this process could be appeared in different form, especially if the welding condition remains unchanged from time to time, as shown in Fig. 1.4. The starting point, which the welding begins, has the higher temperature than the other places. And it influences the other part of pipe, so that the weld bead width becomes wider while the welding torch rotation angle increases.

5
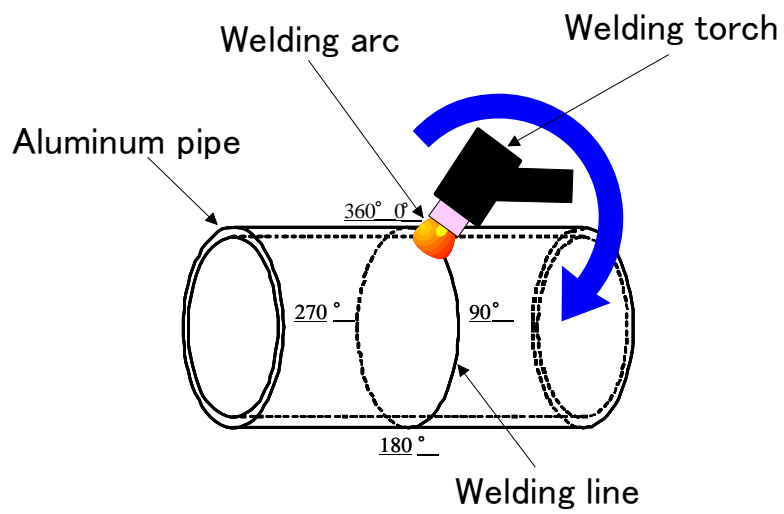
Fig. 1.3 Circumferential TIG welding of pipe

$\theta = 0^{\circ}$ $\theta = 90^{\circ}$

$\theta = 180^{\circ}$ $\theta = 360^{\circ}$
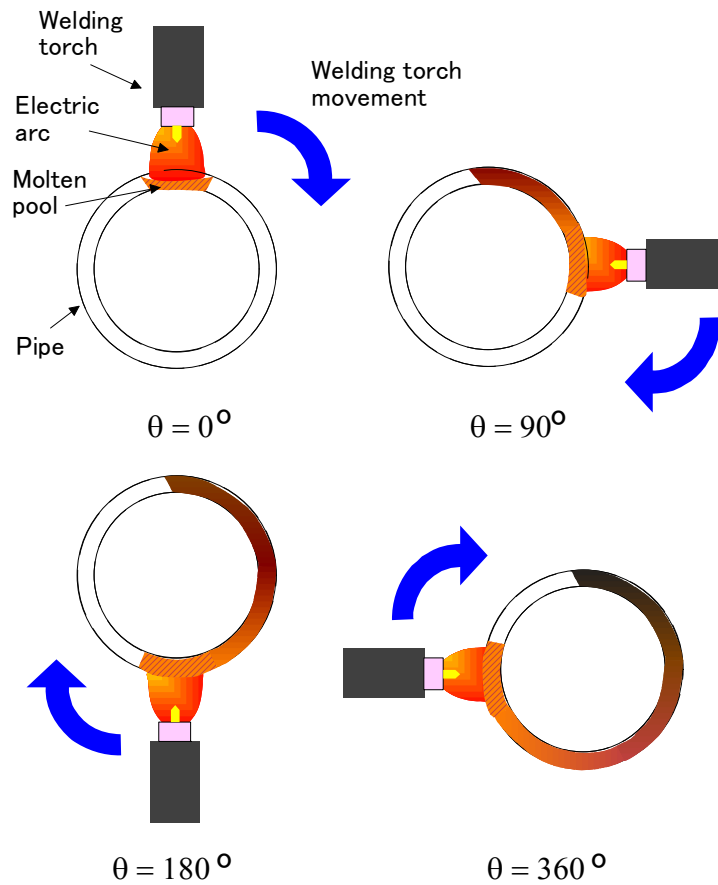
Fig. 1.4 Weld bead profiles during pipe welding

     Piping is a frequent structure in the constructions of welding components such as for the petrochemical industry, power plant, power plant components energy storage,

etc. The fabrication includes welding of individual pipe components to each other and their subsequent heat treatment and nondestructive examination (NDE) to form a unit (piping subassembly) for installation. Piping for nuclear and fossil power plants, chemical plants, refineries, industrial plants, resource recovery, and cogeneration units are most often shop fabricated. Pipelines and other system involving long runs of essential straight pipe sections welded together are usually field assembled. In recent years, the use of new welding processes, new alloys, fracture toughness limitations and mandatory quality assurance (QA) program have made piping fabrication and installation much more complex [28].

Procedure qualification for welding process has established a series of variables. These are base metal, filler metal, position, preheat, postweld heat treatment, shielding gases, joint configuration, electrical characteristics, and technique. Base metal must be also considered the diameter and thickness of the specimen. TIG welding process is one of the commonly used welding processes for fabrication of piping. TIG welding is considered to be the most desirable process for making root welds of highest quality. Techniques using added filler metal as inserts are effective in manual and automatic applications. In automatic TIG welding, welding head orbits the weld joint on a guide track motors and drive wheels need to move the head around the track, a torch to create the arc, and a spool of filler wire. Oscillation and arc energy are adjusted to permit greater dwell time and heat input into the side walls [28]. Orbital welding using TIG or GTAW, Gas Metal Arc Welding (GMAW), or Flux Cored Arc Welding (FCAW) is also used in industry to fabricate high-quality welds pipe-and-tube assemblies, such as tube-to-tube, tube-to-flange, tube-to-header, and nozzle-to-tube welds [29-31].

The example of pipe welding process is construction of welding component at petrochemical industry at Sirz Montaggi srl. The quality requirements are very high and the normal welding processes are TIG for welding the root and SMAW for filling layers [32]. At CIMTAS AS in Turkey, an international fabricator of power plants, power plant components and energy storage, ESAB orbital TIG welding units are used in tube-to-sheet, pipe-to-pipe and header-to-stub welding in the production of heat exchangers, boilers and pipe pre-fabrication [33]. At Zurn energy div., Erie, Pa., nine electronically controlled orbital GTAW machines turn out high-quality tube-to-tube welds that take up 2 miles of tubing, and field constructed boilers might contain over 10 miles of tubing. Tubing averages 2-inch o.d. with 0.165-inch-thick wall and goes into steam generators and auxiliary generator components-superheater, economizers, and

7

combustion air preheaters [34]. The pipeline project of Maui in New Zealand was also successfully welded and inspected to a high standard in an aggressive marine environment for which they were not originally intended. The process used GTAW and GMAW [35].

The example of pipe welding machine is the Arc Machine's Model 15 with low radial clearance for GTAW welding of all pipe sizes from 3 inch pipe (76 mm) up to an unlimited size, including flat plate. It is intended for field use in the nuclear, shipbuilding, chemical, petrochemical and construction industries where weld quality requirements are stringent and the use of the GTAW process is beneficial. These welding torch elements consist of rotation, wire feed, automatic voltage control and cross-seam steering and torch oscillation. The model is shown in Fig. 1.5 [36].
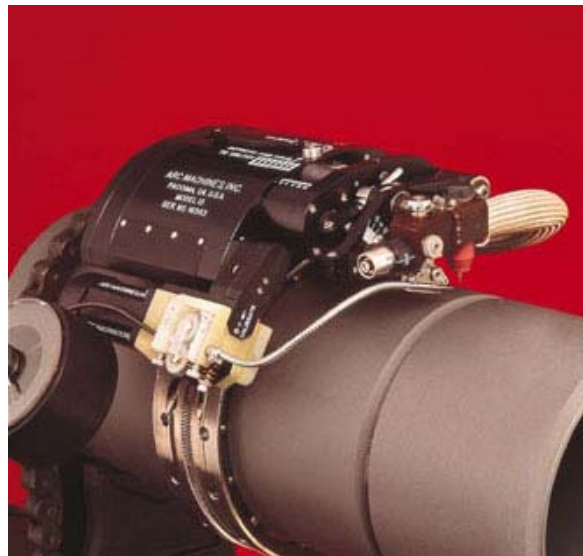
Fig. 1.5 The Arch Machine model 15 (Arc Machine, Inc.)

To reach faster and easier pipe welding, with exceptional weld quality, the automatic pipe welding called Autoweld system, by Lincoln Electric was developed. In pipeline projects that require many joints of uniform high quality to meet code requirements, the system provides dramatic improvements over existing methods [37].

1.3.3 Aluminum Pipe Welding

It is easy to understand that the use of aluminum is increasing in the welding fabrication industry. Manufacturers often adopt this material either through innovation or as a result of demand by their end-users. The unique characteristics of aluminum—light weight, excellent corrosion resistance, high strength, high toughness, extreme

temperature capability, versatility of extruding and recycling capabilities—make it one of the current favored choices of material for many engineers and designers for a variety of welding fabrication applications. Because of the increased use of aluminum as a manufacturing material, the conversion from steel to aluminum within the welding fabrication industry is becoming increasingly common. Some examples of aluminum pipe's application are pipe railing, liquid ammonia heat pipe, architectural structure, irrigation pipe, pipelines, etc.

Most aluminum alloys can be joined by either MIG or TIG, and the weldabilities of aluminum alloys are essentially the same for both processes. The most common alloys are grouped by weldability rating as follows [38]:

a. Readily weldable

- Wrought alloys: Pure aluminum, 1350, 1060, 1100, 2219, 3003, 3004, 5005, 5050, 5052, 5083, 5086, 5154, 5254, 5454, 5456, 5652, 6010, 6061, 6063, 6101, 6151, 7005, 7039
- Casting alloys: 356.0, 443.0, 413.0, 514.0, A514.0

b. Weldable in most applications

- Wrought alloys: 2014, 2036, 2038, 4032
- Casting alloys: 208.0, 308.0, 319.0, 333.0, 355.0, C355.0, 511.0, 512.0, 710.0, 711.0, 712.0

c. Limited weldability

- Wrought alloys: 2024
- Casting alloys: 222.0, 238.0, 295.0, 296.0, 520.0

d. Welding not recommended

- Wrought alloys: 7021, 7029, 7050, 7075, 7079, 7129, 7150, 7178, 7475
- Casting alloys: 242.0

Wrought and casting alloys are listed above by Aluminum Association designations. Wrought alloys most easily welded by gas shielded arc processes are those of the non-heat-treatable 1xxx, 3xxx, and 5xxx series; the alloys in the heat treatable 6xxx series are also easily welded. The major alloying elements found in aluminum wrought alloys are shown in Table 1.1.

The heat of welding removes part or all of the effects of strain hardening; consequently the strength of the heat-affected zone (HAZ) of the weld in a non-heat-treatable alloy may not exceed that of the annealed alloy. The size of the low strength zone depends primarily on the speed of welding. When a heat-treated alloy (T4 or T6 condition) is arc welded, its strength in the as-welded condition is slightly less than that of the unwelded alloy in the T4 condition. Because of the high strength of the base metal and the low strength of the HAZ, weldments of alloys in the T6 condition have a low as-welded joint efficiency and often lack of ductility. Solution heat treatment and aging after welding may restore much of the strength, but ductility loss usually occurs [38].

Table 1.1 The major alloying elements found in aluminum wrought alloys

Major alloying element	Designation
99.0% min aluminum and over	1xxx
Copper	2xxx
Manganese	3xxx
Silicon	4xxx
Magnesium	5xxx
Magnesium and silicon	6xxx
Zinc	7xxx
Other elements	8xxx

TIG welding tends to be limited to the thinner gauges of aluminum, up to 6 mm in thickness. It has a shallower penetration into the base metal than Metal Inert Gas (MIG) welding and difficulty is sometimes encountered penetrating into corners and into the root of fillet welds. Manual TIG welding of aluminum is normally performed using AC where oxide film removal takes place on the electrode positive half cycle and electrode cooling and weld bead penetration on the electrode negative half cycle of the AC sine wave. By using square wave power resources, we can adjust the wave frequency and the balance of positive and negative current by shortening or extending the length of time spent on the positive or negative half cycle. Increasing the frequency produces in a more focused arc, increasing penetration, enabling faster travel speeds to be used and reducing distortion [39].

Compared to the plate welding, the pipe welding is more difficult. If the constant welding conditions are maintained over the full joint length, the bead width becomes wider as the circumferential welding of small diameter pipes progresses.

The previous researches have been conducted by rotating aluminum pipe and keep welding torch static [18-21]. The theoretical and experimental study of heat flow during welding of pipes with seam and girth welding method was carried out [18], which confirmed that under a constant heat input and welding speed, the size of the fusion zone remains unchanged in seam welding but continues to increase in girth welding of pipes with small diameters. The other researches study on parameter optimization in the circumferential GTA welding of aluminum pipes with numerical heat conduction model [19], and semi-analytical finite-element method [20]. Another mathematical method for the determination of the optimum heat input condition to control the temperature field was also conducted [21], which the algorithm was also applied to a circumferential aluminum pipe welding with Gas Tungsten Arc (GTA).

1.3.4 Automatic Welding Process

Arc welding process is nonlinear and multivariable-coupled, because it involves many uncertainties, such as, influences of metallurgy, heat transfer, chemical reaction, arc physics, and magnetization [1]. Therefore, intelligent control systems have been developed for modeling and controlling the welding process, as they derive the control performance based on human experience, knowledge, and logic techniques, instead of mathematical process models. Intelligent technologies for robotic welding which contains computer vision sensing, automatic programming for weld path and technical parameters, guiding and tracking seam, expert robot welding system, intelligent control of welding pool dynamic and quality have been investigated [40-43]. Since the early 1960's sensing and control systems have been successfully implemented in applications where the sensor could be placed on the backside of the weld and moved in synchronism with the welding torch [43]. The development of intelligent control systems has been conducted for modeling and controlling the welding process as they use neural networks [2-7] [44-45], fuzzy techniques [8-12] [46-47] and neuro-fuzzy [11] [48-49].

Vision systems that can monitor weld pool in GTAW welding system have been developed [50-54]. The experiment using the vision sensors to control the TIG weld width for stainless steel [51-52] and aluminum alloy [22] plate was conducted with the

algorithm of image processing and pattern recognition of molten pool's edge. The visual sensing system is analyzed from the point of the view of light intensity and recovers the shape and height of the weld pool by SFS (shape from shading) algorithm from the welding pool image [33] [53-54]. The previous research [45] was successfully conducted to weld stainless steel pipe, with the diameter of pipe was 42.7 mm and 2 mm in thickness. However, this research was conducted for welding aluminum material with smaller size of 37.8 mm in diameter and 2 mm in thickness. Compared with the detected stainless steels image, image of aluminum molten pool has very low brightness.

1.3.5 Computational Intelligence

Human has learned from studies of natural systems using what has been learnt to develop new algorithm to solve complex problems. Some successes have been achieved through the modeling of biological and natural intelligence, resulting "intelligent systems". Intelligence is defined as the ability to comprehend, to understand and profit from experience, to interpret intelligence, having the capacity for thought and reason (especially to a high degree). Other keywords that describe aspects of intelligence include creativity, skill, consciousness, emotion and intuition [55-56].

In the mid-1900s, Alan Turing gave much thought that can computers be intelligent. He believed that machine could be created that would mimic the process of the human brain. In 1950, Turing published his test of computer intelligence, referred to as the Turing test. In this research, we introduced a sub-branch of artificial intelligence (AI), namely computational intelligence (CI) – the study of adaptive mechanisms to enable or facilitate intelligent behavior in complex and changing environments. These mechanisms include the AI paradigms that exhibit an ability to learn or adapt to new situations, to generalize, abstract, discover, and associate. The following CI paradigms are covered: artificial neural networks (NN), fuzzy systems (FS), evolutionary computing (EC) and swarm intelligence (SI) [55].

Figure 1.6 gives a summary of CI techniques. Soft computing, a term coined by Lotfi Zadeh, is a different grouping of paradigms, which usually refers to the collective set of CI paradigms and probabilistic methods. The arrows indicate that techniques from different paradigms can be combined to form hybrid systems. Each of CI paradigms has its origins in biological systems. NNs model biological neural systems, FS originated from studies of how organisms interact with their environment, EC models natural

evolution (including genetic and behavioral evolution) and SI models the social behavior of organisms living in swarms or colonies [55].
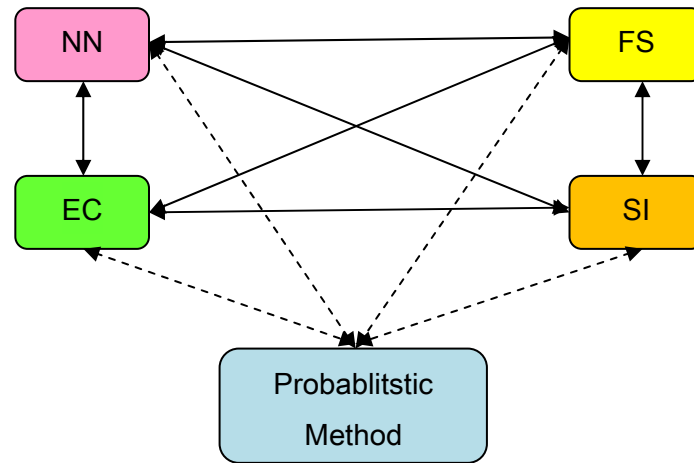
Fig. 1.6 Illustration of CI paradigms

1.3.5.1 Artificial Neural Networks

As the brain is a complex, nonlinear and parallel computer, it has the ability to perform tasks much faster than any computer such as pattern recognition, perception and motor control. In addition to these characteristics, others such as the ability to learn, memorize and generalize, it encouraged research in algorithmic modeling of biological neural systems - referred to as artificial neural networks (NN) [55-56].

An artificial neuron (AN) is a model of a biological neuron (BN). Each AN receives signals from the environment or other ANs, gathers these signals, and when fired, transmits a signal to all connected ANs. Figure 1.7 shows an illustration of artificial neuron. Input signals are inhibited or excited through negative and positive numerical weights associated with each connection to the AN. The firing of an AN and the strength of the exiting signal are controlled via a function, referred to as the activation function. The AN collects all incoming signals, and computes a net input signal as a function of the respective weights. The net signal serves as input to the activation function which calculates the output signal of the AN.

An artificial neural network (NN) is a layered network of ANs. An NN may consist of an input layer, hidden layers and an output layer. ANs in one layer are connected, fully or partially, to the ANs in the next layer. Feedback connections to previous layers are also possible [55].
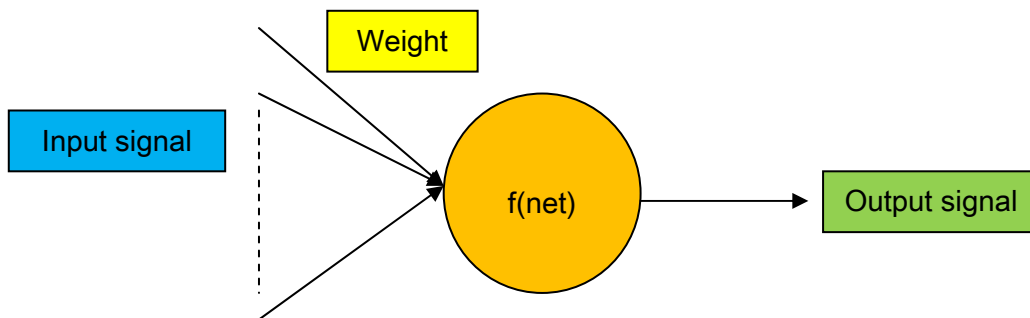
Fig. 1.7 Illustration of an artificial neuron
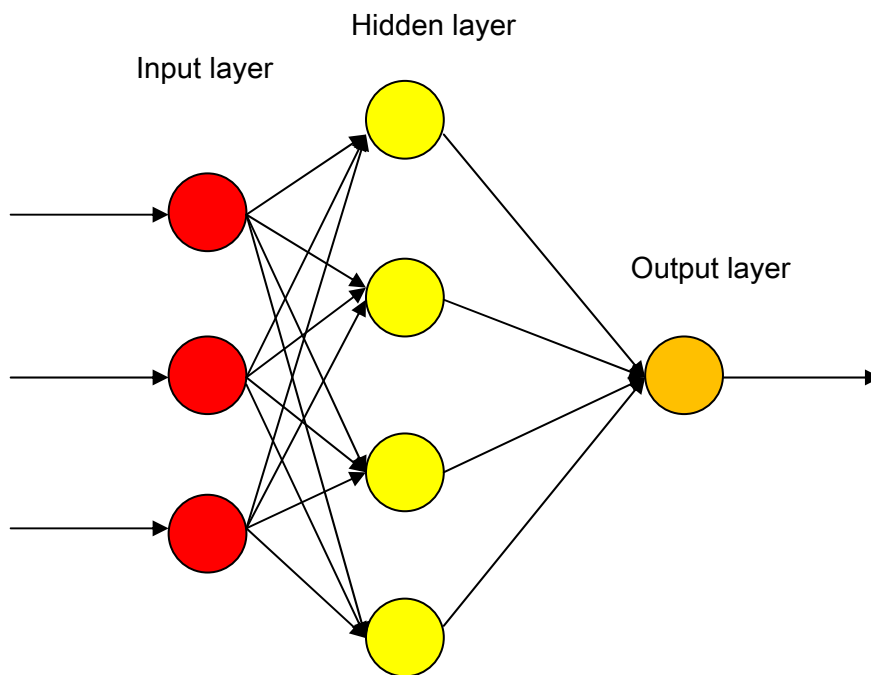
Fig. 1.8 Illustration of an artificial neural network

NN have been used for a wide range of applications, including diagnosis of diseases, speech recognition, data mining, composing music, image processing, forecasting, robot control, credit approval, classification, pattern recognition, planning game strategies, compression and many others. A typical NN structure is depicted in Fig. 1.8 [55].

1.3.5.2 Fuzzy Systems

Traditional set theory requires elements to be either part of a set or not. Likewise, binary-valued logic requires the values of parameters to be either 0 or 1, with similar constraints on the outcome of an inferencing process. Human reasoning is almost always not this exact. Our observations and reasoning usually include a measure of uncertainty [55-56].

Fuzzy sets and fuzzy logic is referred to as approximate reasoning. With fuzzy sets, an element belongs to a set to a certain degree of certainty. Fuzzy logic allows reasoning with these uncertain facts to infer new facts, with a degree of certainty associated with each fact. Therefore, fuzzy sets and logic allow the modeling of common sense. The uncertainty in fuzzy systems is referred to as nonstatistical uncertainty, and should not be confused with statistical uncertainty. Statistical uncertainty is based on the laws of probability, whereas nonstatistical uncertainty is based on vagueness, imprecision and/or ambiguity. Statistical uncertainty is resolved through observations. Nonstatistical uncertainty, or fuzziness, is an inherent property of a system and cannot be altered or resolved by observations [55].
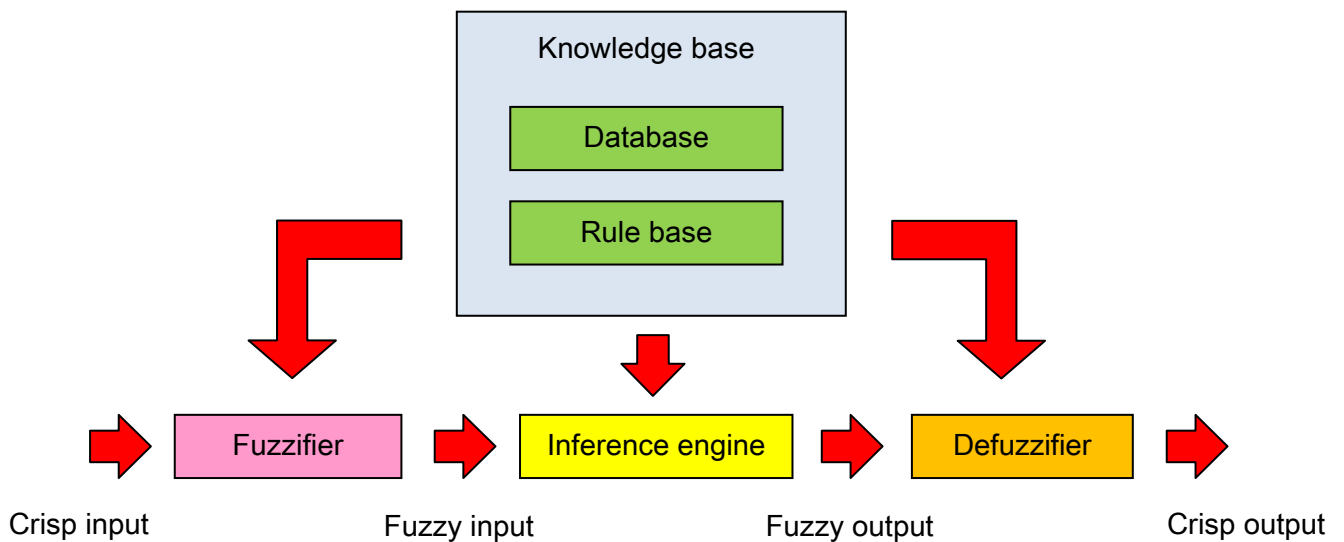
Fig. 1.9 The structure of FIS

The basic structure of a fuzzy system consists of four conceptual components as shown in Fig. 1.9 are [55]:

1. a knowledge base, which consists of a database that defines the membership functions used in the fuzzy rules, a rule base that contains a selection of fuzzy rules;

2. a fuzzifier, that translates crisp inputs into fuzzy values;

3. an inference engine, which applies the fuzzy reasoning mechanism;

4. defuzzifier, that extracts a crisp value from fuzzy output.

Fuzzy systems have been applied successfully to control systems, gear transmission and braking systems in vehicles, controlling lifts, home appliances, controlling traffic signals and many others [55].

1.3.5.3 Evolutionary Computing

Evolutionary computing has its objective of natural evolution, where the main concept is survival of the fittest: the weak must die. In natural evolution, survival is achieved through reproduction. Offspring, reproduced from two parents (sometimes more than two), contain genetic material of both (or all) parents - hopefully the best characteristics of each parent. Those individuals that inherit bad characteristics are weak and lose the battle to survive [55-56].

In evolutionary computing a population of individuals is modeled, where an individual is referred to as a chromosome. A chromosome defines the characteristics of individuals in the population. Each characteristic is referred to as a gene. The value of a gene is referred to as an allele. For each generation, individuals compete to reproduce offspring. Those individuals with the best survival capabilities have the best chance to reproduce. Offspring is generated by combining parts of the parents, a process referred to as crossover. Figure 1.10 shows example of cross-over operator using one point cross-over. Each individual in the population can also undergo mutation which alters some of the allele of the chromosome. There are two type of mutation operators which are random mutate and inorder mutate. Figure 1.11 shows random mutation. The survival strength of an individual is measured using a fitness function which reflects the objectives and constraints of the problem to be solved. Genetic algorithm is one of the methods developed in EC algorithms [55-56].
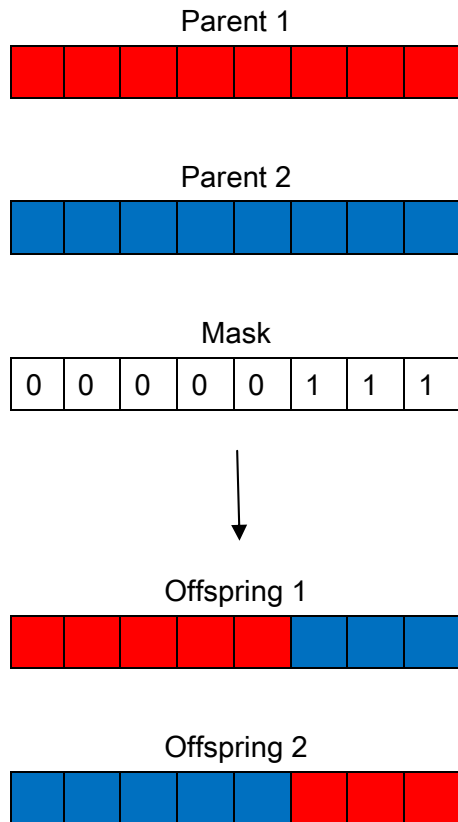
Fig. 1.10 One-point cross over operator
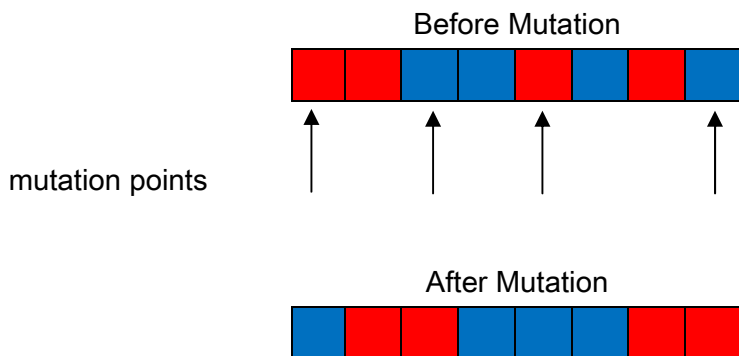
Fig. 1.11 Mutation operator: random mutate

Evolutionary computing has been used successfully in real-world applications, for example, data mining, combinatorial optimization, fault diagnosis, classification, clustering, scheduling and time series approximation [55].

1.3.5.4 Swarm Intelligence

Swarm intelligence originated from the study of colonies or swarms of social organisms. Studies of the social behavior of organisms (individuals) in swarms prompted the design of very efficient optimization and clustering algorithms. For example, simulation studies of choreography of bird flocks led to the design of the particle swarm optimization algorithm and studies of the foraging behavior of ants resulted in ant colony optimization algorithms [55].

Particle swarm optimization (PSO) is a method for global optimization, modeled on the social behavior of bird flocks. PSO is a population-based search procedure where the individuals, referred to as particles, are grouped into a swarm. Each particle in the swarm represents a candidate solution to the optimization problem. In a PSO system, each particle is "flown" through the multidimensional search space, adjusting its position in search space according to its own experience and that of neighboring particles. A particle therefore makes use of the best position encountered by itself and the best position of its neighbors to position itself toward an optimum solution. The effect is that particles "fly" toward the global minimum, while still searching a wide area around the best solution. The performance of each particle is measured according to a predefined fitness function which is related to the problem being solved [55].
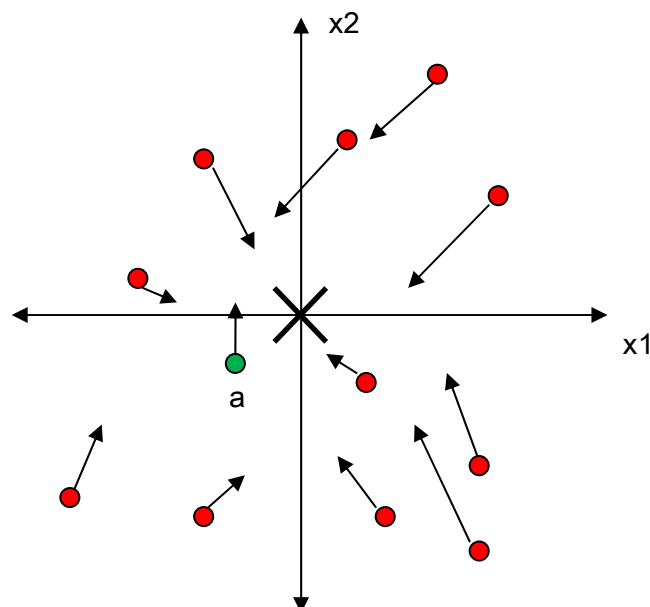
(a) Global best illustrated
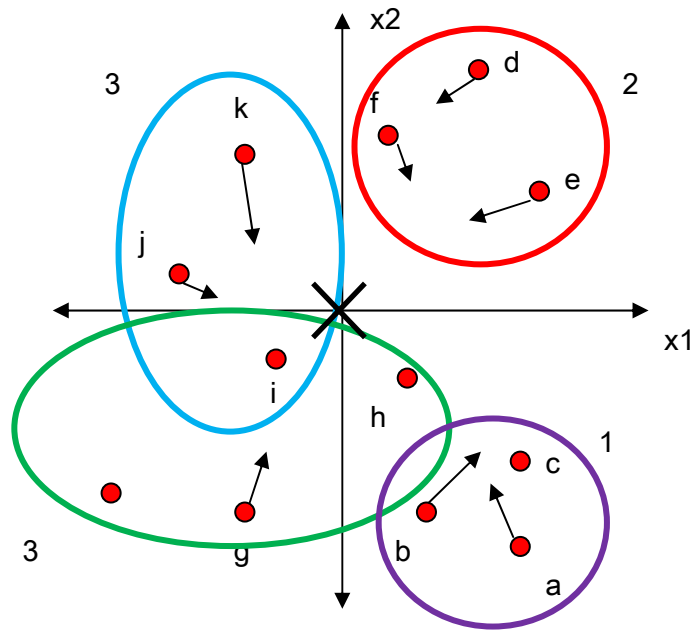
(b) Local best – Initial swarm
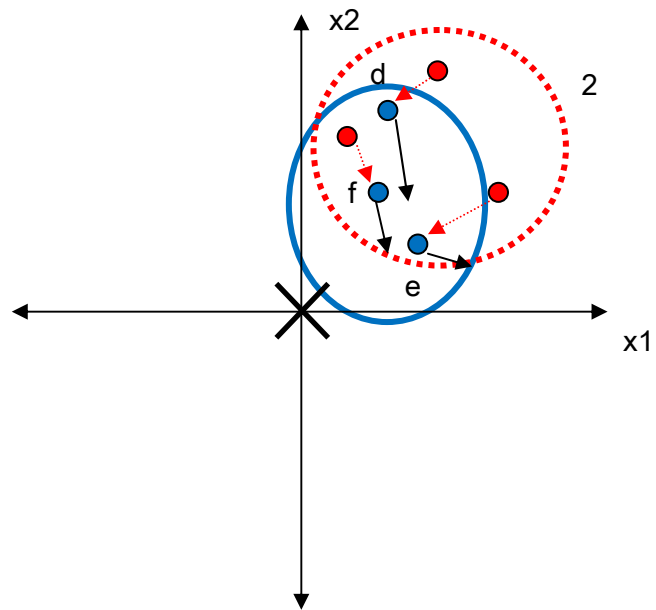
(c) Local best – second swarm

Fig. 1.12 *gbest* and *lbest* illustrated

Figure 1.12 shows the initial swarm of particles as represented by the dots [55]. The optimum point is indicated by a cross. Figure 1.12 (a) illustrates the global best (*gbest*) version of PSO. Particle a is the current global best solution. Initially the own best position (*pbest*) of each individual is its current point. Therefore, only particle a influences the movement of all the particles. The arrows indicate the direction and magnitude of the change in positions. All the particles are adjusted toward particle a.

The local best (*lbest*) version, as illustrated in Figure 1.12 (b), shows how particles are influenced by their immediate neighbors. In neighborhood 1, both particles a and b move toward particle c, which is the best solution within that neighborhood. Considering neighborhood 2, particle d moves toward f, so does e.

For the next iteration, e will be the best solution for neighborhood 2. Now d and f move toward e as illustrated in Figure 1.12 (c) (only part of the solution space is illustrated). The blocks represent the previous positions. Note that e remains the best solution for neighborhood 2.

Applications of PSO include function approximation, clustering, optimization of mechanical structures and solving systems of equations [55].

1.4 Original Contributions

In this thesis, we describe new approach to welding penetration control of fixed aluminum pipes using vision sensors. The following original contributions in intelligent welding system of aluminum pipes are proposed:

1. Welding penetration control of fixed aluminum pipes by monitoring backside image of molten pool using vision sensors was proposed. An algorithm to obtain edge detection's range to detect edge of molten pool was proposed. Image processing based on differential value of brightness was proposed to detect edge of molten pool and the validity of the system was confirmed. As a result of welding experiments, the effectiveness of automatic welding system was demonstrated and sound weld was obtained [57-65].

2. An automatic welding process of aluminum pipe welding system by monitoring backside image of molten pool using fuzzy inference system was constructed. Simulation of welding control using fuzzy inference system was constructed to simulate the welding control process. It shows that fuzzy controller was suitable for controlling the welding speed. As a result of automatic welding control using fuzzy

inference system, it shows the effectiveness of the control system that is confirmed by sound weld of experimental results [66-68].

3. Welding penetration control of aluminum pipes using omnidirectional camera was constructed. An algorithm to obtain to detect edge of molten pool from panorama image of molten pool was proposed. From the experimental results using fuzzy inference system, it shows the effectiveness of the control system [69-72].

4. Genetic Algorithm (GA) and Particle Swarm Optimization (PSO) of edge detection of molten pool in fixed pipe welding were proposed. GA & PSO optimized image processing algorithm was applied into the real time process using omnidirectional vision-based monitoring of molten pool. From the experimental results using fuzzy inference system, it shows the effectiveness of the control system [73-74].

1.5 Organization of Thesis

Each of the original contributions described in the previous section is presented in the following separated chapters.

Chapter 1 describes the background, literature review, contribution and the outline of this work.

Chapter 2 describes the welding penetration control of fixed aluminum pipes by monitoring backside image of molten pool using vision sensors. An image processing algorithm to obtain edge detection's range to detect the edge of molten pool is proposed. Neural network model for welding speed control are constructed to perform the process automatically.

Chapter 3 describes the automatic welding process of aluminum pipes by monitoring backside image of the molten pool using fuzzy inference system. Simulation of welding control using fuzzy inference system is constructed to simulate the welding control process. The simulation result shows that fuzzy controller is suitable for controlling the welding speed and appropriate to be implemented into the welding system. A series of welding control experiments is conducted to evaluate the performance of the fuzzy controller.

Chapter 4 describes welding penetration control of aluminum pipes using an omnidirectional camera. A new image processing algorithm is constructed to process the captured image and to recognize the edge of the molten pool. Back bead width data as the result of detection are delivered into the fuzzy inference system to control welding speed.

Chapter 5 describes PSO and GA optimization for the edge detection of the molten pool in fixed pipe welding. These methods of optimization determine brightness range values for edge detection of molten pool. Fuzzy inference system controls the welding speed using the input data of detected back bead width.

In Chapter 6 the results of this thesis are summarized and future researches are discussed.

Automatic Welding System of Fixed Aluminum Pipes Using Neural Network

2.1 Introduction

Recently, arc welding process of aluminum alloys is very important in the automotive and maritime sectors, and has potential for high strength aerospace alloys due to lighter and cheaper structures [75]. Arc welding techniques such as Metal Inert Gas (MIG) and TIG are widely used in welding aluminum. If the joint is properly designed and suitable welding parameters have been established, result of joint integrity and quality will be high [76]. Compared to plate welding, welding of aluminum pipes is more difficult due to the characteristics of the welding process and aluminum properties. If the constant welding conditions are maintained over the full joint length, the bead width becomes wider as the circumferential welding of small diameter pipes progresses. Therefore, the control of bead width products has been very difficult to perform by constant welding conditions. The automation of bead width control requires the ability to adjust speed of welding torch or control welding arc current.

There have been many studies on welding process of aluminum pipes by rotating the pipe and welding torch was kept static [18-21]. Unfortunately, the welding process was conducted in rotated pipe. Having welded pipe in fixed position, obviously, the excessive arc current yields burn through of metals; in contrary, insufficient arc current produces imperfect welding as shown in Fig. 2.1. In order to avoid these errors and to obtain the uniform weld bead over the entire circumference of the pipe, the welding conditions should be controlled as the welding proceeds, so that the system must be intelligent. For that purpose, this research proposes welding penetration control of fixed

aluminum alloy pipe A6063S-T5 using vision sensors. In this experiment, AC welding machine with square-wave current was used.

(a) Melt down   (b) Imperfect
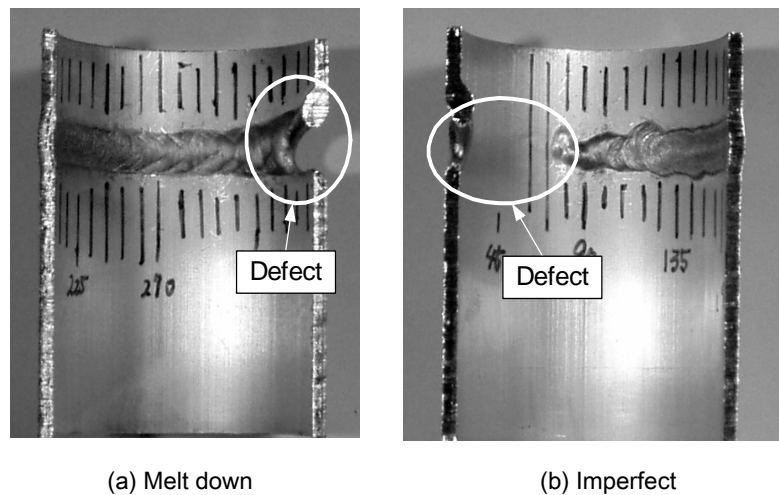
Fig. 2.1 Defects in welding of pipe

The previous research [45] was successfully conducted to weld stainless steel pipe, with the diameter of pipe was 42.7 mm and 2 mm in thickness. However, this research was conducted for welding aluminum material with smaller size of 37.8 mm in diameter and 2 mm in thickness. Compared with the detected stainless steel's image, image of aluminum molten pool has very low brightness. Therefore, new technique in detecting molten pool edge was proposed in this research. In order to show the validity of the image processing algorithm, the results of detected image of molten pool and measured back bead data were compared. Several experiments without control were conducted to provide the training data for control system. In this study, neural network model was utilized to control the welding penetration by modifying speed as welding parameter.

2.2 Experimental Devices

The experimental device, which was used in this experiment, is shown in Fig. 2.2. The overall system used the circumferential welding system, CCD camera and the image digitizer (256×220pixels, 8bit), the personal computer (CPU: 700 MHz), two stepping motors which are used for the revolution and longitudinal movement of the welding torch, the small-sized stepping motor which was used for arc length control, arc current measurement equipment, the gearbox, and the TIG welding machine.

24
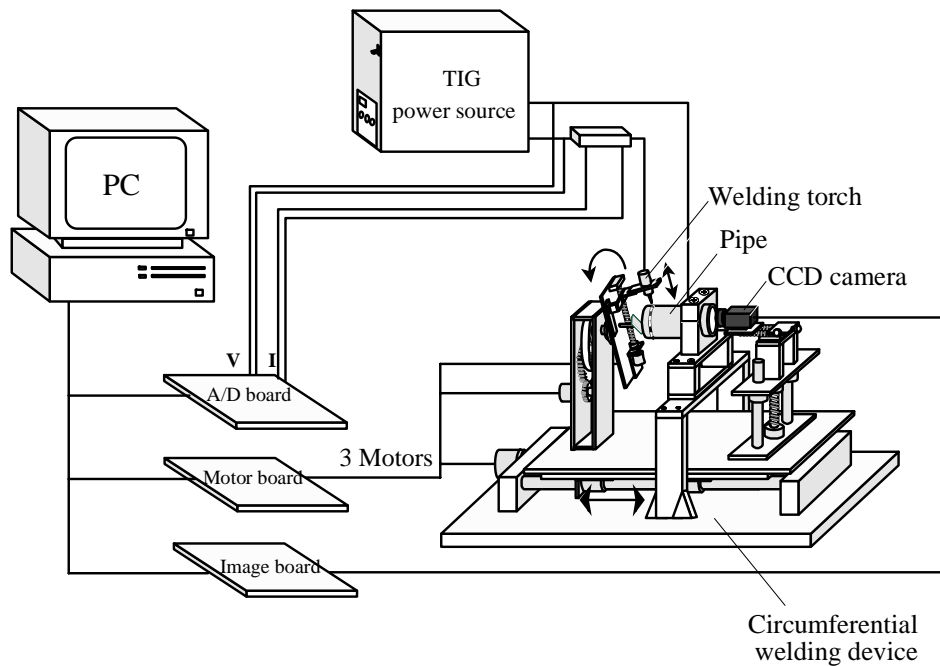
Fig. 2.2 Schematic of experimental device

A CCD camera was used for monitoring of molten pool and sent the image data to personal computer through the image digitizer. Time required for capturing a single frame was 1/30s. The backside image of molten pool was processed in the personal computer to detect the image parameter of molten pool. Base metal used in this experiment was aluminum alloy pipe A6063S-T5. Pulsed TIG AC welding machine with square-wave current and pure argon shielding gas was used. To obtain good image of molten pool, the back shield gas with pure argon was utilized. The method of the study was conducted using several experimental works, which are: image processing algorithm construction to recognize the molten pool, welding process without control for determining welding and image parameters to train the neural network system, and finally conducting the experiment with control using neural network control system.

2.3 Monitoring of Molten Pool

In this section, the image processing algorithm to recognize the molten pool image and result of preliminary experiment using the image processing algorithm are described.

2.3.1 Image Processing Algorithm

In order to capture the backside molten pool image, CCD camera was used for acquisition of reflected image from the mirror. The arrangement of mirror and camera is

shown in Fig. 2.3 (a). The mirror with the size of 29 x 20 mm was set with 60° about the horizontal axes. The mirror rotates along the welding torch during the pipe welding process and reflects the image into the CCD camera. The example result of backside image of molten pool is shown in Fig. 2.3 (b).
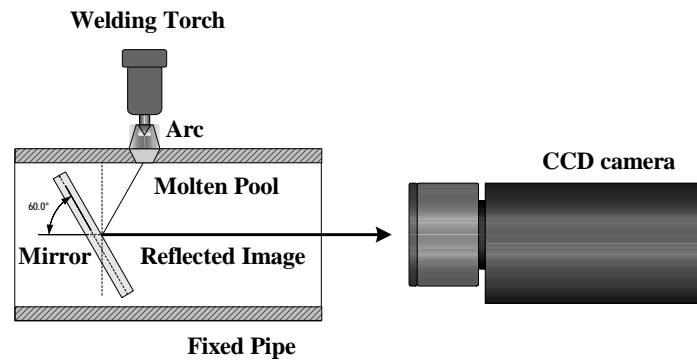
(a) Schematic of monitoring system
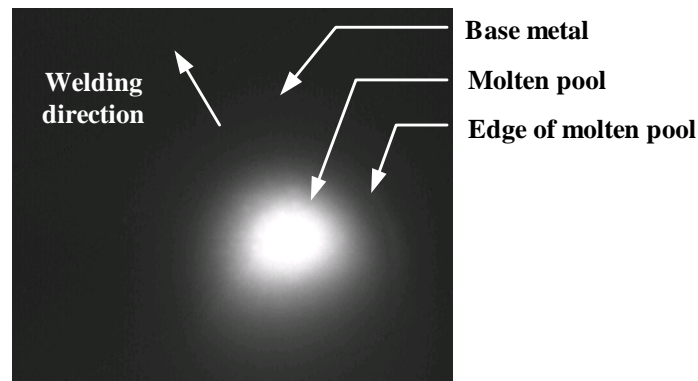
(b) Backside image of molten pool

Fig. 2.3 Monitoring system and backside image of molten pool

Figure 2.4 presents the flowchart of image processing algorithm. According to the low brightness of aluminum's molten pool due to the low melting point, the stable and robust image processing algorithm must be constructed. Applying ellipse approximation (top and bottom ellipse) as an improvement of previous algorithm (only top ellipse) [57] [59], this process produced the improved image parameters of width (W), length (L) and area (A).

```
┌─────────────────────────┐              ┌───────────────────────────────┐
│   Molten Pool Image     │──────────┐   │  Correction of Maximum and    │
└─────────────────────────┘          │   │      Minimum Position         │
            │                         │   └───────────────────────────────┘
            ▼                         │                  │
┌─────────────────────────┐          │                  ▼
│    Rotate the Image     │          │   ┌───────────────────────────────┐
└─────────────────────────┘          │   │     Find the Maximum Width     │
            │                         │   └───────────────────────────────┘
            ▼                         │                  │
┌─────────────────────────┐          │                  ▼
│ Histogram Analysis and  │          │   ┌───────────────────────────────┐
│  Scan the Edge          │          │   │      Max and Min of Y,         │
│  Detection's Range      │          │   │  Left and Right Edges at Max   │
└─────────────────────────┘          │   │           Width                │
            │                         │   └───────────────────────────────┘
            ▼                         │                  │
┌─────────────────────────┐          │                  ▼
│  Edge Detection's Range │          │   ┌───────────────────────────────┐
└─────────────────────────┘          │   │     Ellipse Approximation      │
            │                         │   └───────────────────────────────┘
            ▼                         │                  │
┌─────────────────────────┐          │                  ▼
│ Top and Bottom Edge     │          │   ┌───────────────────────────────┐
│      Detection          │          │   │     Image parameters of        │
└─────────────────────────┘          │   │          W, L, A               │
            │                         │   └───────────────────────────────┘
            ▼                         │
┌─────────────────────────┐          │
│ Left and Right Edge     │──────────┘
│      Detection          │
└─────────────────────────┘
```
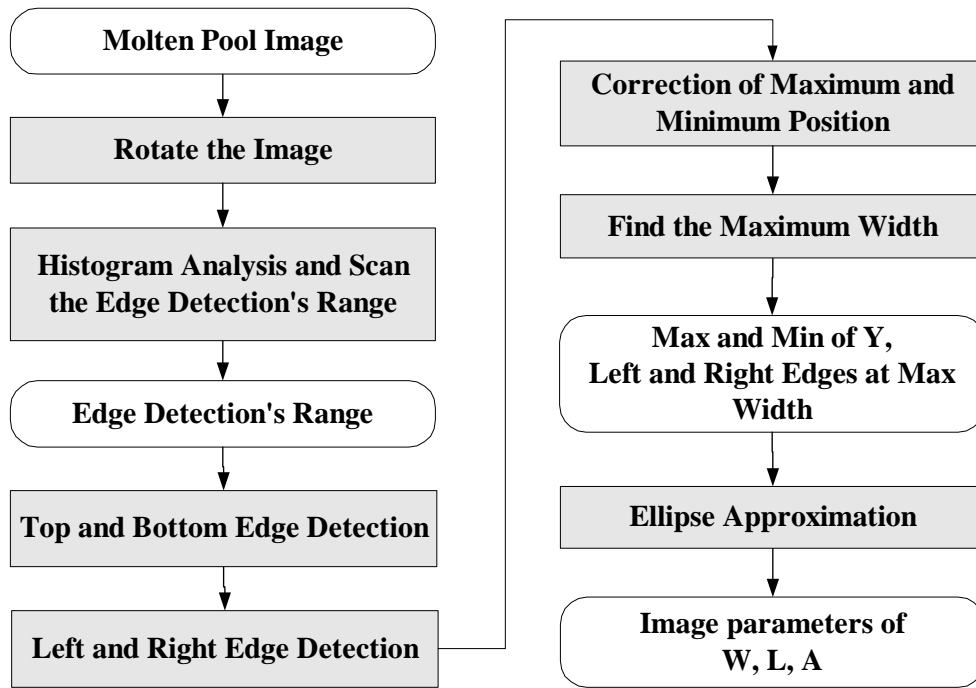
Fig. 2.4 Flowchart of image processing algorithm

The detail of image processing algorithm will be discussed as follows.

(1) Rotation of image: The first process of the recognition was to rotate the original image into uniform position as shown in Fig. 2.5 (a), (b), and (c). After reading the image, the histogram process was conducted. With threshold value produced from minimum scan of histogram frequency, the binarization was conducted as shown in Fig. 2.5 (b). In order to eliminate noises, the pick noise process was performed. Then the center of gravity of the bright area was obtained from the binary image. The image was aligned by rotating the center of gravity to the center of image to produce the image as shown in Fig. 2.5 (c).

(2) Histogram analysis and scan the edge detection's range: From the histogram analysis, the frequency of brightness value of the image was obtained. The brightness average, g_{avg} and accumulation of the percentage of brightness average, p_{avg} were obtained by the Eqs. (2.1) and (2.2), respectively.

$$g_{avg} = \frac{\sum_{i=0}^{i=255}\left(f(i)\times i\right)}{\sum_{i=0}^{i=255}i} \qquad (2.1)$$

27

$$p_{avg} = \frac{\sum\limits_{i=0}^{i=avg} f(i)}{\sum\limits_{i=0}^{i=255} f(i)} \times 100\%$$

(2.2)

where $f(i)$ is the frequency of brightness at i.

(a) Original Image	(b) Binary Image	(c) Rotated Image
(d) Vertical Scanning	(e) Top and Bottom	(f) Maximum and Minimum Position
(g) Horizontal Scanning	(h) Left and Right Edges	(i) Ellipse Approximation
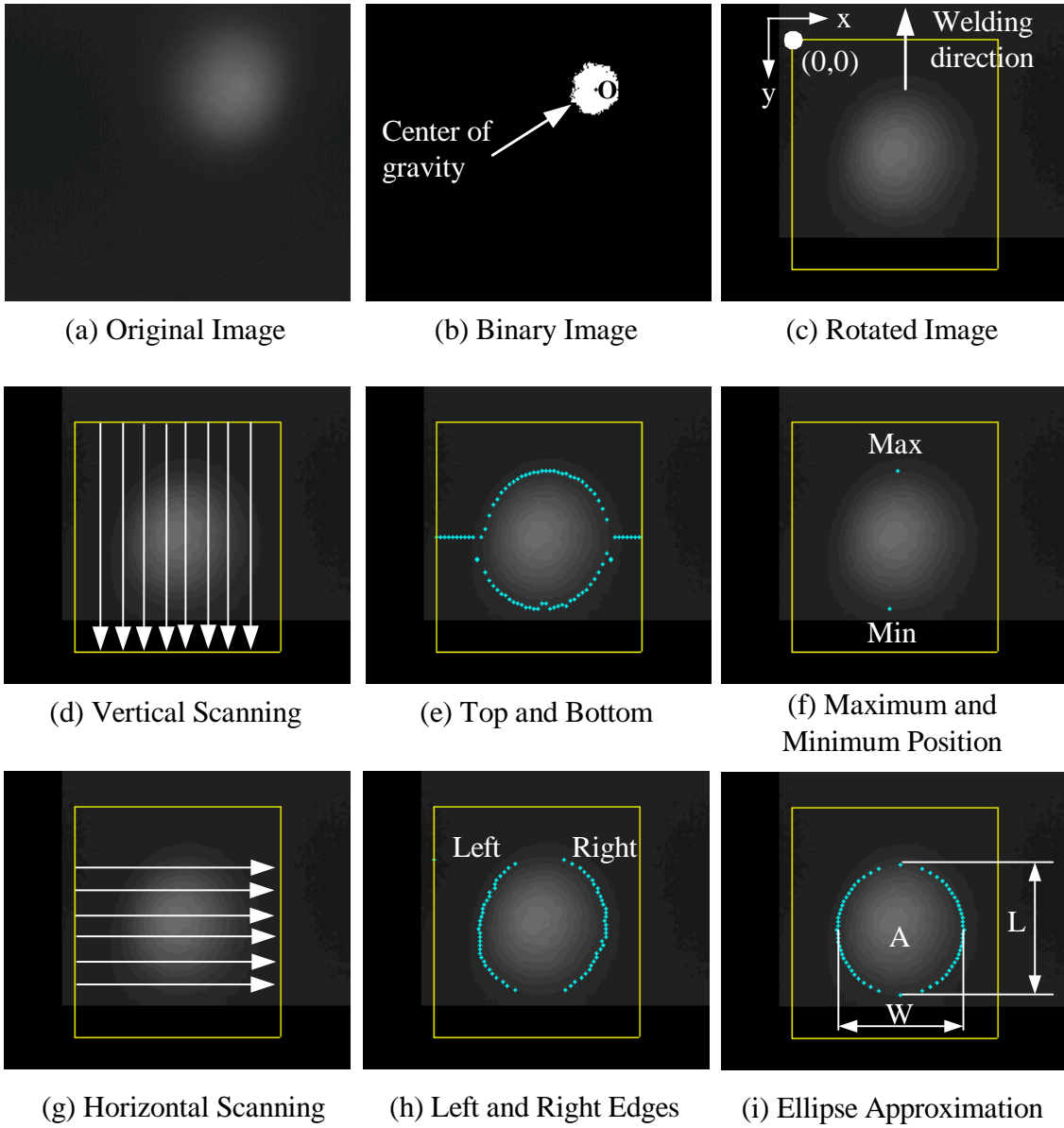
Fig. 2.5 Results of image processing
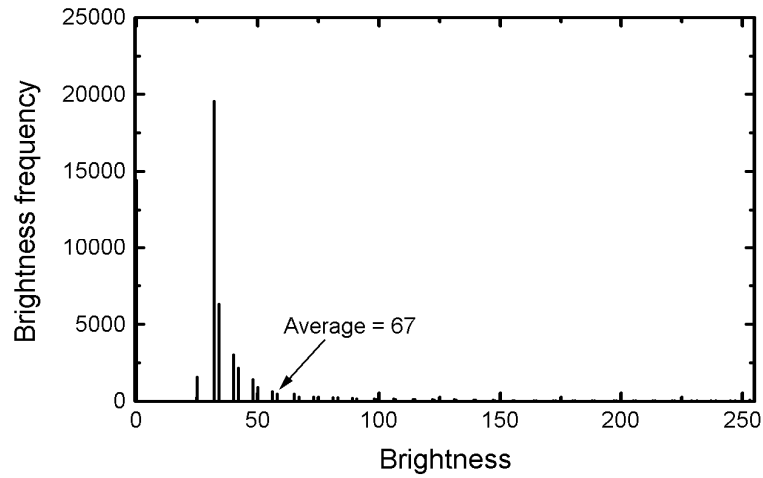
(a) Brightness frequency of molten pool image
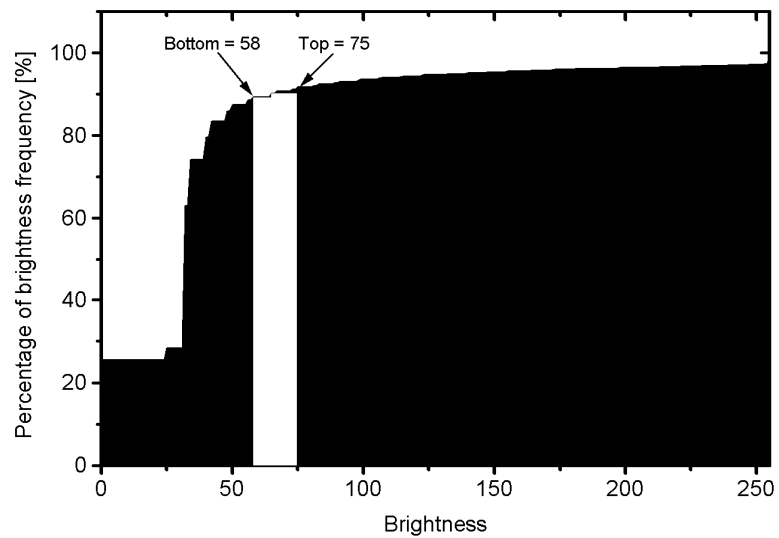
(b) Percentage of brightness frequency to find top and bottom brightness of edge detection

Fig. 2.6 Method to find top and bottom brightness of edge detection

By evaluating the frequency of brightness at 255, brightness average, g_{avg} and percentage at brightness average, p_{avg}, the range of threshold value could be determined. Several rules that have been determined from the observation and experience were applied to obtain the percentage of top threshold, p_{top} and bottom threshold, p_{btm} as shown in Table 2.1. Then the value of brightness at that percentage could be determined. Figure 2.6 shows the example of method to find top and bottom brightness of edge detection. With the brightness average of 67 in Fig. 2.6 (a) and applying the rules in Table 2.1, top brightness of 75 and bottom brightness of 58 could

be determined as shown in Fig. 2.6 (b). This process improved the previous process [57][59] that used contrast enhancement.

Table 2.1 Rules of top and bottom brightness of edge detection

Brightness Average (g_{avg})	Percentage at Brightness Average (p_{avg})	Histogram Frequency at Brightness of 255 ($f(255)$)	Percentage of Top Brightness (p_{top})	Percentage of Bottom Brightness (p_{btm})
< 35	All values	< 1000	$p_{top} = p_{avg} + 2.0\%$	$p_{btm} = p_{avg} + 1.0\%$
> 35 and < 48	< 90.0%	< 1000	$p_{top} = p_{avg} + 1.0\%$	$p_{btm} = p_{avg} - 1.0\%$
> 35 and < 48	> 90.0%	< 1000	$p_{top} = p_{avg} + 0.5\%$	$p_{btm} = p_{avg} - 0.5\%$
> 48 and < 70	< 90.0%	> 1000	$p_{top} = p_{avg} + 2.0\%$	$p_{btm} = p_{avg} - 2.0\%$
> 48 and < 70	> 90.0%	> 1000	$p_{top} = p_{avg} + 1.0\%$	$p_{btm} = p_{avg} - 1.0\%$
> 70	All values	> 1000	$p_{top} = p_{avg} + 0.5\%$	$p_{btm} = p_{avg} - 0.5\%$

(3) Maximum and Minimum Position: The differential values of brightness along vertical axis $g_v{'}(i,j)$ were obtained with the following formula.

$$g_v{'}(i, j) = g(i, j+1) - g(i, j) \qquad (2.3)$$

where $g(i,j)$ is the brightness value of a pixel at (i,j)

Because the position of top and bottom position was very difficult to be decided from differential value of brightness distribution, the top and bottom threshold values were utilized as range of edge scanning. Figure 2.7 shows the example of detection of top and bottom position of molten pool's edge. In Fig. 2.7 (a) and (b) the brightness distribution at x = 136 and differential value of brightness distribution was shown, respectively. The top position was detected from the edge detection's range with the biggest value of differential value as shown in Fig. 2.7 (c). On the contrary, the bottom position was detected as the smallest value of differential value as shown in Fig. 2.7 (d). The process was repeated along x position inside the set window as shown in Fig. 2.5 (e). Finally, by comparing the highest and lowest position of top and bottom as shown in Fig. 2.5 (f), we could find the maximum position y_{top} and minimum position y_{btm} as shown in Fig. 2.5 (g).

30

(4) Left and Right Edges: The process to detect left and right edges was same as the process to find maximum and minimum position described at previous section. The differential values of brightness along horizontal axis $g_h'(i,j)$ were obtained, with the formula below.

$$g_h'(i, j) = g(i+1, j) - g(i, j) \qquad (2.4)$$

By applying the top threshold and bottom threshold as the edge detection's range, the left and right edges were detected. This process was repeated along the y position inside the set window from the maximum position until the minimum position as shown in Fig. 2.5 (h). Finally, all of the left and right edges were detected as shown in Fig. 2.5 (i).
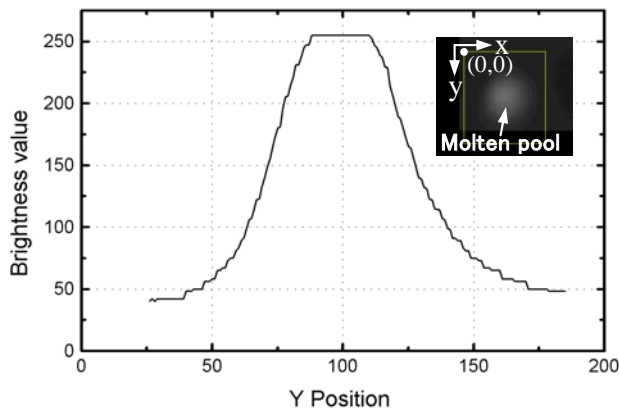
(a) Brightness distribution at x = 136
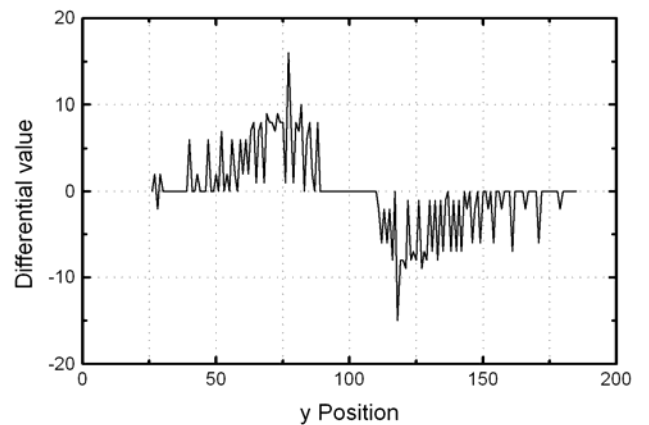
(b) Differential value of brightness distribution at x = 136
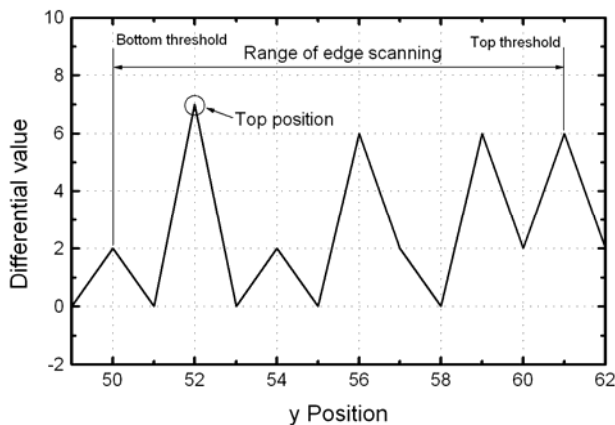
(c) Determination of top position
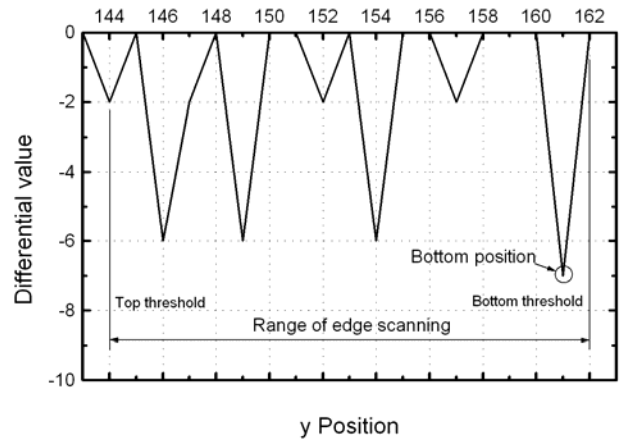
(d). Determination of bottom position

Fig. 2.7 Example of detection of top and bottom position of molten pool's edge

(5) Error Correction: Detected edges from previous process may have the error possibility due to reflection image that occurs usually at above of 350°, so that the error correction must be performed. The detected error occurred below the y_{top} and above y_{btm} for some certain range. With the error filtering process, the new y_{top} and y_{btm} were obtained.

(6) Maximum Width Detection: In order to find the maximum width, the scanning of widest value of left and right edges below y_{top} was conducted. At the maximum width, the left edge L_{lmax} and right edge L_{rmax} were determined. These points were used for the building of ellipse approximation.

(7) Ellipse Approximation: The detected edges were not used directly to get the image parameters of molten pool. The more robust image processing algorithm by ellipse approximation was constructed to avoid the error possibilities and unsteady of detected edge. The inputs to build the ellipse approximation were: (1) Maximum position, y_{top}, (2) Minimum position, y_{btm}, (3) Left edge at maximum width, L_{lmax}, and (4) Right edge at maximum width, L_{rmax}. With the construction of ellipse along the detected edge, it overcame the lack of detected edges. The result of ellipse approximation is shown in Fig. 2.5 (j).

2.3.2 Results of Image Processing Algorithm

In order to show the validity of the proposed image processing algorithm, the algorithm was applied to the current system. Figure 2.8 shows the result of preliminary experiment without control to examine the image processing algorithm. Result of detected edge is shown in Fig. 2.8 (a). The relation between welding speed, measured back bead width and detected molten pool width are shown in Fig. 2.8 (b). Image resolution is 0.06 mm/pixel. It is clearly seen that that image processing algorithm could detect the molten pool width with good approximation. However, some errors still occur during the monitoring process with the average error is 0.3 mm and standard deviation is 0.6 mm.

The cause of the errors might come from the detected threshold values as the brightness range for scanning the edge of molten pool. The judgment of rules to obtain top and bottom brightness of edge detection could provide error in judgment of edge detection. Very low brightness of molten pool due to higher welding speed also generated poor detection of threshold values; therefore the edge detection could be failed.

θ = 4.5°   θ = 22.5°   θ = 49.5°   θ = 72.5°

θ = 99°   θ = 117°   θ = 139.5°   θ = 117°

θ = 184.5°   θ = 207°   θ = 229.5°   θ = 252°

θ = 270o   θ = 292.5°   θ = 319.5°   θ = 360°
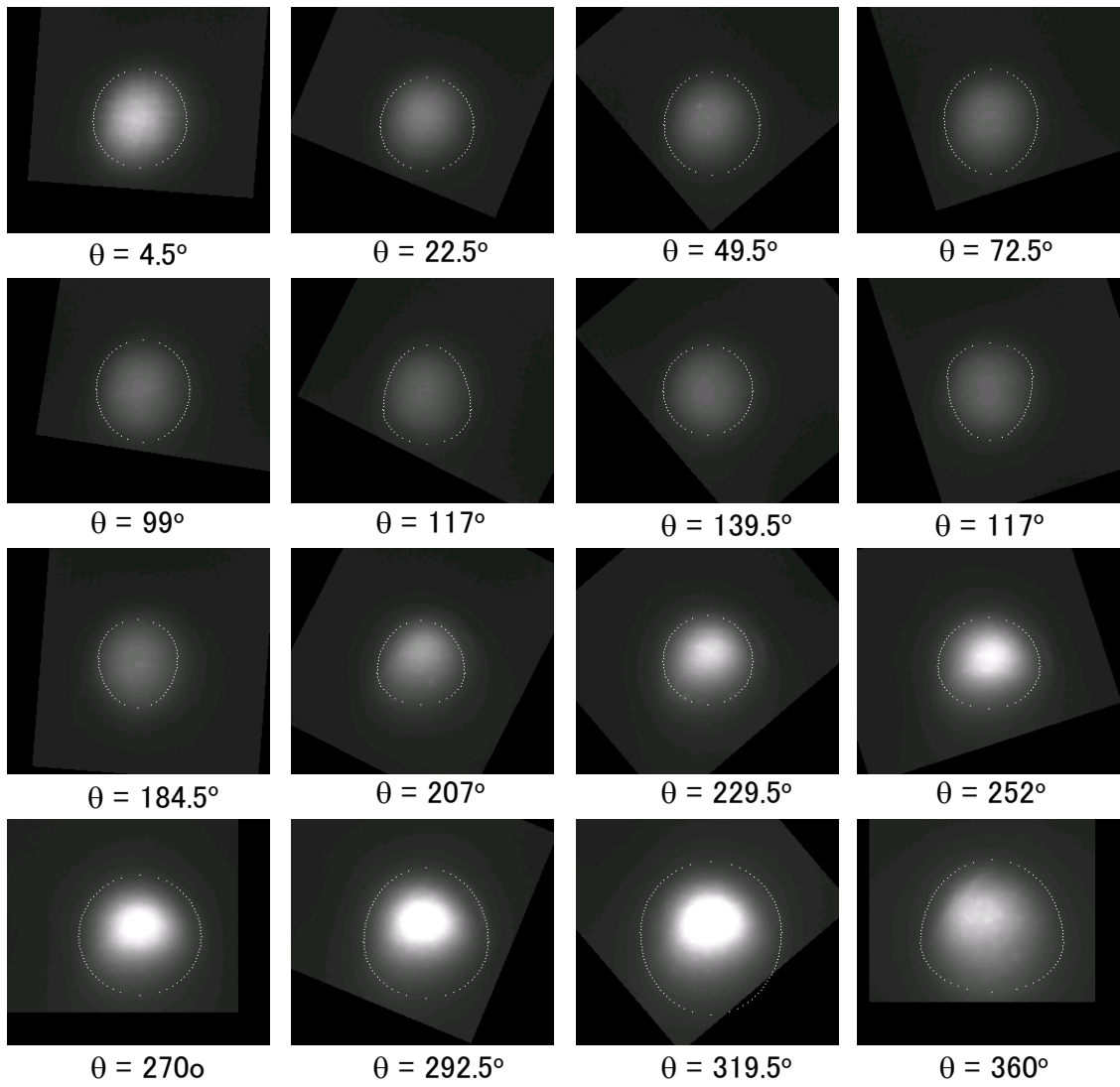
(a) Results of edge detection
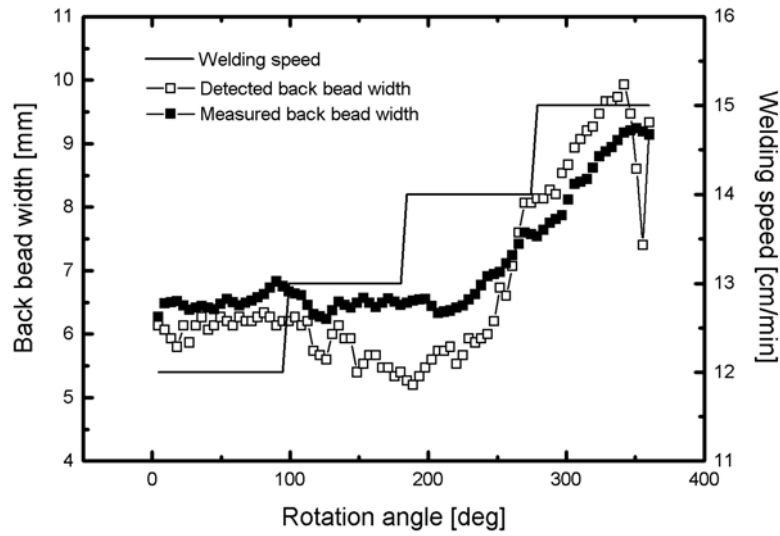
(b) Comparison between detected and measured back bead width
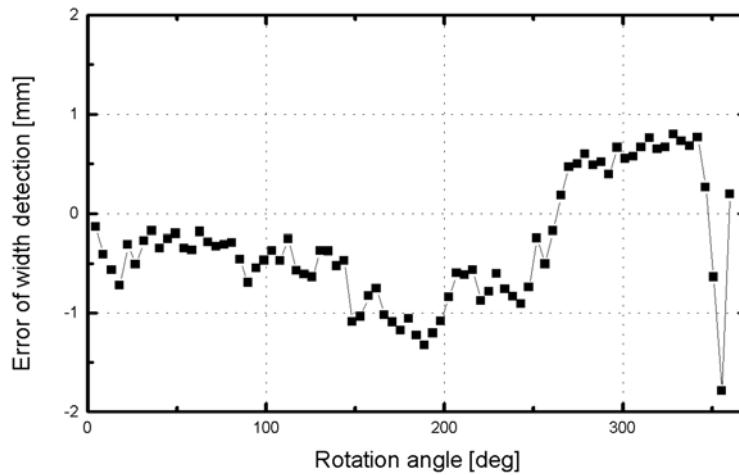
(c) Error of detected back bead width

Fig. 2.8 Result of preliminary experiment

At the end of the rotation, some errors might occur due to reflection from the surface of welded back bead to the molten pool image. Another reason of this error came from the error of the measurement of back bead width using digital vernier caliper. Although the image processing algorithm had some errors, the algorithm with ellipse approximation was considered as the good approach. It could be assured that the ellipse approximation detected edge of molten pool robustly. Compared with previous research [57] [59], this image processing algorithm has improved the detection.

2.4 Experiment

Experiments were conducted in two ways: experiment without control to collect training data and experiment with control using neural network control system.

2.4.1 Experiment Without Control

The material properties and welding conditions of this study is shown in Table 2.2. Welding experiments were conducted in TIG welding to find the training data by welding the pipe with several different welding speeds. The welding speed of 12 – 20 cm/min was implemented at four range of rotation angle, which notated as shown in Table 2.3.

Table 2.2 Material properties and welding conditions

Base metal	Al-6063S-T5
Diameter of pipe (mm)	37.8
Thickness of pipe (mm)	2.0
Density (g/cm^3)	2.69
Melting point (^{o}C)	615-655
Thermal conductivity (W/m.K at 25°C)	209
Welding machine	AC
Electrode	2% Th-W ($\varnothing$ 2.4 mm)
Nominal arc length (mm)	1.5
Welding current, I (A)	50 ~ 70
Pulse current frequency (Hz)	50
EN ratio	0.5
Welding speed, v (cm/min)	12 ~ 26
Shielding gas	100% Ar
Shielding gas, q (l/min)	8 ~ 15
Back shielding gas, 1 (l/min)	8 ~ 10

Table 2.3 Notation of welding speed

Notation	Range of rotation angle
v_1	0° – 90°
v_2	90° – 180°
v_3	180° – 270°
v_4	270° – 360°

Welding process was conducted autogenously for 360° of circumference and in fixed position of pipe. To begin with, the torch started to initiate the arc until the initial penetration was produced. Then by controlling the welding speed, $v_1 - v_4$, the experiment without control was conducted. In constant welding current of 60 A, all the training data consisted of the image parameters: width (W), length (L) and area (A), rotation angle (θ), and welding speed (v) were obtained.

2.4.2 Welding Speed Control with Neural Network

The experiment with control is conducted with the neural network model as control system. Neural network is a biologically inspired computational model that consists of processing elements (neurons) and connections between them, as well as of training and recall algorithms. The structure of neural network is defined by inputs, an input function and a signal function. Inputs have weight bound to them. An input function calculates the aggregated net input signal to a neuron coming from all its inputs. A signal function calculates the activation level of a neuron as a function of its aggregated input signal and its previous state. An output signal equal to the activation value is emitted through the output of the neuron. A multilayer feedforward network is an important class of neural networks that typically consists of a set of sensory units (source nodes) that constitute the input layer, one or more hidden layers of computation nodes, and an output layer of computation nodes. The input signal propagates through the network in a forward direction, on a layer by-layer basis. These neural networks are commonly referred to as multilayer perceptrons (MLPs), which represent a generalization of the single-layer perceptrons. Multilayer perceptrons have been applied successfully to solve some difficult and diverse problems by training them in a supervised manner with a highly popular algorithm known as the errors *back-propagation algorithm* [77].

The back propagation neural network model is shown in Fig. 2.9. The input data from experiment without control were used to train the process and outputted the weight of neural network. There were three layers structure consisted of six units in the input layer, eleven units in the hidden layer, and two units in the output layer.
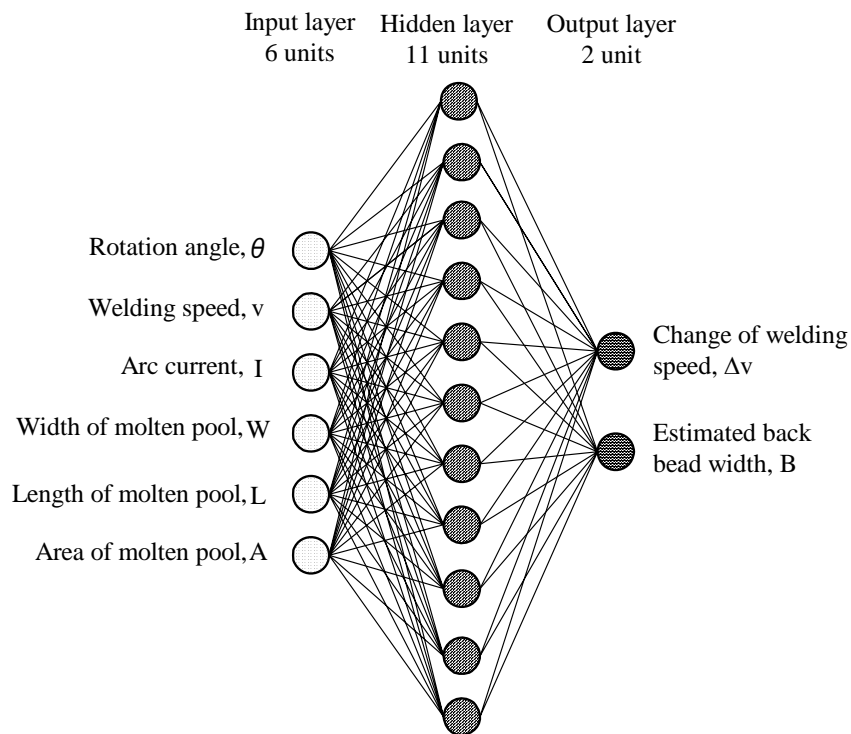
Fig. 2.9 Neural network model
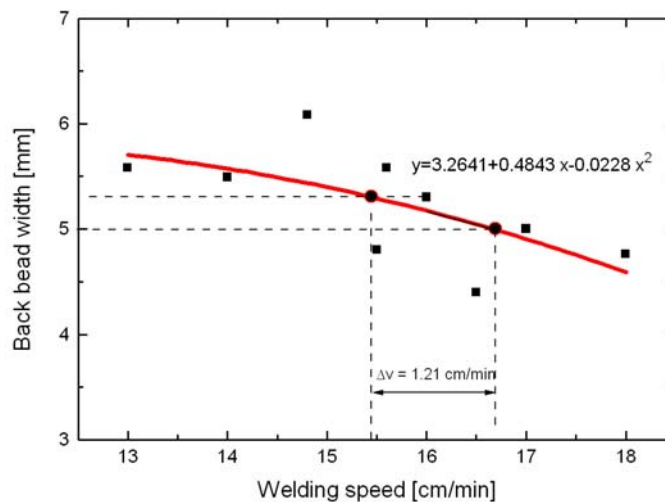
Fig. 2.10 Second degree polynomial regression of welding speed at θ = 216°

At the constant welding current of 60 A, the welding speed was controlled by the input data of welding torch rotation angle (θ), welding speed (v), arc current (I), image width (W), image length (L), and image area (A). From the collected data from the experiment without control, the process to find the change welding speed (Δv) was performed for every 4.5° of rotational increment using linear regression or second degree of polynomial regression of the data. The equation of regression was used to

find the change of welding speed to the target of back bead width. Figure 2.10 shows the example of second degree of polynomial regression of welding speed at θ = 216°. If the real back bead width was 5.3 mm and the polynomial coefficients were: a = - 0.0228, b = 0.4843, and c = 3.2641, then we could calculate the real speed at width of 5.3 mm yielded 15.47 cm/min. If the target back bead width was 5 mm, then with same procedure above we could find the real speed was 16.68 cm/min. As the result, we obtained the difference of welding speed was, Δv = 16.68 - 15.47 = 1.21 cm/min. In this experiment, the target of back bead width was 5±1 mm.

The first output of neural network Δv was inputted directly into the motor control to rotate the welding torch. The second output of neural network B was used to estimate the back bead width using neural network. The 387 pairs of data were composed and processed into neural network training. Finally, the result of control welding was measured and analyzed.

2.5 Results and Discussion

During the experiment, pipe welding system exactly performed the decided sequence of welding torch movement which shows a very flexible aspect of the system. For experiment without control, detection of molten pool image was conducted for every 4.5° of rotation angle. The results of experiment without control by monitoring backside image of molten pool are shown in Fig. 2.11.

In Fig. 2.11 (a), three kind of welding speed with same values of $v_1 - v_2$ and different values of $v_3 - v_4$ were observed. In this experiment, by increasing the values of v_3 and v_4 at 16 and 17 cm/min, respectively, the back bead width could be decreased until 6 mm. In contrary, by inputting $v_3 - v_4$ with the value around 13 – 14 cm/min produced the final back bead width of about 8 mm. However, for achieving the target value of back bead width of 5 mm, the welding speed was still not enough. Therefore, it was necessary to observe the last three value of welding speed of $v_2 - v_4$.

Figure 2.11 (b) shows the welding result with different welding speed of $v_2 - v_4$. At the beginning of welding process with θ = 0° – 180°, all of the different welding speed showed the same values around the target value of back bead width. However, by increasing the welding speed at $v_3 - v_4$, the back bead width showed the different result at the range of 6 – 7 mm. The smallest value of welding speed of v_4 was set at 19.5 cm/min. From these experiments, it was shown that the value of welding speed of v_2 was very important. Although by increasing the value of v_2 produces almost the same

back bead width at $\theta = 90^o - 180^o$, but it influenced the next welding result at $\theta = 180^o - 360^o$.
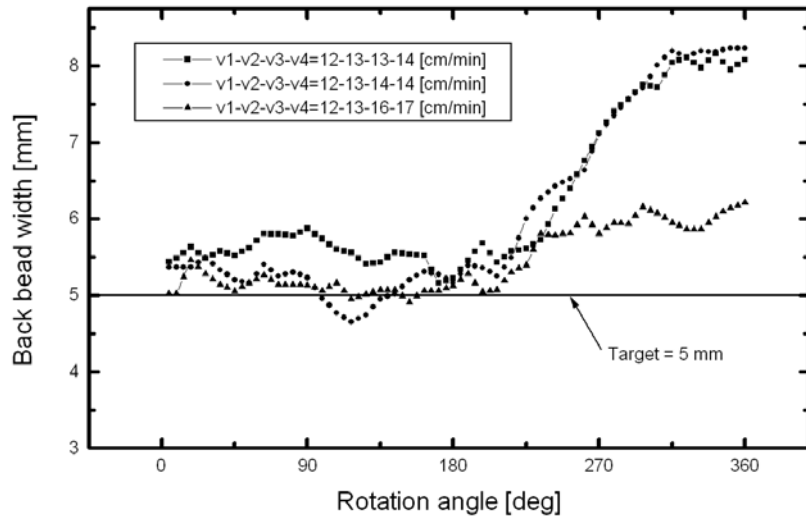
(a) Welding result with different welding speed of $v_3 - v_4$
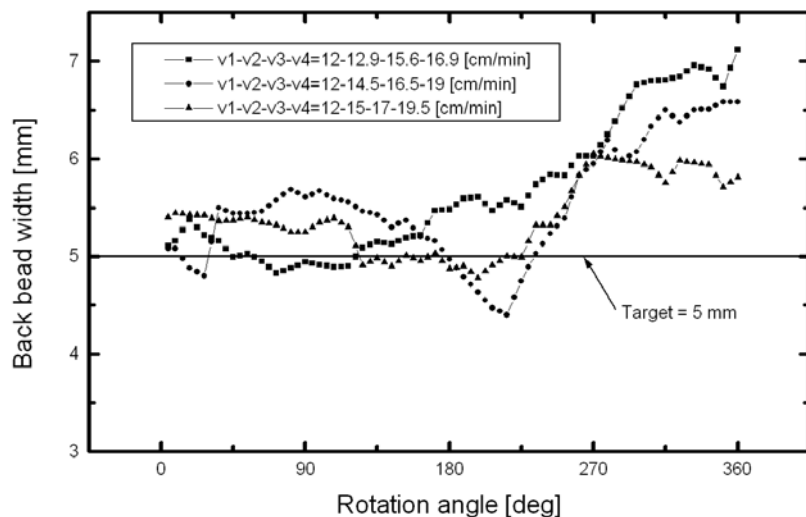
(b) Welding result with different welding speed of $v_2 - v_4$

Fig. 2.11 Results of experiment without control

From the experiment to evaluate the neural network system, the comparison between back bead width obtained from the neural network and measurement is shown in Fig. 2.12. In this experiment, to produce stable arc condition, the welding speed of 12 cm/min at $\theta = 0^o - 45^o$ was kept constant. Figure 2.12 (a) shows the comparison between estimated back bead width using neural network and measured back bead width. In Fig. 2.12 (b) presents the error of back bead width estimation. At $\theta = 45^o - 135^o$ estimated back bead width error was about -1 mm, and at $\theta = 270^o - 360^o$, error was

more than 1 mm. Nevertheless, most of the errors were aligned in the tolerance value of 4 – 6 mm and the average error of the estimation was –0.1 mm. The possible cause of errors could come from the error of measurement of back bead width. Another reason of these errors was the training data for neural network were not sufficient.
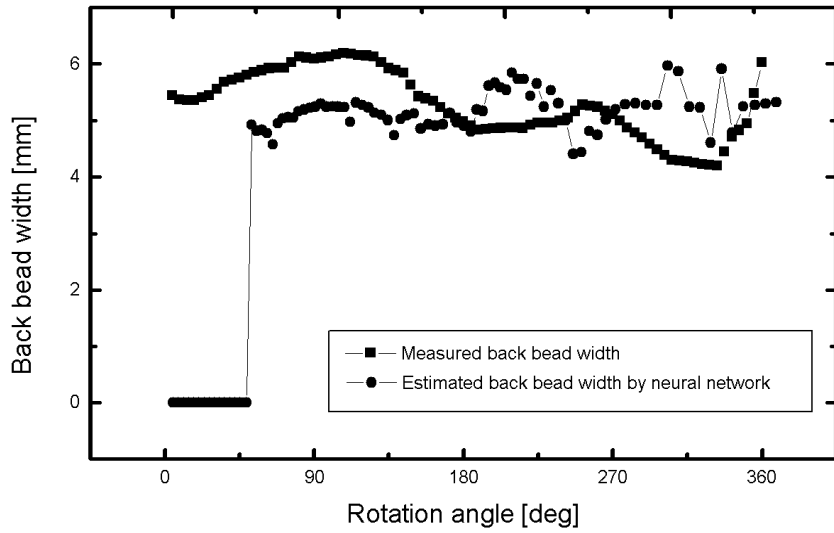
(a) Comparison between estimated and measured back bead width
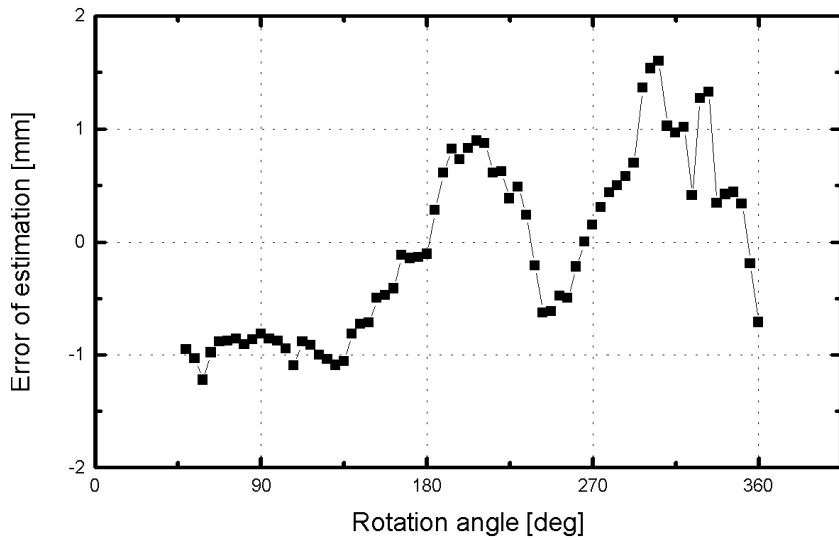
(b) Error of the estimation of back bead width

Fig. 2.12 Result of estimated back bead width using neural network
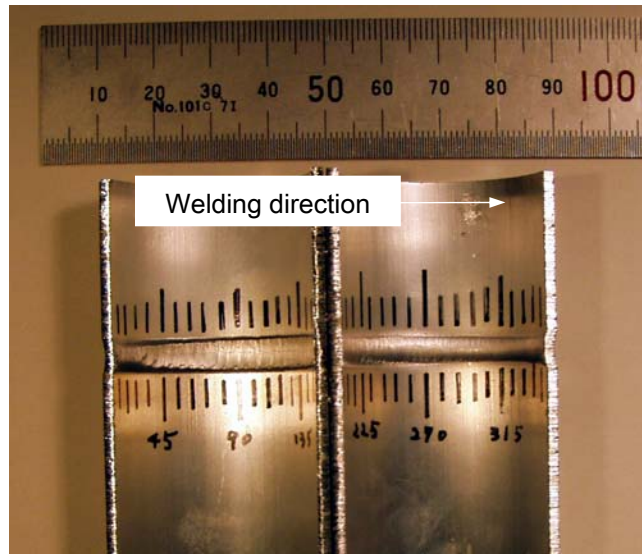
(a) Back bead
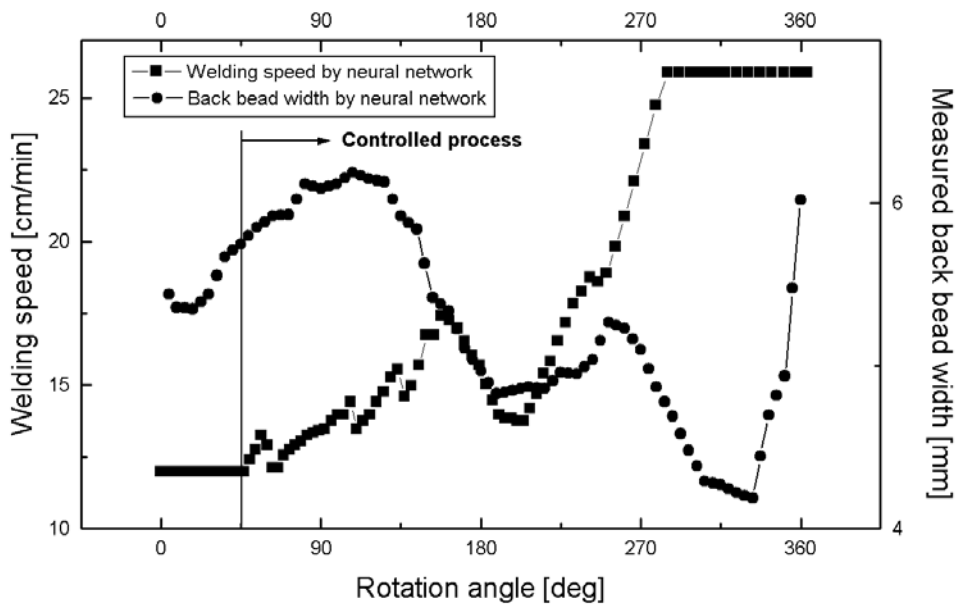
(b) Welding speed and back bead width

Fig. 2.13 Result of experiment using neural network control

The experiment result using neural network is shown in Fig. 2.13. Figure 2.13 (a) shows sound weld of back bead. The cleaning area in with and without control results were almost same at 10 – 12 mm in width. Having this result, the cleaning area was not influence greatly in the control process. The welding speed and measured back bead width is shown in Fig. 2.13 (b). At $\theta = 45° – 135°$, the welding speed increased slowly from 12 – 15 cm/min and the error of back bead width increased and exceeded 1 mm.

However, by increasing the welding speed until 17.5 cm/min, the error of back bead width decreased to 0 mm at θ = 180°. Then, the welding speed was reduced to 14 cm/min at θ = 180° and increased again up to 26 cm/min to saturated value of welding speed at θ = 270°. This welding speed has decreased error of back bead width less than 0 mm and more than -1 mm. In general, the average error and standard deviation of back bead with using neural network model was 0.3 mm and 0.6, respectively.

This experiment result shows a good agreement with previous experiment without control that the welding speed at θ = 90° – 180° was very important to affect next welding result. Accordingly, by proper control of welding speed, it will produce excellent back bead width. The experiment result shows that the bead was smooth in appearance and there was no crack, porosity, undercut and burn through along the circumference. The back bead width also aligned in the range target of 4 – 6 mm in width. In this study, the welding condition was changed during the welding proceeded along the circumference of the pipe. However, the suitable welding condition for producing the good result was obtained at welding current, I = 60 A, pulsed current frequency, f = 50 Hz, minimum welding speed, v_{min} = 12 cm/min, and maximum welding speed, v_{max} = 26 cm/min. In general, the proposed automatic welding system produced sound weld of aluminum pipes by monitoring backside image of molten pool.

2.6 Conclusions

Main results obtained by the investigation are summarized as follows.

1. An automatic welding process of aluminum pipe welding system by monitoring backside image of molten pool using vision sensors was constructed.

2. An algorithm to obtain edge detection's range to detect edge of molten pool was proposed. Image processing based on differential value of brightness was proposed to detect edge of molten pool and the validity of the system was confirmed.

3. As a result of welding experiments, the effectiveness of automatic welding system using neural network was demonstrated and sound weld was obtained.

Welding Penetration Control of Fixed Aluminum Pipes Using Fuzzy Inference System

3.1 Introduction

Improved automation of welding process has become increasingly important in the need for higher weld quality and reduced manufacturing cost. Advanced welding robot technology offers the reduced manufacturing cost however its use requires a means of sensing and monitoring the errors of the workpiece and the robot itself.

Among the variety of welding processes, Tungsten Inert Gas (TIG) welding is frequently used, primarily because of its optimum weld quality, minimum distortion, operatively in all positions, and good visibility because the gas around the arc is transparent and weld pool is clean. A number of problems in automating arc welding processes include sensing, monitoring, joint tracking, and lack of adequate mathematical model for parameter prediction and quality control. Moreover, the welding penetration control is essential to the production quality welds with a specified geometry. Problems with parameter setting and quality control occur frequently in the TIG welding process, because welding process is nonlinear and multivariable-coupled which involves many uncertainties, such as, influences of metallurgy, heat transfer, chemical reaction, arc physics and magnetization [1].

Therefore, it is very difficult to obtain a practical and useful controllable model of an arc welding process through classical modeling approaches. Welding bead width accuracy is difficult to be controlled due to the non-linearity and uncertainties of the process. As a result, intelligent control systems have been developed for modeling and controlling the welding process, as they derive the control performance based on human experience, knowledge, and logic techniques, instead of mathematical process

models. Hence, an approach adapted to provide modeling difficulties is Fuzzy Inference System that provides an approximate but effective means of describing the behavior of the system. A fuzzy inference system is a rule-based system that uses fuzzy set and fuzzy logic to reason about data. Fuzzy logic is a computational paradigm that provides a mathematical tool for representing information in a way that resembles human linguistic information and reasoning processes [77-83]

Many industrial applications in arc welding process using fuzzy inference system have been reported [8-12] [46-47] [78]. An important application field where fuzzy inference system may play a significant role is in the control of welding speed under constant arc current in pipe welding. Compared to plate welding, obviously, welding of fixed pipe is more difficult due to the characteristics of the welding process and material properties. For fixed pipe welding, if the constant welding conditions are maintained over the full joint length, the bead width becomes wider as the circumferential welding of small diameter pipes progresses. Therefore, the control of bead width products has been very difficult to perform by constant welding conditions.

The previous research was successfully conducted to weld stainless steel pipes [45] and aluminum pipes [57-61] [63-65] using neural network. The same material with neuro and fuzzy controller was also observed [62]. However, by using neural network great number of training data was necessary. In this research, welding penetration control of fixed aluminum alloy pipe A6063S-T5 using fuzzy inference system was proposed. By using this control system, the experimental data used in this study were less than in previous experiment using neural networks [57-65]. AC welding machine with square-wave current was used. The constant current of TIG welding process was considered with the controlled welding speed derived from the back bead width of molten pool image. Simulations were conducted to assess the performance of fuzzy modeling and fuzzy controller. A series of experiment were conducted to investigate the effectiveness of fuzzy controller.

3.2 Experiment

The pipe welding system developed in this study is same as in Section 2.2. Material properties and welding condition is shown in Table 3.1.

44

Table 3.1 Material properties and welding conditions

Base metal	Al-6063S-T5
Diameter of pipe (mm)	37.8
Thickness of pipe (mm)	2.0
Density (g/cm³)	2.69
Melting point (°C)	615-655
Thermal conductivity (W/m.K at 25°C)	209
Welding machine	AC
Electrode	2% Th-W ($\varnothing$ 2.4 mm)
Nominal arc length (mm)	1.5
Welding current, I (A)	50 ~ 70
Pulse current frequency (Hz)	50 ~ 70
EN ratio	0.5
Welding speed, v (cm/min)	12 ~ 24
Shielding gas	100% Ar
Shielding gas, q (l/min)	8 ~ 15
Back shielding gas, 1 (l/min)	8 ~ 10

3.2.1 Image Processing Algorithm

A mirror with the size of 29 x 20 mm was set with 60° about the horizontal axes reflected the backside molten pool image into the CCD camera as shown in Fig. 3.1 (a). The mirror rotates along the welding torch during the pipe welding process. Backside image of molten pool is shown in Fig. 3.1 (a).

Fig. 3.1 (b) - (g) presents the results of image processing algorithm. According to the low brightness of aluminum's molten pool due to the low melting point, the stable and robust image processing algorithm must be constructed as follows.

1. The image of molten pool was captured by CCD camera. The center of image was obtained and it was rotated along the center of image to get uniform image.

2. Edge detection was performed using the differential value of brightness distribution. Firstly, histogram analysis was performed to find the edge detection's range consists of top and bottom threshold values. Secondly, edge position was determined within this range.

3. The vertical scanning within the defined set window obtained the maximum and minimum position of edge. And then the horizontal scanning determined the left and right edges.

4. Finally the width of molten pool (w) was determined as a largest width of the left and right edges.
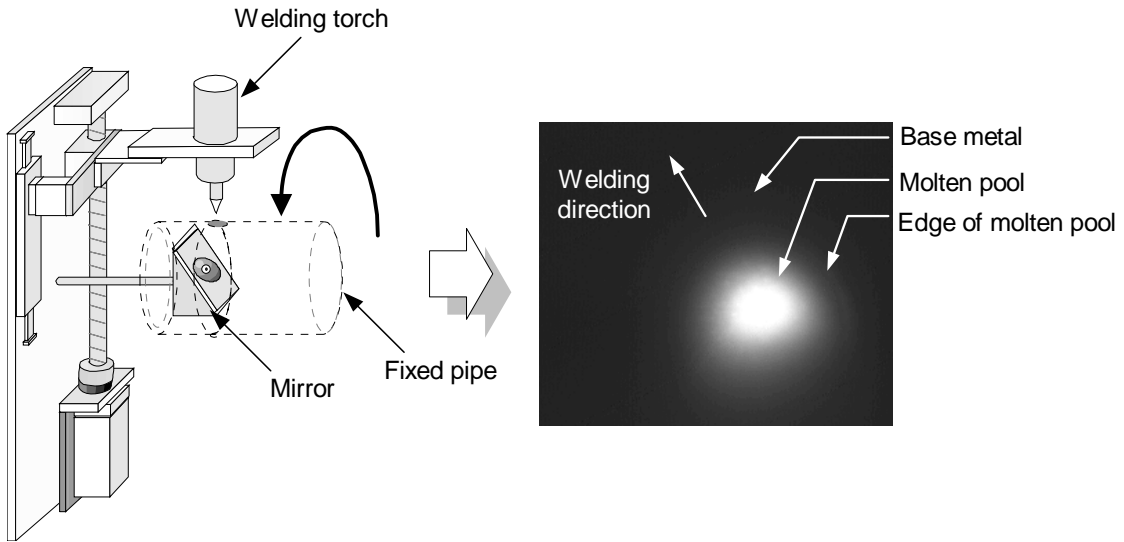
(a) Schematic of monitoring
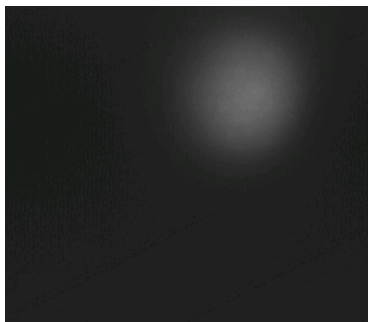
(b) Original image
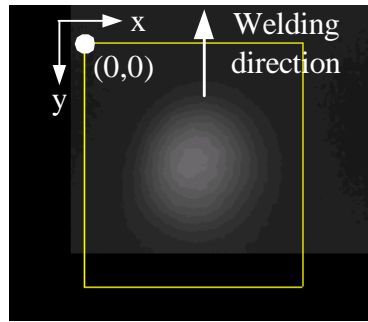
(c) Rotated image
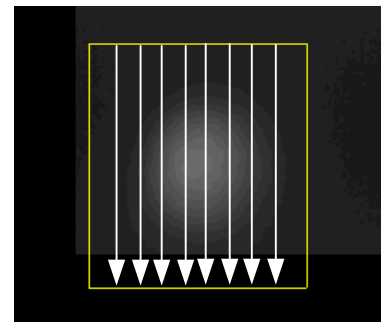
(d) Vertical scanning
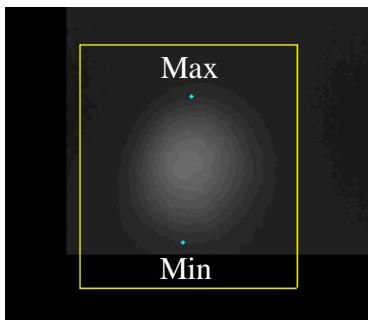
(e) Maximum and minimum edge positions
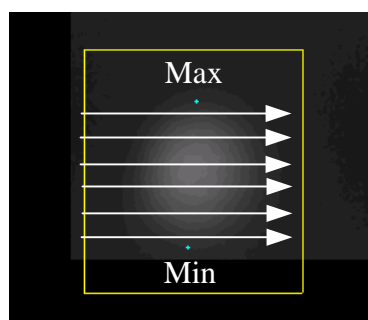
(f) Horizontal scanning
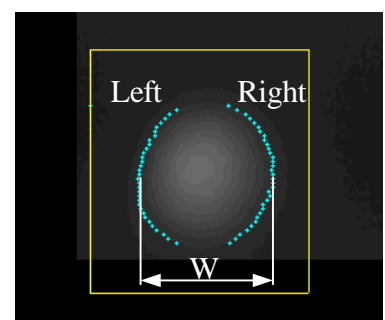
(g) Left - right edges and width of molten pool

Fig. 3.1 Monitoring of molten pool

3.2.2 Preliminary Experiment

Preliminary experiments were conducted to find the preliminary data by welding the pipe with several different welding speeds. The welding speed of 12 – 20 cm/min was implemented at four range of rotation angle: θ_1 = 0° – 90°, θ_2 = 90° – 180°, θ_3 = 180° – 270°, and θ_4 = 270° – 360°.

Welding process was conducted autogenously for 360° circumference of fixed pipe. In constant welding current of 60 A, the torch started to initiate the arc until the initial penetration was produced. Then by controlling the welding speed, $v_{\theta 1}$ – $v_{\theta 4}$, the preliminary experiment was conducted. The relationship between welding speed, rotation angle and back bead width is shown in Fig. 3.2. The result shows that at the constant welding speed, the more rotation angle, the larger back bead width.
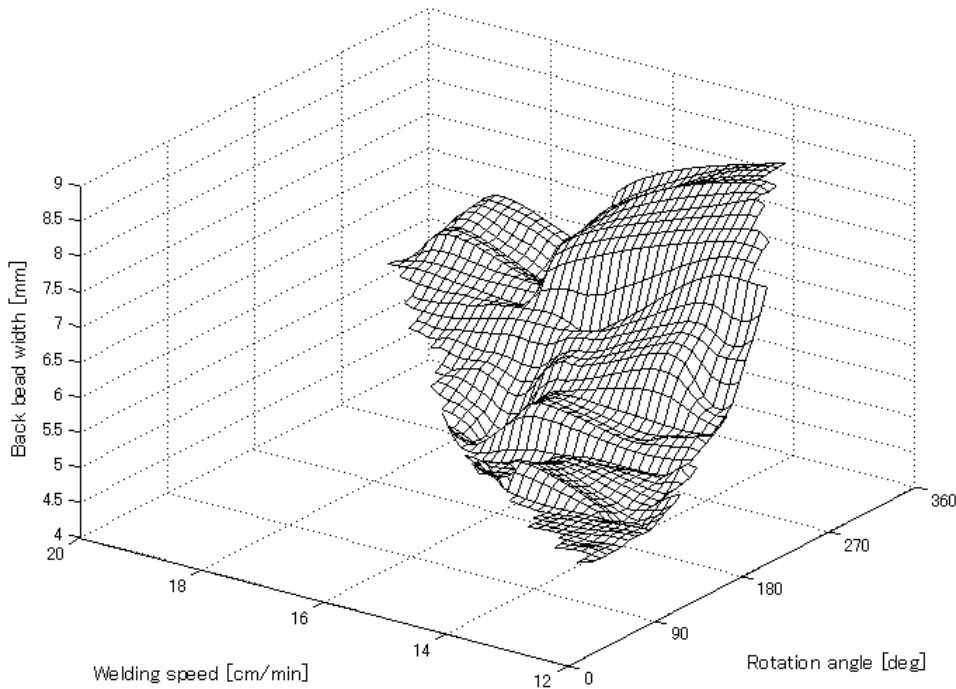
Fig. 3.2 Results of preliminary experiment

3.3 Experiment

To evaluate process control in pipe welding, the simulation of welding speed control system was proposed as shown in Fig. 3.3. The output from the fuzzy modeling, which is the estimated back bead width (w) will be compared to the reference back bead width (w_r) to produce error (e). Together with the change of error (Δe), correction of welding speed (Δv) was determined. For simulating the welding process model, the process was

47

constructed by considering the welding distance (s) and control time (t_{cont}) that includes image processing time and control process time which was set to 0.08 s. To initiate the welding speed, v_0 of 12 cm/min was set. By adding the correction of speed to the previous welding speed, the new welding speed was determined. Welding distance and rotation angle (θ) will be determined by multiplying welding speed with control time. This process will be repeated for the welding distance that set from initial point until reach the end of the circumference of pipe.

3.3.1 Modeling of Welding Process

In pipe welding using constant arc current, welding speed is an important process parameter. Understanding the relationship between welding speed and rotation angle is essential to exercise the level of back bead width desired. In general, this is a difficult task because of the problems associated with many uncertainties of welding process. The objective of this work is to develop a model of welding process by means of fuzzy inference system. In this work, the back bead width is estimated from the welding speed and rotation angle of welding torch. The data from preliminary experiments without control have been used to perform the modeling process.
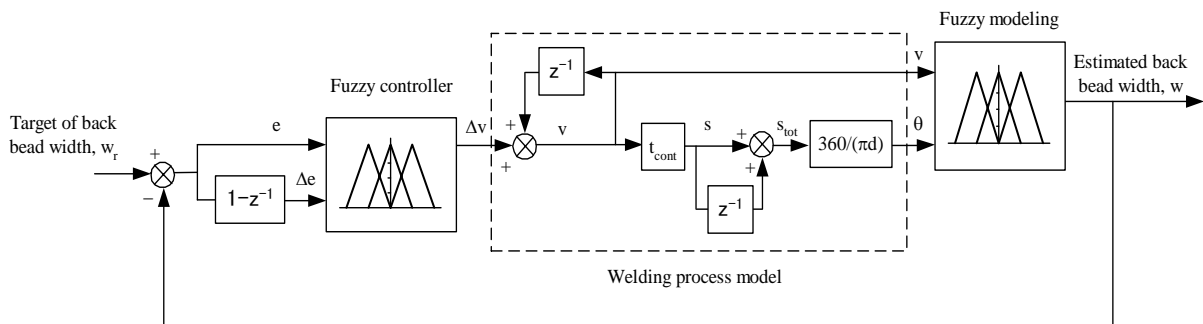
Fig. 3.3 Block diagram of welding speed control system

First input to the fuzzy modeling is welding speed (v). At constant welding speed for every degree of rotation angle produces different back bead width. Hence, the rotation angle (θ) was adopted as another input to the fuzzy modeling. Five kinds of membership (Z – Zero, S – Small, M – Medium, L – Large, VL – Very Large) and triangular membership functions were used to fuzzify the inputs. Figure 3.4 illustrates the membership functions and ranges for each fuzzy variable. The optimization of the

48

assignment was done through trial and error for achieving optimum performance of fuzzy inference system.

(a) Input: welding speed [cm/min]

(b) Input: rotation angle [deg]

(c) Output: back bead width [mm]
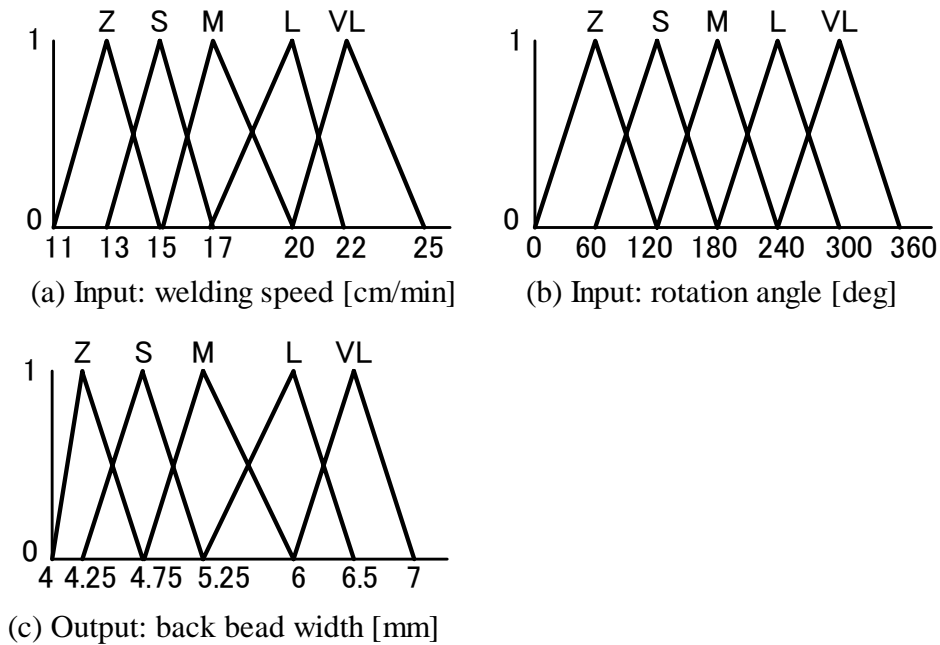
Fig. 3.4 Membership function of fuzzy modeling of back bead width

Table 3.2 Decision table for the fuzzy modeling of back bead

θ \ v	Z	S	M	L	VL
Z	M	S	Z	Z	Z
S	L	M	S	Z	Z
M	L	L	M	S	Z
L	VL	L	L	M	S
VL	VL	VL	L	L	M

A set of rules that describe the operation of the fuzzy inference system should be constructed to specify which action to be taken under which conditions. These rules usually take the form of IF-THEN rules and can be obtained from a human expert. The decision table matrix for fuzzy modeling of back bead width is shown in Table 3.2.
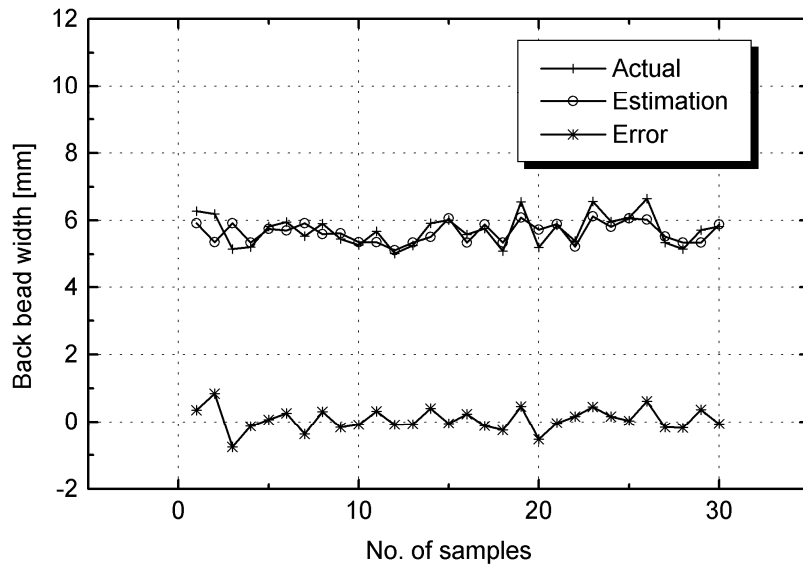
Fig. 3.5 Error curve of the fuzzy modeling

The heuristics guidelines in establishing this matrix are based on the following statements.

1. When welding speed increases, the back bead width will decrease.
2. When rotation angle increases, the back bead width will increase.

Most common and simplest way to define the rule is the "max-min" inference method which is used here. These bring to the final step, defuzzification of the fuzzy output. And the weighted average method was used to convert the output values into a nonfuzzy result.

For the purpose of validating the models, the data set was set randomly split into 1245 training samples and 400 test samples. The partitioning is repeated 10 times independently. The precision (mean square error) of the method is 0.5 mm. Figure 3.5 shows the error curves of the method. The modeling results shows that the fuzzy modeling has good performance and suitable to estimate back bead width.

3.3.2 Fuzzy Controller Design

The flowchart of control process is shown in Fig. 3.6. First, when the program executed, the arc will be started. In order to get the penetration at the starting point and stable arc, the welding torch must be kept static for a certain time. Then, the welding torch starts to move along the pipe. During the welding process, the rotational angle is

50

monitored and checked whether more than 360° or not. If the rotation angle less than 360°, then the backside image of molten pool is captured by CCD camera and send to the PC to be processed.

The output of the image processing is the width of molten pool, w. This value becomes the input of fuzzy controller. The output of fuzzy control is the correction of welding speed. After adjusting the welding speed, motor waits for several milliseconds to make sure the CCD camera captures the molten pool image. All of the processes will be repeated until the rotation angle reaches 360°. Finally, the program commands to stop the motor and the welding arc will stop.

Fig. 3.6 Flowchart of control process

N   Z   P

(a) Input: back bead width
error, e [mm]

N   Z   P

(b) Input: back bead width
error deviation, Δe [mm]

N   Z   P

(c) Output: welding speed
correction, Δv [cm/min]
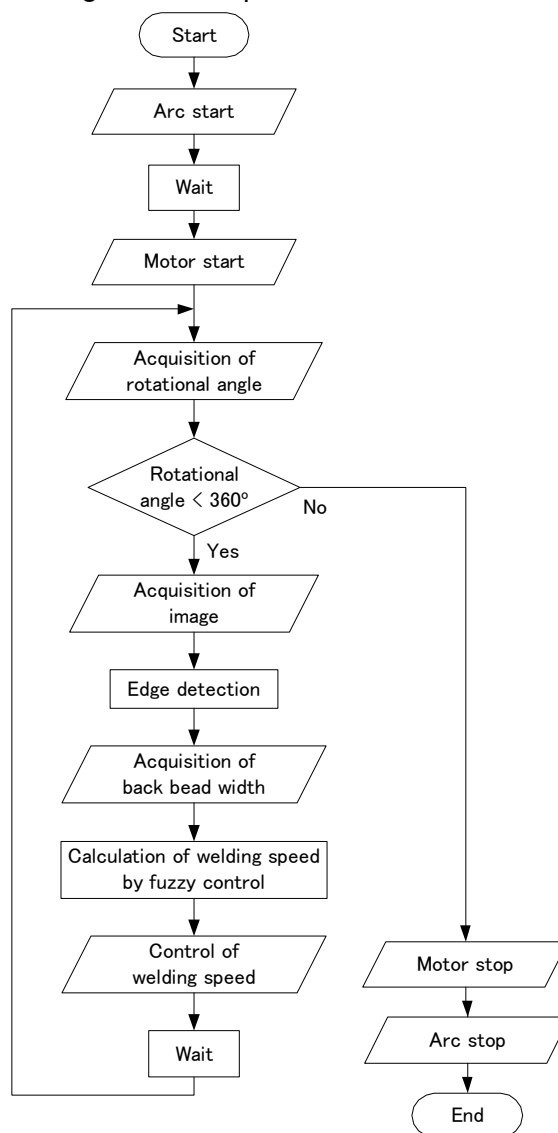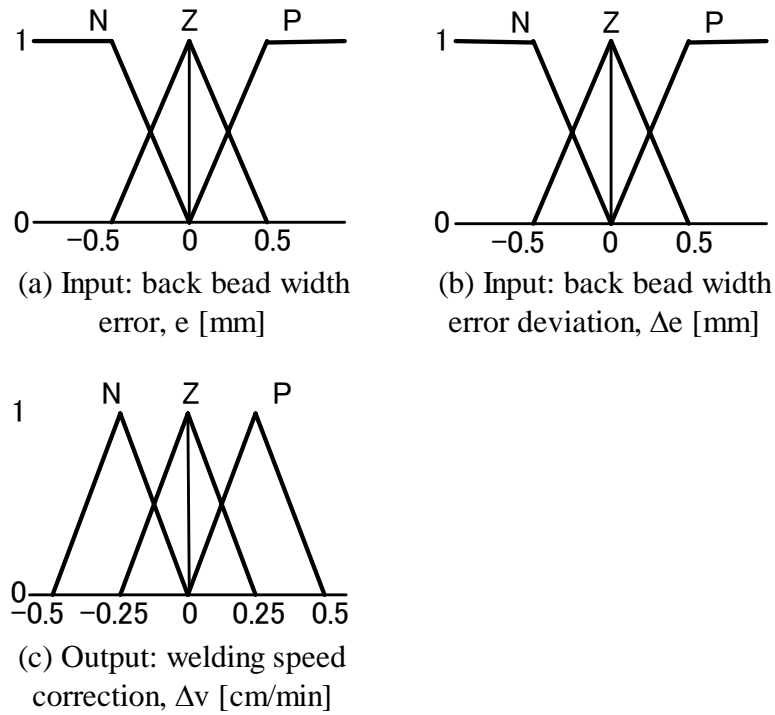
Fig. 3.7 Membership function of fuzzy control

Table 3.3 Decision table for the fuzzy control of welding speed

Δe \ e	N	Z	P
N	1) N	4) N	7) Z
Z	2) N	5) Z	8) P
P	3) Z	6) P	9) P

In this step, the proposed fuzzy control took two variables to be fuzzified. One was an error (e_n), which was the difference of back bead width (w_n) at the concerned time step (n) from the reference back bead width (w_r):

$$e_n = w_r - w_n \tag{3.1}$$

and w_r was set at 5 mm.

The other was the change of an error defined as:

$$\Delta e_{n+1} = w_{n+1} - w_n \tag{3.2}$$

Back bead width
w [mm]

Δv -> Positive (+)   Δv -> Positive (+)   Δv -> Zero (0)

9) w_{n+1} 8)   7) w_n Error = $w_r - w_n$

w_n w_n w_{n+1} w_{n+1}

Error < 0

Δv -> Positive (+)   Δv -> Zero (0)   Δv -> Negative (-)

6)   5)   4) w_n

Target width w_{n+1} w_{n+1} Error = 0

w_n w_n w_{n+1} w_{n+1}

Error > 0

Δv -> Zero (0)   Δv -> Negative (-)   Δv -> Negative (-)

3) w_{n+1} 2)   1) w_n

w_n w_n w_{n+1} w_{n+1}

Rotation angle θ [deg]
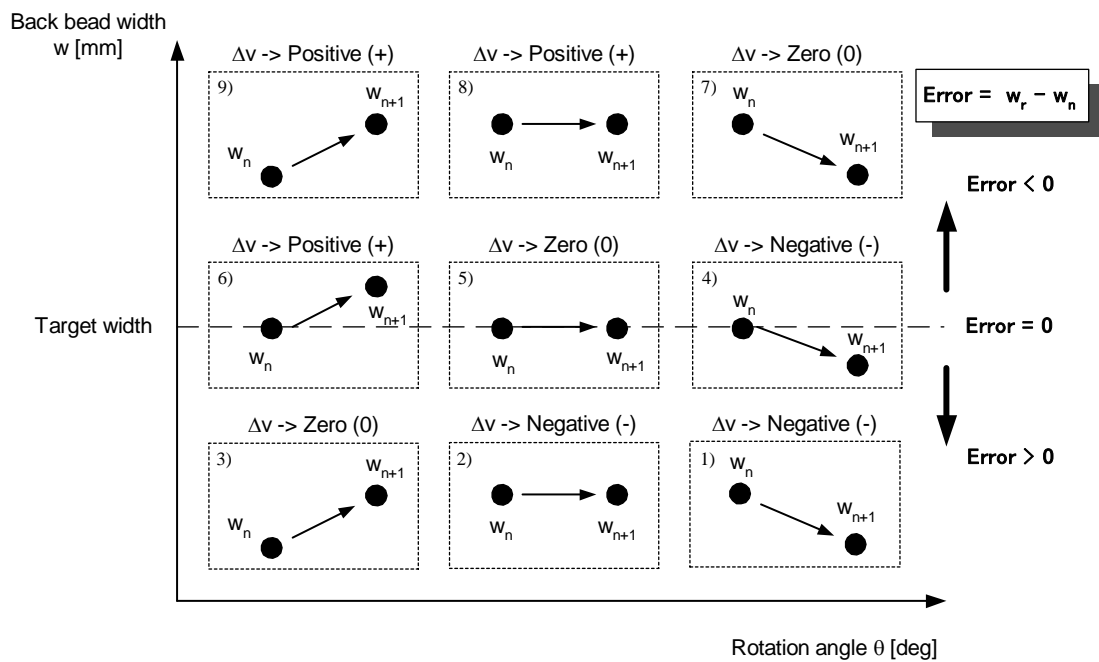
Fig. 3.8 Summary of input – output relationship

Three kind of membership (N – Negative, Z – Zero, P – Positive) and triangular membership functions were used to fuzzify the inputs. Figure 3.7 shows the membership functions and ranges for each fuzzy variable. The decision table for fuzzy control of welding speed is shown in Table. 3.3. The following knowledge was utilized to determine a new welding speed.

1. If back bead width error is negative, ($e(n) < 0$) and becomes smaller ($\Delta e(n) < 0$), then back bead width should be increased and set much lower of welding speed ($\Delta v < 0$).

2. If back bead width error is negative, ($e(n) < 0$) and not changed ($\Delta e(n) = 0$), then back bead width should be increased and set much lower of welding speed ($\Delta v < 0$).

3. If back bead width error is negative, ($e(n) < 0$) and becomes larger ($\Delta e(n) > 0$), then back bead width should be decreased and set no change of welding speed ($\Delta v = 0$).

4. If back bead width error is zero, ($e(n) = 0$) and becomes smaller ($\Delta e(n) < 0$), then back bead width should be increased and set much lower of welding speed ($\Delta v < 0$).

5. If back bead width error is zero, ($e(n) = 0$) and not changed ($\Delta e(n) = 0$), then back bead width should be decreased and set no change of welding speed ($\Delta v = 0$).

53

6. If back bead width error is zero, (e(n) = 0) and becomes larger (Δe(n) > 0), then back bead width should be decreased and set much higher welding speed (Δv > 0).

7. If back bead width error is positive, (e(n) > 0) and becomes smaller (Δe(n) < 0), then back bead width should be decreased and set no change of welding speed (Δv = 0).

8. If back bead width error is positive, (e(n) > 0) and not changed (Δe(n) = 0), then back bead width should be decreased and set much higher welding speed (Δv > 0).

9. If back bead width error is positive, (e(n) > 0) and becomes larger (Δe(n) > 0), then back bead width should be decreased and set much higher welding speed (Δv > 0).

    The summary of input-output relationship is shown in Fig. 3.8.

    The simulation result of back bead width and welding speed is shown in Fig. 3.9. It shows that the fuzzy control maintained the back bead width over the reference within the range of 5$\pm$1 mm. The root mean square error (RMSE) and mean square error (MSE) of fuzzy control are 0.3 mm and 0.6 mm, respectively. The welding speed gradually increased to keep the back bead width under the certain tolerance. Based on this result, the fuzzy control was suitable for controlling the welding speed and appropriate to be implemented into the real automatic control system. This control system also performed the process more effective, because it used the experimental data 70 percent less than in the study using neural network [65].
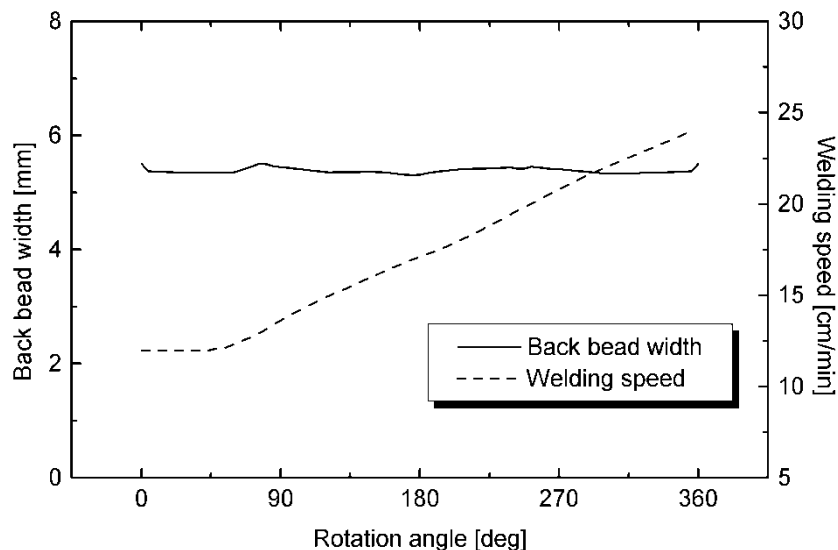
Fig. 3.9 Result of simulation

3.4 Results and Discussion

In this experiment, to produce stable arc condition, the welding speed of 12 cm/min at θ = 0° – 45° was kept constant. Figure 3.10 shows the experiment result at different

arc current and same pulse current frequency. At constant arc current, I = 60 A, and pulse current frequency, f = 50 Hz, the result shows that the back bead width could be kept in the target range of 5±1 mm with the average error and standard deviation are -0.1 mm and 0.4 mm, respectively as shown in Fig. 3.10 (a).

This setting was set as baseline to the next experiment. Welding speed was increased by fuzzy controller to reach the target of back bead width. On the other hand, by increasing the arc current, obviously the higher heat input was delivered. Therefore the system designed to produced back bead width conformed to the reference back bead width by increasing welding speed. The welding speed at increased arc current is higher as shown in Fig. 3.10 (b). The correction welding speed was kept higher by fuzzy control, although the values were saturated to the 0.25 cm/min as shown in Fig. 3.10 (c). The result after increasing arc current at I = 62.5 A and f = 50 Hz yields the average error and standard deviation are -0.3 mm and 0.5 mm, respectively.
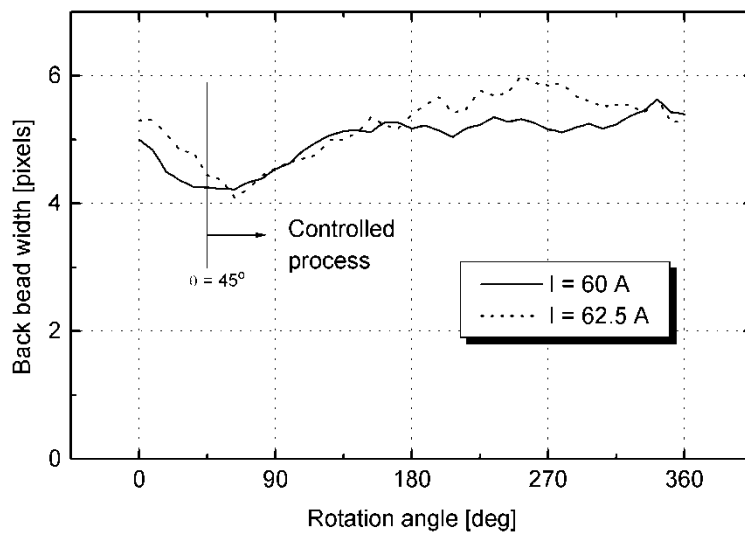
(a) Back bead width
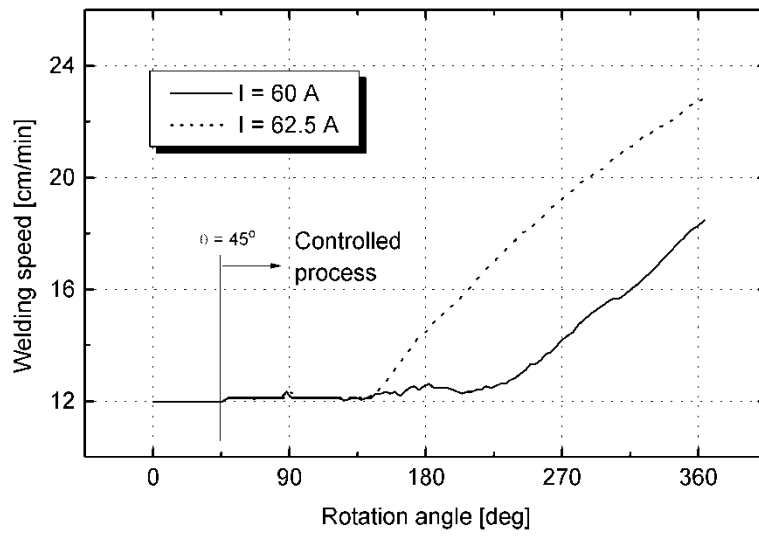
(b) Welding speed
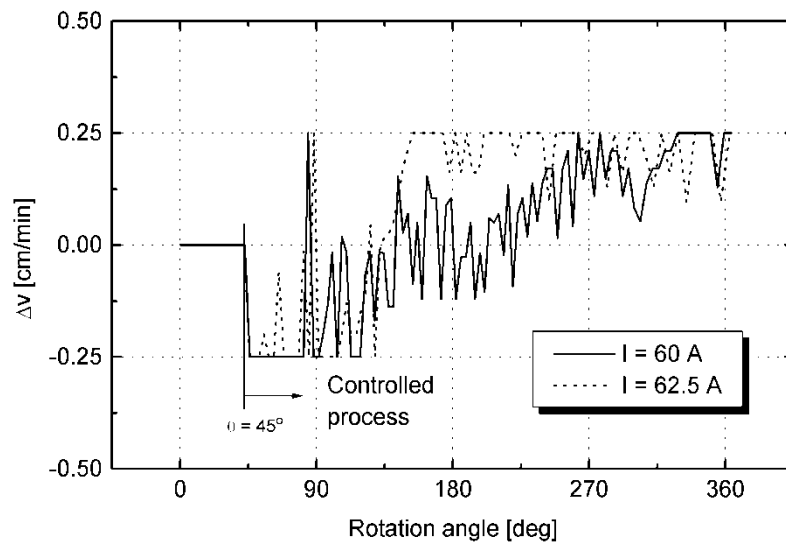
(c) Correction of welding speed

Fig. 3.10 Results at different arc current and same frequency (f = 50 Hz)
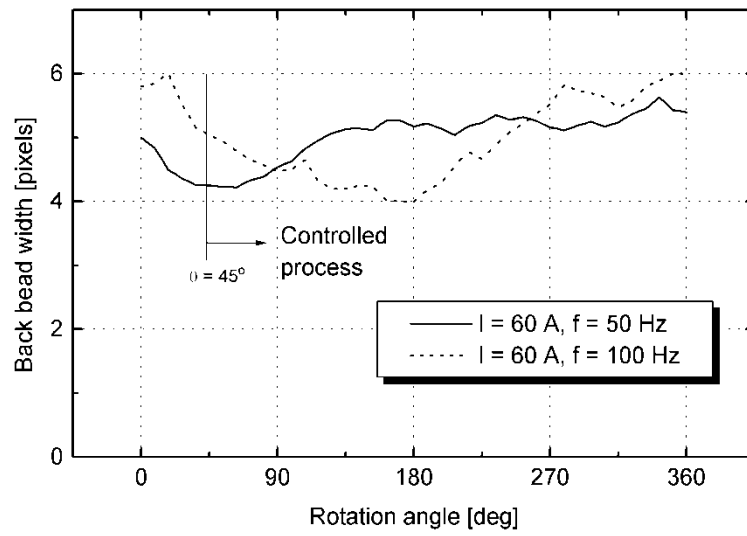
(a) Back bead width
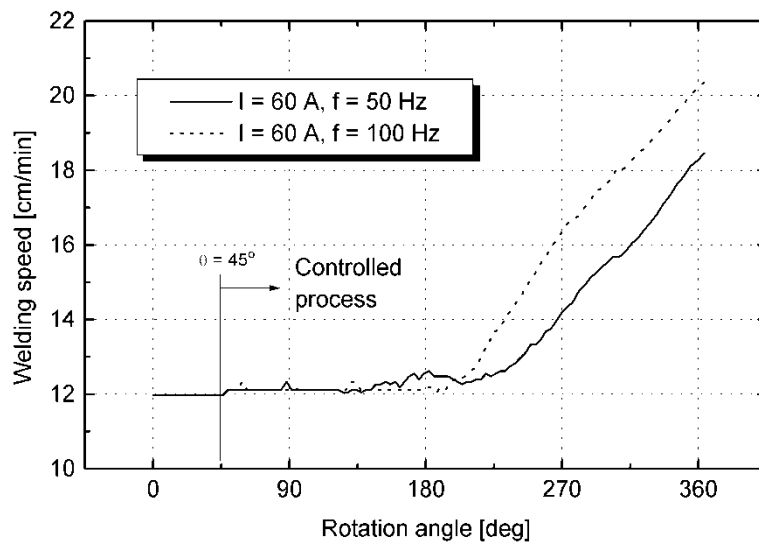
(b) Welding speed
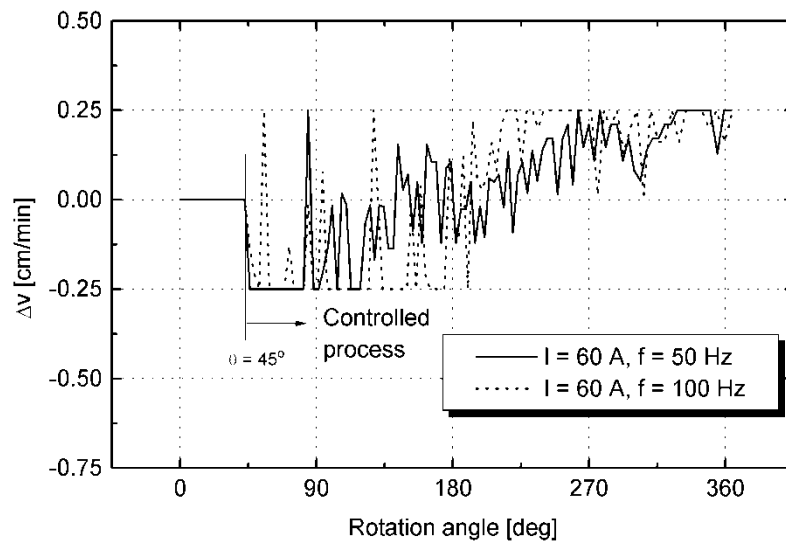
(c) Correction of welding speed

Fig. 3.11 Results at different pulse current frequency

Figure 3.11 shows the experimental result at same arc current and different pulse current frequency. At I = 60 A and f = 100 Hz, it is clearly understood that the heat input also increased. It shows that the back bead width could be maintained in the target range of 5±1 mm with the average error and standard deviation are -0.1 mm and 0.6 mm, respectively as shown in Fig. 3.11 (a).

However, back bead width decreased because the welding speed increased and it increased gradually after welding speed was corrected as shown in Fig. 3.11 (b). The correction of welding speed was kept higher by fuzzy controller, although some corrections were saturated to the ±0.25 cm/min as shown in Fig. 3.11 (c).

These experimental results indicate that fuzzy controller can perform the correction of welding speed to get the target of back bead width. However the results of back bead width using increased arc current and increased pulse current frequency were not as good as the baseline's result. Some errors occurred may correspond to the error of image processing and welding speed control. By adjusting the membership function of fuzzy controller, target back bead width can be obtained.

Figure 3.12 shows four pictures illustrating each result of experiment without and with welding penetration control, respectively. Figure 3.12 (a) shows the result of the welding for welding speed of $v_{\theta 1} - v_{\theta 4}$ = 12.1 – 12.8 – 14.8 – 16.7 cm/min and the

58

standard deviation is 0.66 mm. On the contrary, the welding process with fuzzy control provides sound weldment as shown in Fig. 3.12 (b), (c) and (d).
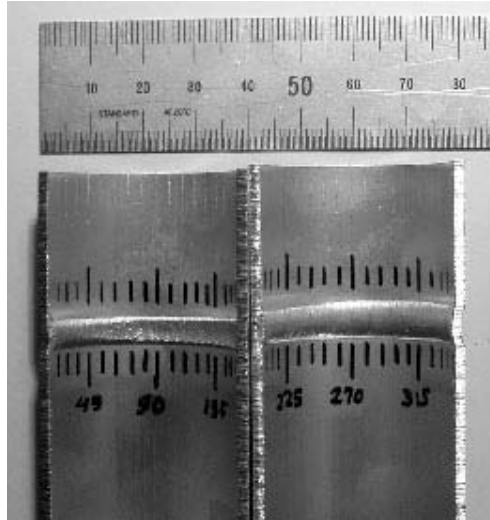
(a) Experiment without control

(I = 60 A, f = 50 Hz)
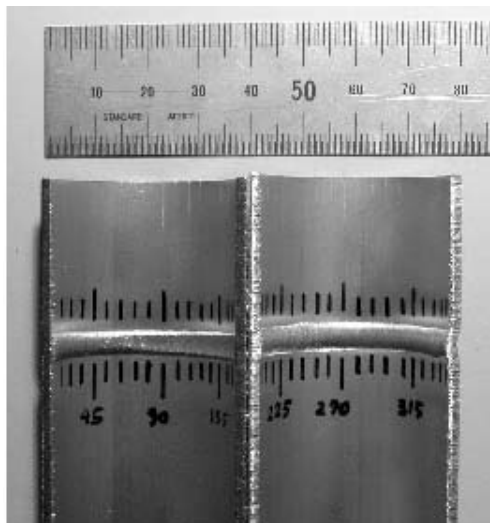
(b) Experiment with control

(I = 60 A, f = 50 Hz)
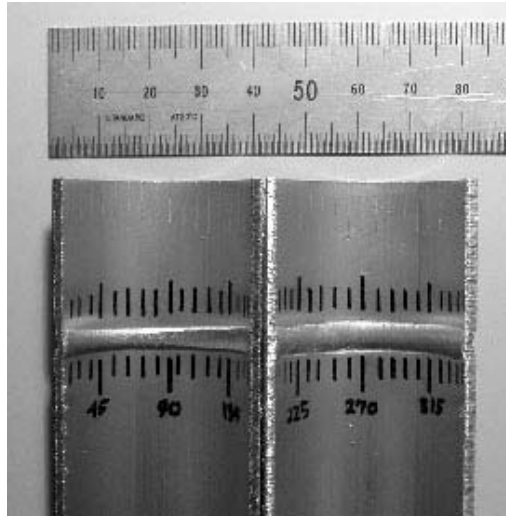
(c) Experiment with control, at different arc current and same frequency

(I = 62.5 A, f = 50 Hz)
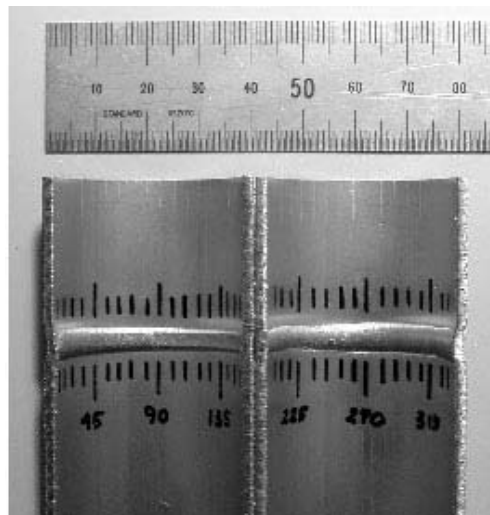
(d) Experiment with control, at same arc current and different frequency

(I = 60 A, f = 100 Hz)

Fig. 3.12 Back bead appearance

The experiment results show that there were no crack, porosity, undercut and burn through along the circumference and the bead was smooth in appearance. Moreover, the back bead width also aligned in the range target of 5±1mm in width. In this study, the welding condition was changing during the welding proceeded along the circumference of the pipe. However, the suitable welding condition for producing the good result was obtained at welding current, I = 60 A, pulse current frequency, f = 50 Hz, minimum welding speed, v_{min} = 12 cm/min, and maximum welding speed, v_{max} = 24 cm/min.

In general, the proposed automatic welding system using fuzzy inference system produced sound weld of aluminum pipes by monitoring backside image of molten pool.

3.5 Conclusions

Main results obtained by the investigation are summarized as follows.

1. An automatic welding process of aluminum pipes by monitoring backside image of molten pool using fuzzy inference system was constructed.

2. Simulator of welding control using fuzzy inference system was constructed to simulate the welding control process. It shows that the fuzzy controller was suitable for controlling the welding speed.

3. As a result of automatic welding control using fuzzy inference system, it shows the effectiveness of the control system that is confirmed by sound weld of experimental results.

New Monitoring System of

Backside Image of Molten Pool

Using Omnidirectional Camera

4.1 Introduction

For many applications in automation of welding process, the need for higher weld quality and reduced manufacturing cost has become increasingly important. Advanced welding technology takes part to reduce manufacturing cost, however its use requires a means of sensing and monitoring of error in the process. As the application of pipe welding in power stations, offshore structures, and process industries, it is important to investigate the characteristic of the welding process.

There have been problems in automating arc welding processes such as sensing, monitoring and line tracking. The difficulty in welding process related to nonlinear and multivariable-coupled which involves many uncertainties, such as influences of metallurgy, heat transfer, chemical reaction, arc physics, and magnetization [1].

Therefore, to achieve full automation of aluminum pipe welding, the welding penetration should be controlled. Intelligent control systems have been developed for modeling and controlling the welding process as they derive the control performance based on human experience, knowledge, and logic techniques. Many industrial applications and welding processes have been studied using neural networks [2-7] [44-45] [57-65] and fuzzy techniques [8-12] [46-47] [65-68]. Another difficulty in controlling an arc welding process is how to detect weld pool geometrical features, such as weld bead width and penetration, either from the topside or backside, conveniently and in real-time. Various efforts have been made to sense weld pool sizes in real-time from the topside, such as ultrasonic detection, infrared sensing, pool image processing, and radiographic sensing to produce weld quality control [13-16]. The experiment using

the vision sensing to control the TIG weld width for stainless steel [45] and aluminum alloy [57-68] pipe has been conducted with the algorithm of image processing to detect molten pool's edge.

In order to avoid the defects during aluminum pipe welding and to obtain the uniform weld bead over the entire circumference of the pipe, the welding conditions should be controlled as the welding proceeds. The previous research was successfully conducted to weld stainless steel pipes [45] and aluminum pipes [57-68] using plain mirror that rotates along the welding torch during the pipe welding process. This research studies the intelligent welding process of aluminum alloy pipe 6063S-T5 in fixed position using the AC welding machine. The proposed monitoring system used new monitoring system backside image of molten pool by using an omnidirectional camera. Recently, an omnidirectional camera which provides a wide view of 360° has been popularly applied to mobile robots [84-89]. The omnidirectional camera consists of a perspective camera and a curved mirror to allow a central projection by reflected rays such as by paraboloidal, ellipsoidal and hyperboloidal mirrors. A geometry model and design method for an omnidirectional camera with a hyperboloidal mirror is presented [84]. In [86], the geometry of image formation of an omnidirectional camera with paraboloidal and hyperboloidal mirror was developed. A general framework was described for computing ego-motion using the optical flow in an omnidirectional camera. The image velocity vectors were mapped into a sphere using the Jacobian of the transformation to estimate ego-motion [87].

AC welding machine with square-wave current was used. The constant current of TIG welding process was used and controlled welding speed derived from the back bead width of molten pool image was performed. Panorama image of molten pool was developed and image processing algorithm was constructed to detect edge of molten pool. In this experiment, the fuzzy inference system was used to control welding penetration by modifying speed. Automatic welding process was conducted to evaluate the performance of the system.

4.2 Experimental Device

The pipe welding system developed in this study is same as Section 2.2. The major functional elements of the experimental system are a circumferential welding manipulator, CCD camera and the image board (256×220pixels, 8bit), the personal computer (CPU: 700 MHz), A/D board to measure arc current and voltage, TIG welding

machine, and motor board to control stepping motors. Material properties and welding conditions is shown in Table 4.1.

4.3 Image Processing Algorithm

4.3.1 Omnidirectional Vision

Omnidirectional vision developed in this research consists of a CCD camera and a hyperboloidal mirror. This system improved the previous design of monitoring which used plain mirror that rotated along the welding torch [57-68]. With this mirror, there is no rotated part in the monitoring system. Figure 4.1 (a) presents the top view of the hyperboloidal mirror used in this study. The dimension of the mirror is shown in Fig. 4.1 (b).

Table 4.1 Material properties and welding conditions

Base metal	Al-6063S-T5
Diameter of pipe (mm)	37.8
Thickness of pipe (mm)	2.0
Density (g/cm^3)	2.69
Melting point (^{o}C)	615-655
Thermal conductivity (W/m.K at 25°C)	209
Welding machine	AC
Electrode	2% Th-W ($\varnothing$ 2.4 mm)
Nominal arc length (mm)	1.5
Welding current, I (A)	50 ~ 70
Pulse current frequency, f (Hz)	50 ~ 100
EN ratio	0.5
Welding speed, v (cm/min)	12 ~ 20
Shielding gas	100% Ar
Shielding gas, q (l/min)	8 ~ 15

(a) Top view
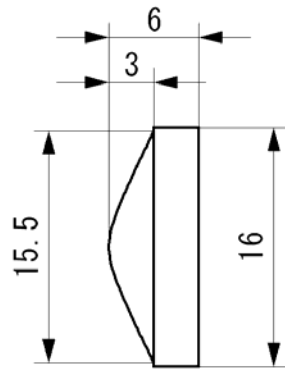
(b) Size of hyperboloidal mirror [mm]

Fig. 4.1 Hyperboloidal mirror
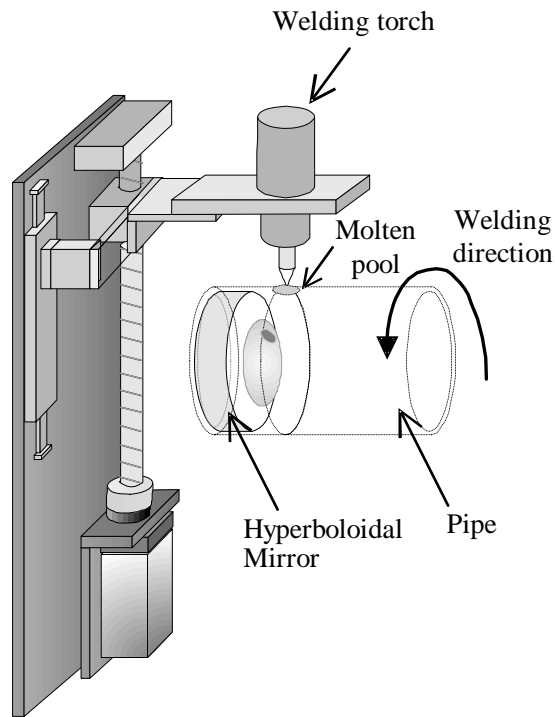
(a)　Schematic of monitoring
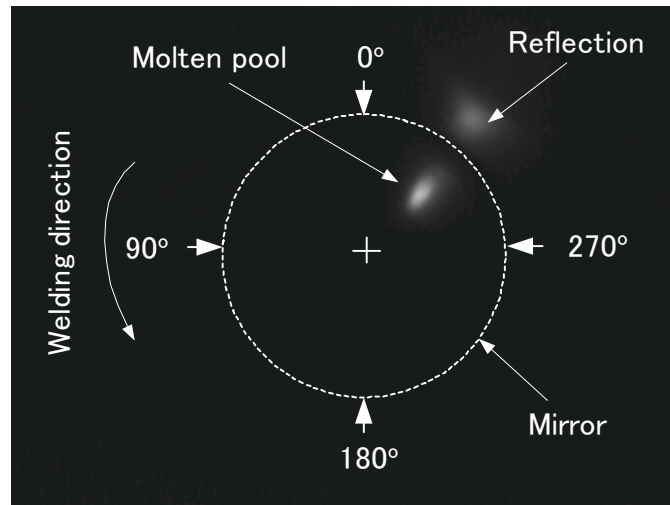
(b)   Example of original image of molten pool.

Fig. 4.2 Monitoring of molten pool

The schematic of monitoring and example result of original image of molten pool are shown in Fig. 4.2 (a) and (b), respectively. The detail geometry of the hyperbolic omnidirectional camera is shown in Fig. 4.2. Hyperboloidal mirror reflects the backside image of molten pool circumferentially to the CCD camera. Omnidirectional vision used in this research was developed from [89]. The origin of the coordinate system (x, y, z) is the center point of camera. An omnidirectional image on an image plane u–v is generated through the following process. First, a light ray goes ahead to the mirror focal point $Om(0, 0, 2C + D)$ from any object point $P(X,Y,Z)$ in the real-world. Next, a light ray is reflected toward a camera lens focal point $Oc(0, 0, D)$ from a mirror intersection point as shown in Fig. 4.4.
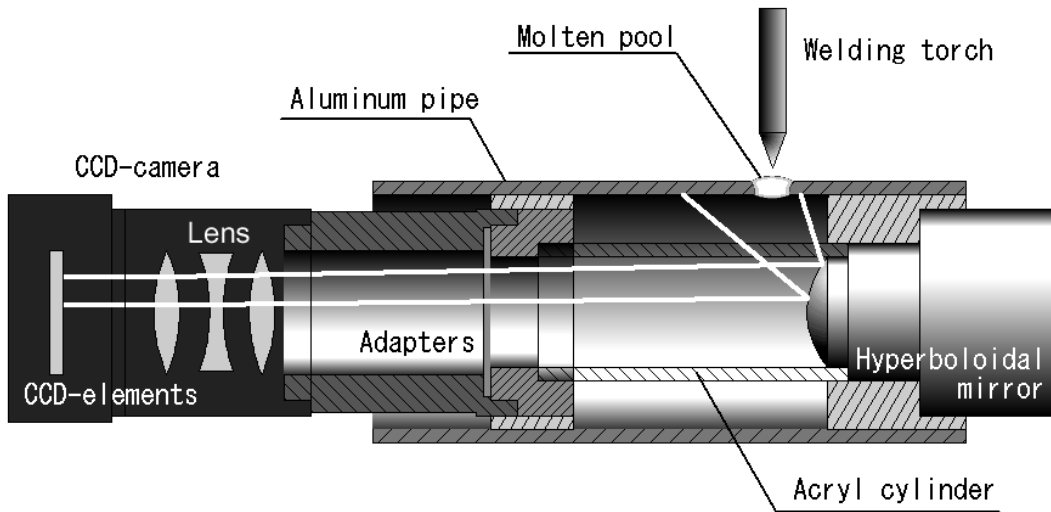
Fig. 4.3 Detail of monitoring system
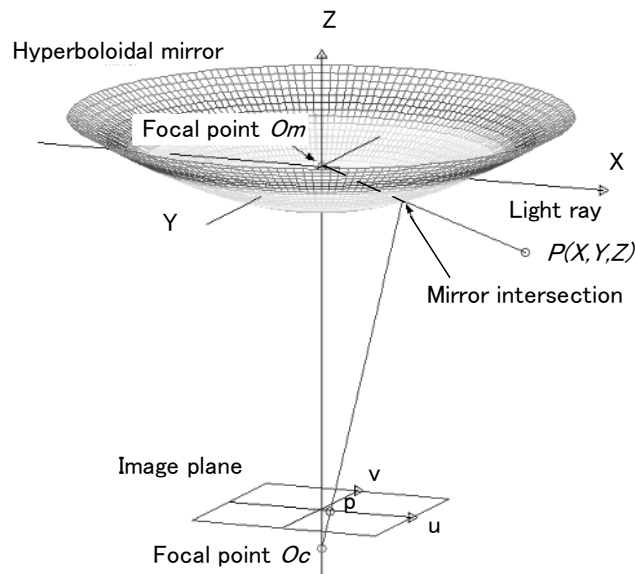
Fig. 4.4 Geometry of a hyperboloidal omnidirectional camera

The hyperboloidal equation of the proposed mirror is represented as:

$$\frac{X^2 + Y^2}{A^2} - \frac{\left(Z + \left(C + D\right)\right)}{B^2} = -1 \qquad (4.1)$$

where A and B are parameters of the hyperboloidal mirror shape, $C = \sqrt{X^2 + Y^2}$, and D is the distance between lens to a center point of the camera. The relationship

equation between an image coordinate $p(u, v)$ and a real-world three-dimensional position $P(X, Y, Z)$ is presented as follows:

$$\binom{u}{v} = \frac{f\left(B^2 - C^2\right)}{\left(B^2 + C^2\right)\left(Z - (2C + D)\right) - 2BC\sqrt{X^2 + Y^2\left(Z - (2C + D)\right)^2}} \binom{x}{y} \qquad (4.2)$$

where f is the focal length of a CCD camera. Relationship equations between Z and X, Z and Y in the image coordinate $p(u, v)$ are described as follows:

$$Z = \frac{-f\left(B^2 + C^2\right)2BC\sqrt{u^2 + v^2 + f^2}}{\left(C^2 - B^2\right)u} X + (2C + D) \qquad (4.3)$$

$$Z = \frac{-f\left(B^2 + C^2\right)2BC\sqrt{u^2 + v^2 + f^2}}{\left(C^2 - B^2\right)v} Y + (2C + D) \qquad (4.4)$$

For the proposed omnidirectional camera, $A = 1$, $B = 2$, $D = 16$ mm, $f = 1.6$ mm and the size of CCD is 6.59 mm × 4.94 mm.

4.3.2 Edge Detection of Molten Pool

Figure 4.5 presents the flowchart of image processing algorithm. Due to the low melting point of aluminum, brightness of molten pool is low; therefore the stable and robust image processing algorithm must be constructed. The detail of edge detection of molten pool will be discussed as follows.

(a) Histogram Analysis: First, the image of molten pool will be analyzed to get the histogram information. Compared to the stainless steel, the edge of molten pool in aluminum is very difficult to be detected. After the observation to find the exact position of molten pool and compared to the real back bead width, it is found that the edge of molten pool aligned between the edge detection range. This range defined as the range between inner and outer brightness as shown in Fig. 4.6 (a). In this study, the same method of [65] to find the edge was applied.

```
┌─────────────────────┐                    ┌─────────────────────┐
│  Molten pool image  │              ┌────▶│  Create set window  │
└──────────┬──────────┘              │     └──────────┬──────────┘
           ▼                         │                ▼
┌─────────────────────┐             │     ┌─────────────────────┐
│  Histogram analysis │             │     │     Set window      │
└──────────┬──────────┘             │     └──────────┬──────────┘
           ▼                         │                ▼
┌─────────────────────┐             │     ┌─────────────────────┐
│ Edge detection's    │             │     │  Vertical scanning  │
│ range               │             │     └──────────┬──────────┘
└──────────┬──────────┘             │                ▼
           ▼                         │     ┌─────────────────────┐
┌─────────────────────┐             │     │ Top and bottom edge │
│Panorama             │             │     └──────────┬──────────┘
│transformation       │             │                ▼
└──────────┬──────────┘             │     ┌─────────────────────┐
           ▼                         │     │Find the max width   │
┌─────────────────────┐             │     │of edge              │
│  Transformed image  │             │     └──────────┬──────────┘
└──────────┬──────────┘             │                ▼
           ▼                         │     ┌─────────────────────┐
┌─────────────────────┐             │     │ Width of molten pool│
│Find center of       │─────────────┘     └─────────────────────┘
│gravity              │
└─────────────────────┘
```
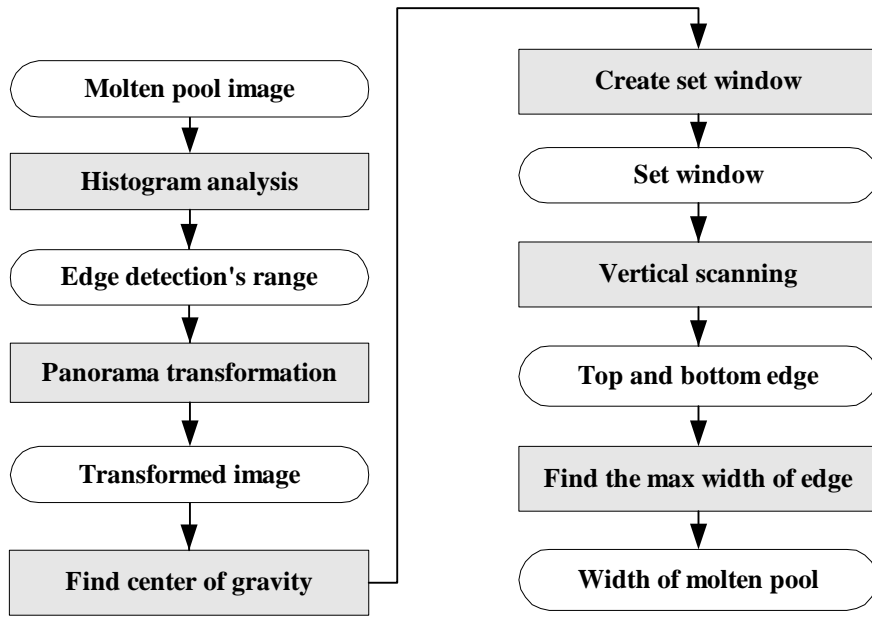
Fig. 4.5 Flowchart of image processing

(a) Illustration image of molten pool

69
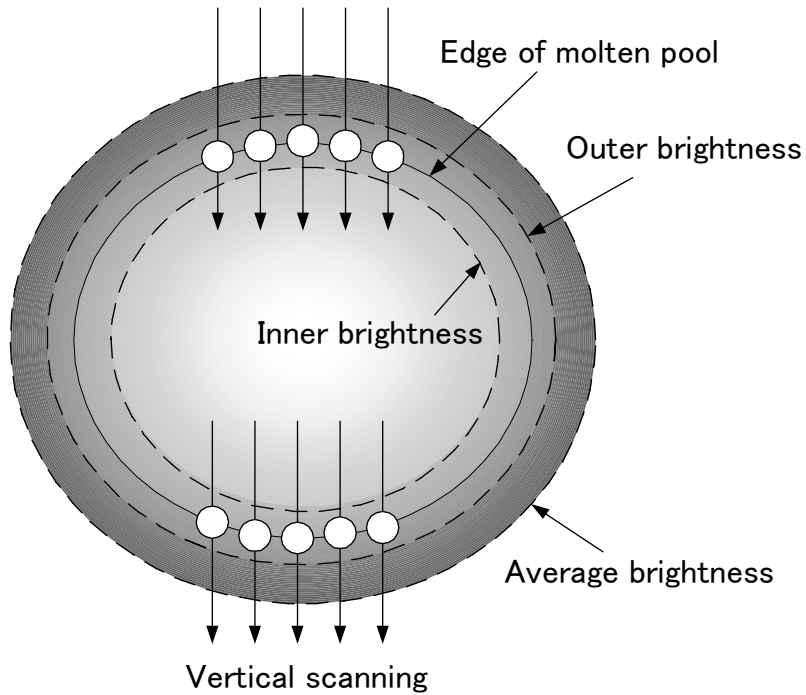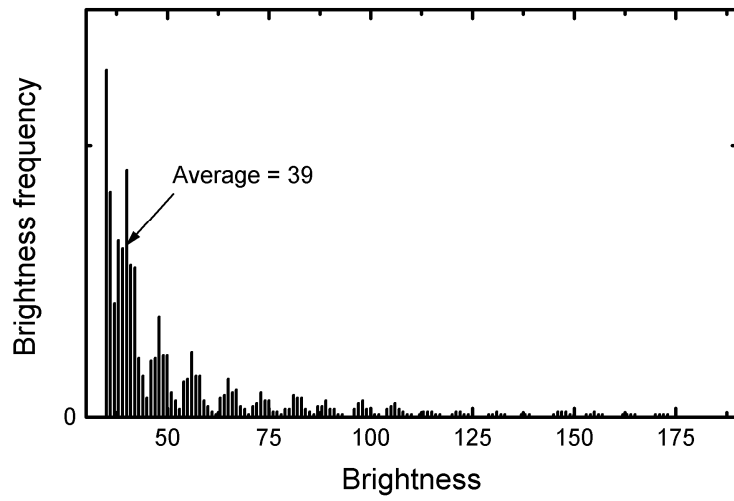
(b) Frequency of average brightness ($\theta=180°$)
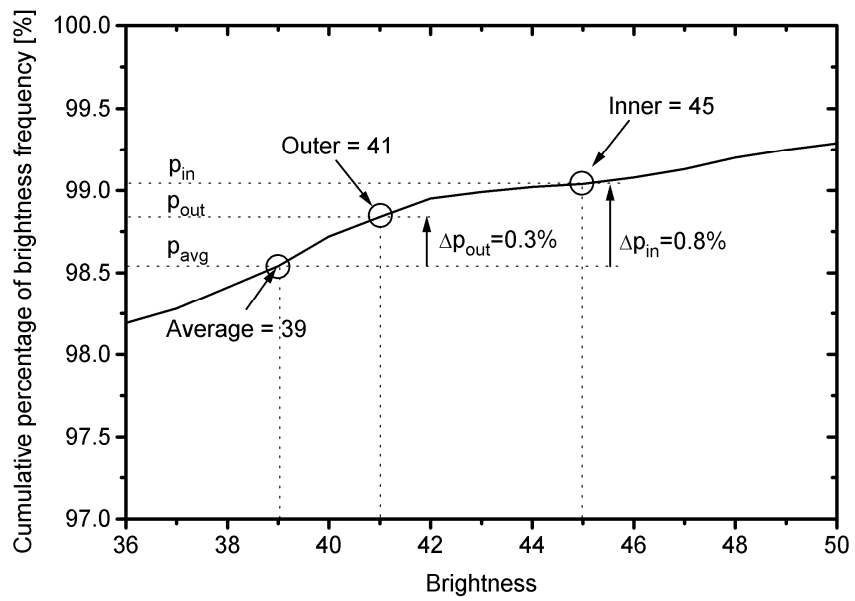
(c) Inner and outer brightness frequency ($\theta=180°$)
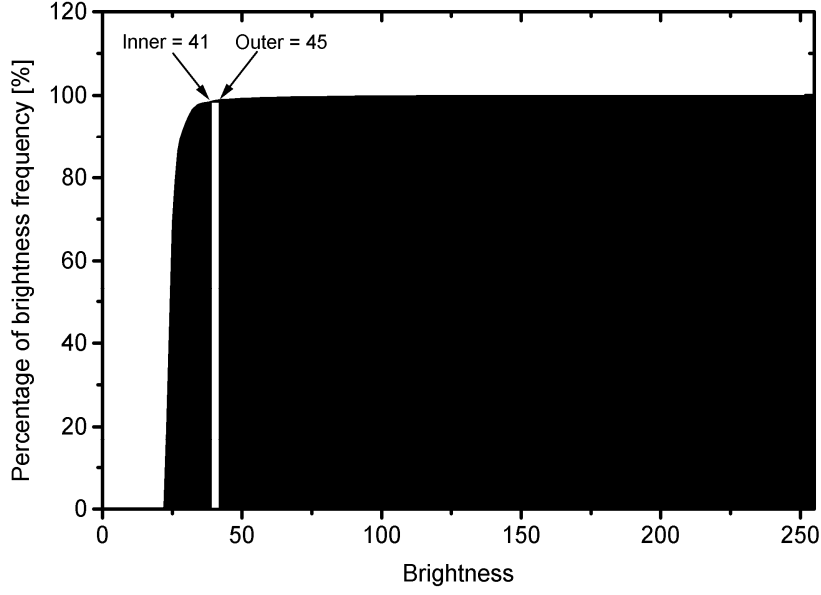
(d) Cumulative percentage of brightness (θ=180º)

Fig. 4.6 Histogram analysis for edge detection

From the histogram analysis, the frequency of brightness value of the image was obtained. The average brightness, g_{avg} and accumulation of the percentage of average brightness, p_{avg} were obtained by the Eqs. (4.5) and (4.6), respectively.

$$g_{avg} = \frac{\sum_{i=0}^{i=255}(f(i) \times i)}{\sum_{i=0}^{i=255} i} \tag{4.5}$$

$$p_{avg} = \frac{\sum_{i=0}^{i=avg} f(i)}{\sum_{i=0}^{i=255} f(i)} \times 100\% \tag{4.6}$$

where $f(i)$ is the frequency of brightness at i.

Figure 4.6 (b) presents the location of brightness average in brightness frequency. Unlike the previous method which applied some rule to obtain the percentage of top threshold or outer brightness, p_{out} and bottom threshold or inner brightness, p_{in} [65], the new method directly add the constant into the value of those percentages, which are defined as:

$$p_{out} = p_{avg} + \Delta p_{out}(\%) \tag{4.7}$$

$$p_{in} = p_{avg} + \Delta p_{in}(\%) \tag{4.8}$$

71

In this experiment as shown in Fig. 4.6 (c), the value of Δp_{out} and Δp_{in} are 0.3% and 0.8%, respectively. Then the value of outer brightness, g_{out} = 45 and outer brightness, g_{in} = 41 can be obtained as shown in Fig. 4.6 (d).

(a) Original image
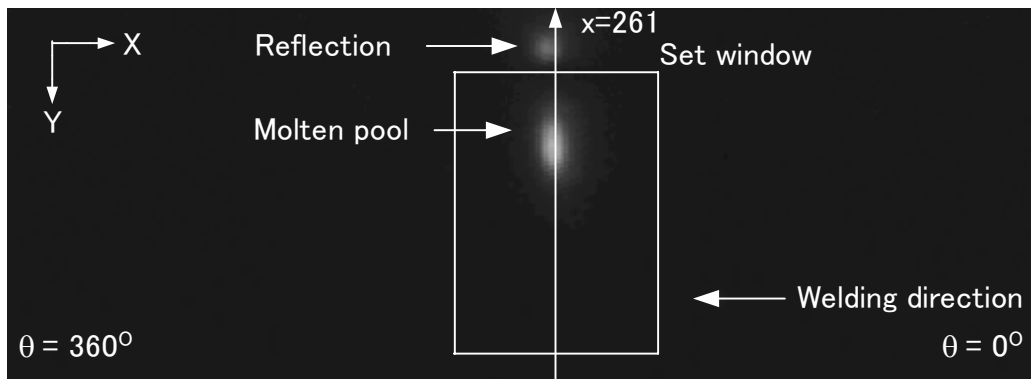
(b) Panorama transformed image
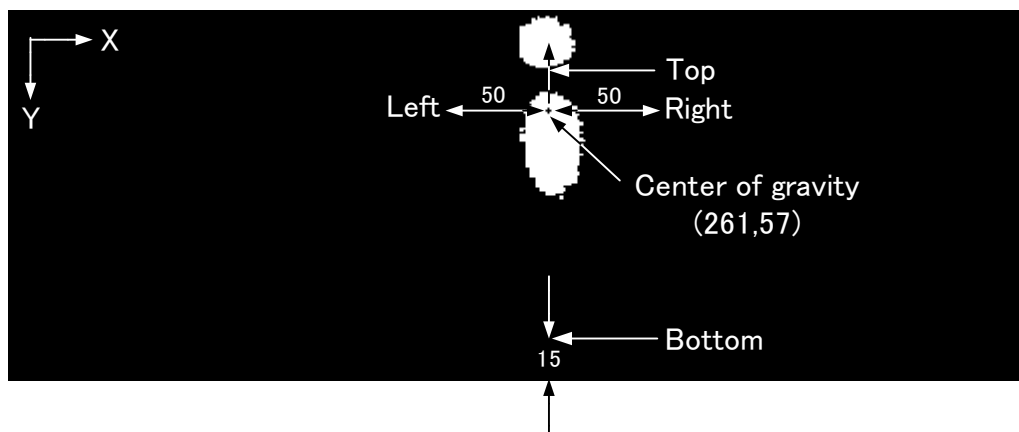
(c) Detection of set window from center of gravity after binarization at brightness of 40
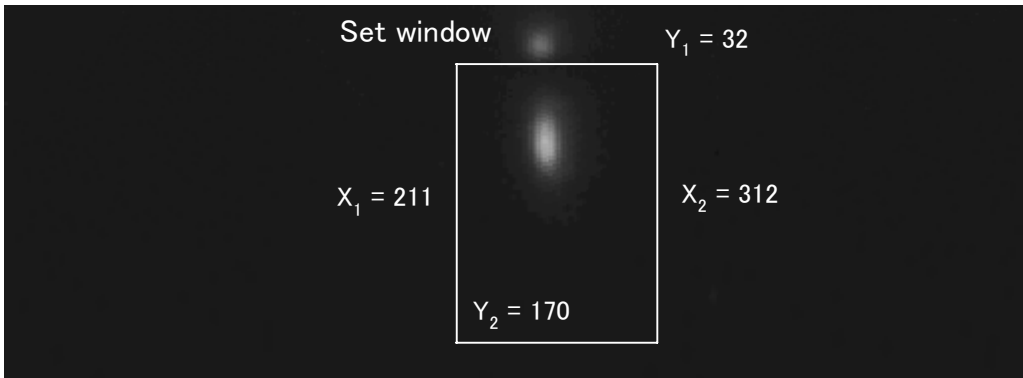
(d) Set window at θ = 180°
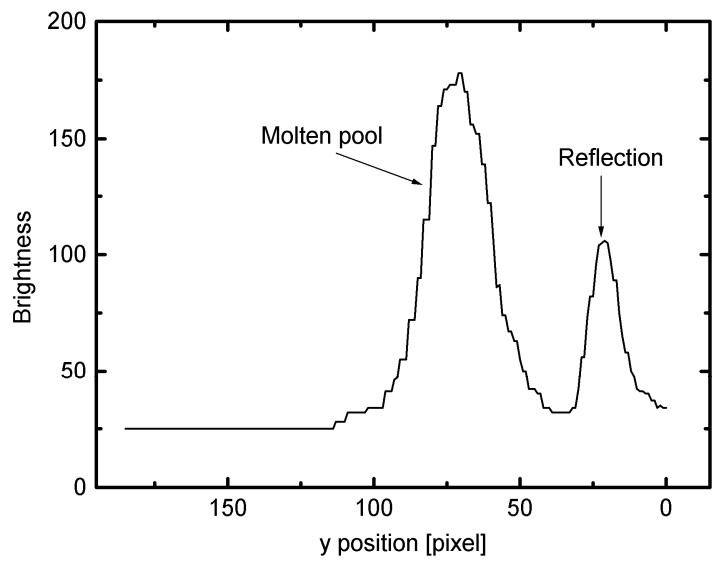
(e) Brightness at x=261
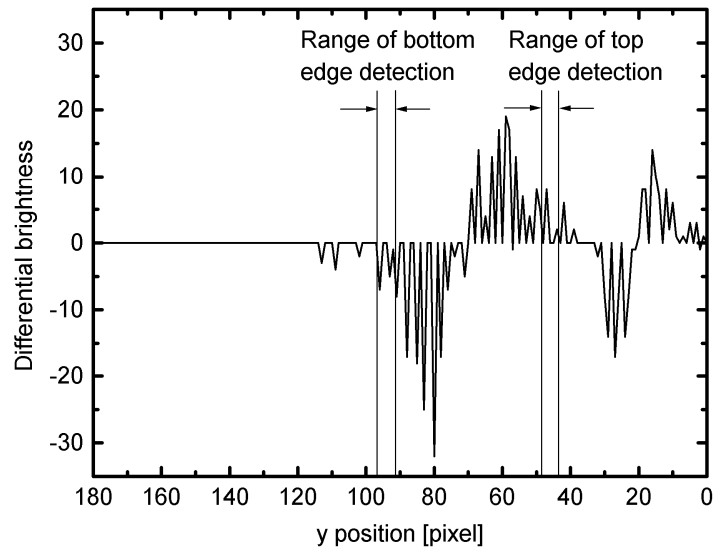
(f) Differential brightness at x=261
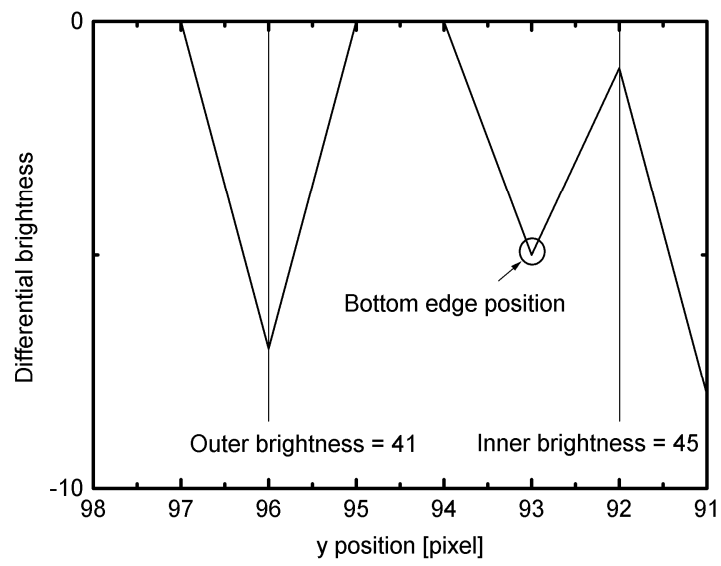
(g) Bottom edge position
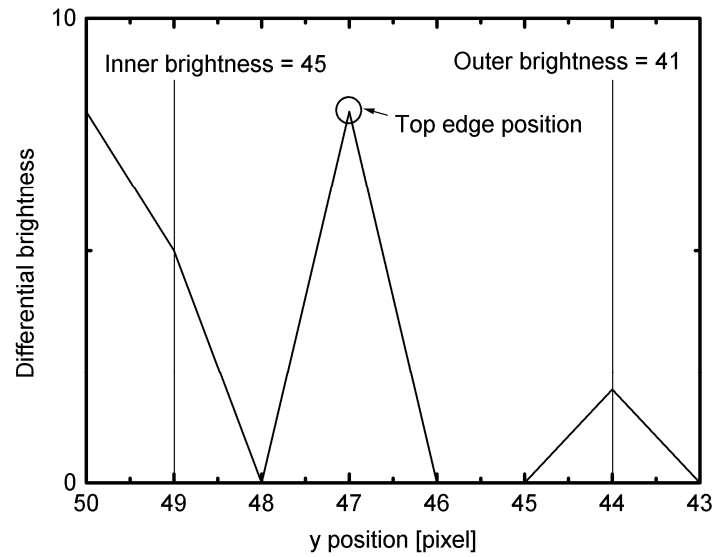
(h) Top edge position
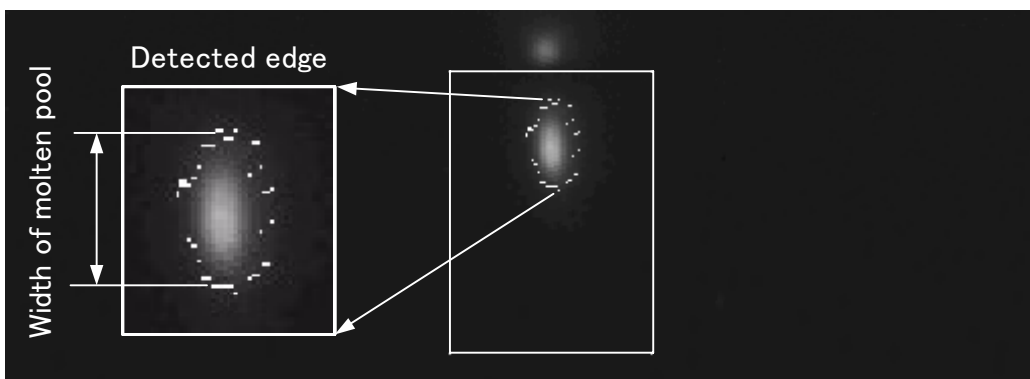
(i) Detected edge and width of molten pool

Fig. 4.7 Edge detection of molten pool

(b) Panorama Transformation: Figure 4.7 (a) shows the omnivision image of molten pool. Every image will be transformed into panorama transformed image using Eqs (4.1) – (4.4) as shown in Fig. 4.7 (b).

(c) Set Window: After finding the center of gravity, set window was created automatically to locate the scanning area and reduce the time of edge detection as shown in Fig. 4.7 (c). The set window was created from the points of left, right, top and bottom as shown in Fig. 4.7 (d). Maximum size of set window was 150 x 100 pixels.

(d) Top and Bottom Edge Detection: From the panorama transformed image inside set window, the vertical scanning was performed to find top and bottom edge detection as shown in Fig. 4.7 (b). Figure 4.7 (e) shows the brightness frequency at x = 261. It is shown that there are two peaks of brightness distribution which are molten pool and its reflection.

Edge detection was performed on the differential value of brightness along vertical axis $g'(i,j)$:

$$g'(i, j) = g(i, j+1) - g(i, j) \tag{4.9}$$

where $g(i,j)$ is the brightness value of a pixel at (i,j) as shown in Fig. 4.7 (f). Edge position was determined within this range of searching. By applying the inner brightness and outer brightness, the bottom edge position can be detected by finding the minimum position within the range as shown in Fig. 4.7 (g). In contrary, the top edge position was detected from maximum position within the range as shown in Fig. 4.7 (h). This process was repeated along x position inside the set window.

(d) Width Detection: In order to find the width of molten pool, the scanning of widest value of top and bottom edges was conducted. Figure 4.7 (i) shows the detected edge and width of molten pool.
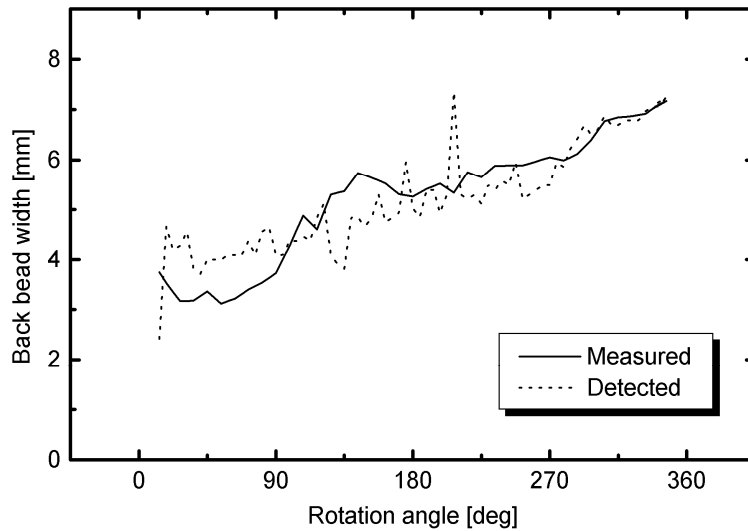
Fig. 4.8 Comparison result of measured back bead width and detected molten pool

4.3.3 Result of Image Processing Algorithm

Figure 4.8 shows the comparison of measured back bead width and detected molten pool width using proposed image processing algorithm in preliminary experiment without control. Image resolution is 0.093 mm/pixel. It is clearly seen that image processing algorithm could detect the molten pool width with good approximation. However, some errors still occur during the monitoring process with the average error is 0.0 mm and standard deviation is 0.4 mm. The cause of the errors might come from the detected inner and outer threshold brightness as the range for scanning the edge of molten pool. Another reason of this error came from the error of the measurement of back bead width.

Although the image processing algorithm had some errors, edge detection using panorama transformation from omnivision image were considered as the good approach. With this result, the algorithm is appropriate to the real time monitoring of the welding process.

4.4 Experiment with Control

Welding process was conducted autogenously for $360°$ of circumference and in fixed position of pipe. In constant welding current of 60 A, the torch started to initiate the arc until the initial penetration was produced. The experiment with control was conducted using fuzzy inference system as control system [66-68]. The output of the image processing which is the width of molten pool, w will become the input of fuzzy control. The output of fuzzy control is the correction of welding speed. After adjusting

the welding speed, motor waits for several millisecond to make sure the CCD camera capture the molten pool image. All of the processes will be repeated until the rotation angle reaches $360°$. Finally, the program commands to stop the motor and the welding arc will stop.

In this step, the proposed fuzzy control took two variables to be fuzzified. One was an error (e_n), which was the difference of back bead width (w_n) at the concerned time step (n) from the reference back bead width (w_r):

$$e_n = w_r - w_n \tag{4.10}$$

and w_r was set at 5 mm.

The other was the change of an error defined as:

$$\Delta e_{n+1} = w_{n+1} - w_n \tag{4.11}$$

Three kind of membership (N – Negative, Z – Zero, P – Positive) and triangular membership functions were used to fuzzify the inputs. Figure 4.9 (a), (b) and (c) show the membership functions and ranges for each fuzzy variable. The decision table for the fuzzy control of welding speed is shown in Fig. 4.9 (d).

(a) Input: back bead width
error, e [mm]

(b) Input: back bead width
error deviation, Δe [mm]

(c) Output: welding speed
correction, Δv [cm/min]

(d) Decision table

Δe \ e	N	Z	P
N	N	N	Z
Z	N	Z	P
P	Z	P	P
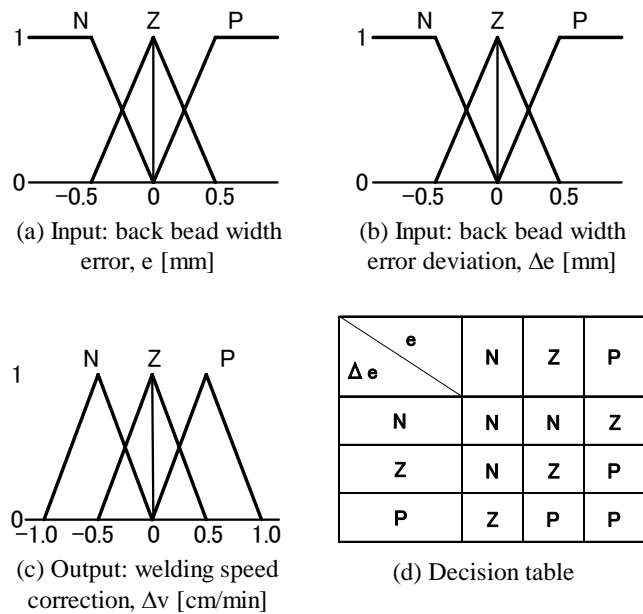
Fig. 4.9 Fuzzy sets and decision table for fuzzy control of welding speed
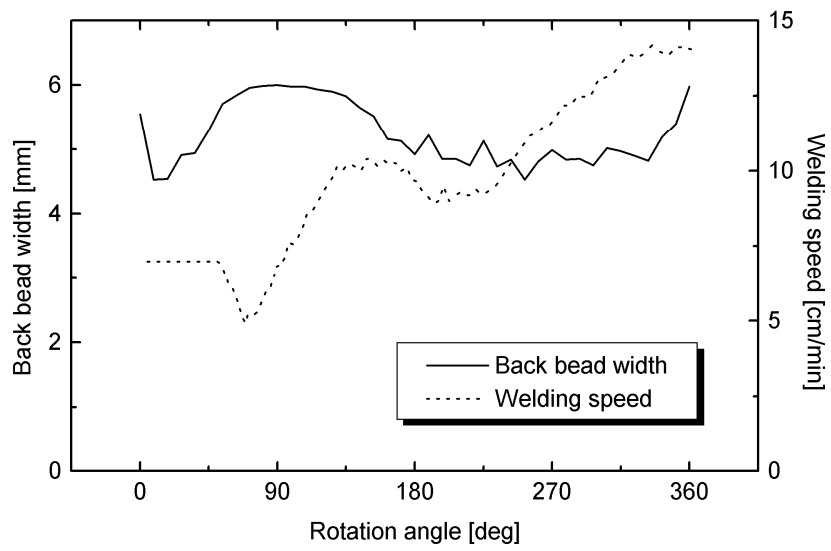
(a) Back bead width and welding speed
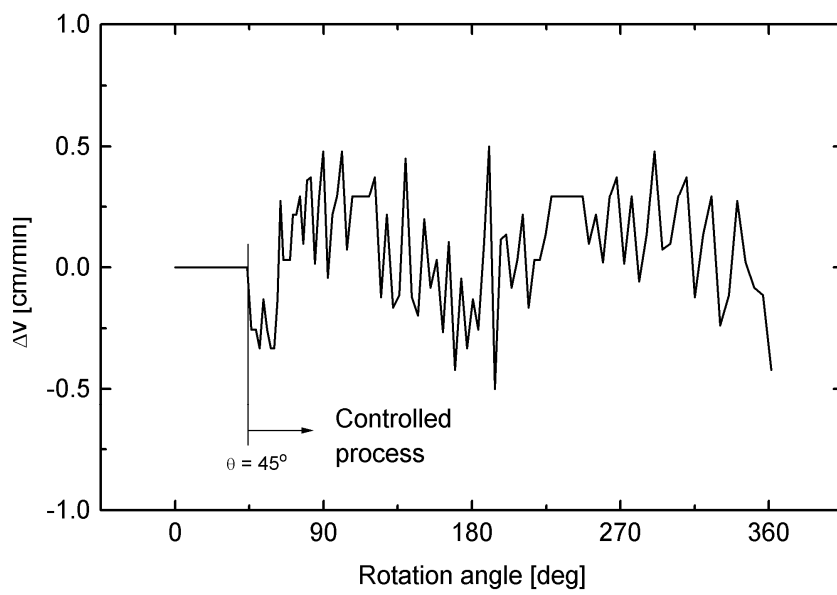
(b) Correction of welding speed

78
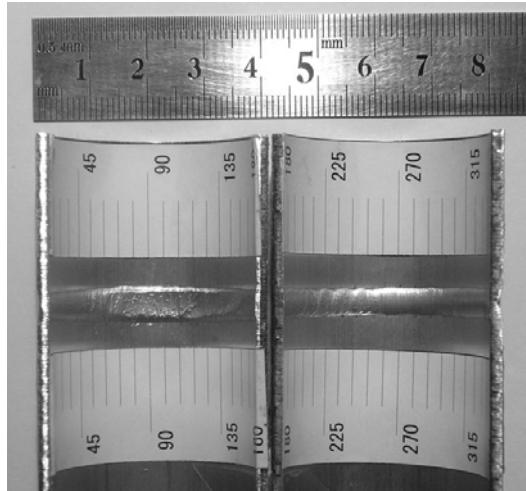
(c) Back bead appearance

Fig. 4.10 Result of experiment with control

4.5 Results and Discussion

In control experiment, to produce stable arc condition, the welding speed of 7 cm/min at $\theta = 0^o – 45^o$ was kept constant. Figure 4.10 (a) shows the experiment result of back bead width and welding speed using fuzzy controller. Figure 4.10 (b) presents that fuzzy control determined the correction of welding speed to keep the back bead width in the target range of 5 ± 1 mm. The result of experiment with control yields the average error, root mean square error (RMSE), and standard deviation are -0.3 mm, 0.3 mm is 0.5 mm, respectively. At $\theta = 45^o – 135^o$, the welding speed increased from $5 – 10$ cm/min and the back bead width increased.

However, by maintaining and increasing the welding speed until 14 cm/min, the back bead width was kept to 5 mm at $\theta = 180^o$. Accordingly, by proper control of welding speed, it will produce excellent back bead width. The experiment result shows that the bead was smooth in appearance and there was no crack, porosity, undercut and burn through along the circumference as shown in Fig. 4.10 (c). The back bead width also aligned in the range target of $4 – 6$ mm. In this study, the welding condition was changed during the welding proceeded along the circumference of the pipe. However, the suitable welding condition for producing the good result was obtained at welding current, I = 60 A, pulsed current frequency, f = 50 Hz, minimum welding speed, v_{min} = 7 cm/min, and maximum welding speed, v_{max} = 15 cm/min. In general, the proposed automatic welding system produced sound weld of aluminum pipes by monitoring backside image of molten pool using omnidirectional camera.

79

4.6 Conclusions

The conclusions of this chapter are summarized as follows.

1. Welding penetration control of aluminum pipes using omnidirectional camera was constructed.

2. An algorithm to obtain to detect edge of molten pool from panorama image of molten pool was proposed. As a result of the experiment using fuzzy inference system, the effectiveness of the control system was confirmed.

Particle Swarm Optimization (PSO) and Genetic Algorithm (GA) Optimization of Edge Detection of Molten Pool in Fixed Pipe Welding

5.1 Introduction

Advanced welding technology offers the reduced manufacturing cost, however its use requires a means of sensing and monitoring of error of the workpiece. Tungsten Inert Gas (TIG) welding is one of the frequently used. In welding fixed pipe, to obtain the uniform weld bead over the entire circumference of the pipe, the welding conditions should be controlled as the welding proceeds.

The difficulty to control arc welding process is how to detect weld pool geometrical features, such as weld bead width and penetration in real-time. The previous researches using the welding system with plain mirror to reflect the backside image of molten pool have been successfully conducted to weld stainless steel pipes [45], and to aluminum pipes [57-68]. In this study we propose new method using omnidirectional vision-based molten pool monitoring. The monitoring system was constructed by hyperboloidal mirror and CCD camera. However, compared to the detected stainless steel's image, image of aluminum molten pool has very low brightness. Therefore, new technique of optimization in detecting edge of molten pool was proposed in this research.

Particle Swarm Optimization (PSO) and Genetic Algorithm (GA) are two kinds of widely used optimization method in evolutionary computation (EC). PSO [90-93] is a population-based search algorithm and is initialized with a population of random solution, called particles. Unlike the other evolutionary computation techniques, each particle in PSO is also associated with a velocity which is dynamically adjusted according to the flying experience of its own and its companions. Therefore, a population of particles is updated on a basis of information about each particles previous best performance and the best particle in the population [94]. A lot of research results have been reported in the literature [90-92]. The genetic algorithm (GA) is an optimization and search technique based on the principles of genetics and natural selection. A GA allows a population composed of many individuals to evolve under specified selection rules to a state that maximizes the "fitness" (i.e., minimizes the cost function) [94-95]. GA combined with neural network trained with convective heat flow calculations is used to adapt GTAW geometry. Good agreement between the model predictions and the experimental data of weld pool penetration and width for various welding conditions shows that the approach is promising [96]. Other application of GA to optimize welding parameters was investigated. A welding economic design has been developed to recognize welding quality at different ranges of welding parameters at minimum cost. This approach integrates neural network and GA to study the welding economic design as a mathematical model [97].

In this experiment, automatic welding system of fixed aluminum alloy pipe A6063S-T5 using omnidirectional vision-based molten pool monitoring was conducted. New image processing algorithm was developed by transforming the original image of molten pool into panorama image. In application of the edge detection of molten pool, a method for determining brightness range values for edge detection using PSO or GA was proposed. This new search method could reduce the computational cost and error of detection. The constant current of TIG welding process was used in the controlled welding speed using fuzzy inference system derived from the back bead width of molten pool image.

5.2 Edge Detection of Molten Pool

The experimental device, which was used in this experiment, is same as in Section 2.2. The material properties and welding conditions used are given in Table 5.1.

82

5.2.1 Monitoring of Molten Pool

In order to capture the backside molten pool image, a hyperboloidal mirror was used for acquisition of reflected image. The schematic of monitoring system is shown in Fig. 5.1 (a). The hyperboloidal mirror reflected the molten pool image into the CCD camera as shown in Fig. 5.1 (b). Figure 5.1 (c) presents the result after transformation process into panorama image using proposed equation in [87]. According to the low brightness of aluminum's molten pool due to the low melting point, the stable and robust image processing algorithm must be constructed. The focus of the optimization was in the histogram analysis process.

Table 5.1 Material properties and welding conditions

Base metal	Al-6063S-T5
Diameter of pipe (mm)	37.8
Thickness of pipe (mm)	2.0
Density (g/cm^3)	2.69
Melting point (^{o}C)	615-655
Thermal conductivity (W/m.K at 25°C)	209
Welding machine	AC
Electrode	2% Th-W ($\varnothing$ 2.4 mm)
Nominal arc length (mm)	1.5
Welding current, I (A)	50 ~ 70
Welding speed, v (cm/min)	7 ~ 25
Shielding gas	100% Ar
Shielding gas, q (l/min)	8 ~ 15

In the histogram analysis process, the brightness average (g_{avg}) and accumulation of the percentage of brightness average (p_{avg}) were obtained by the Eq. (5.1) and (5.2), respectively [45].

$$g_{avg} = \frac{\sum_{i=0}^{i=255}(f(i) \times i)}{\sum_{i=0}^{i=255} i} \tag{5.1}$$

$$p_{avg} = \frac{\sum_{i=0}^{i=avg} f(i)}{\sum_{i=0}^{i=255} f(i)} \times 100\% \tag{5.2}$$

where:

$f(i)$ = the frequency of brightness at i.

By adding the percentage at brightness average (p_{avg}) with some values which are difference percentage of outer brightness (Δp_{out}) and difference percentage of inner brightness (Δp_{in}), the value of percentage of outer brightness (p_{out}) and inner brightness (p_{in}) could be determined as shown in Eq. (5.3) and (5.4), respectively.

$$p_{out} = p_{avg} + \Delta p_{out} \tag{5.3}$$

$$p_{in} = p_{avg} + \Delta p_{in} \tag{5.4}$$
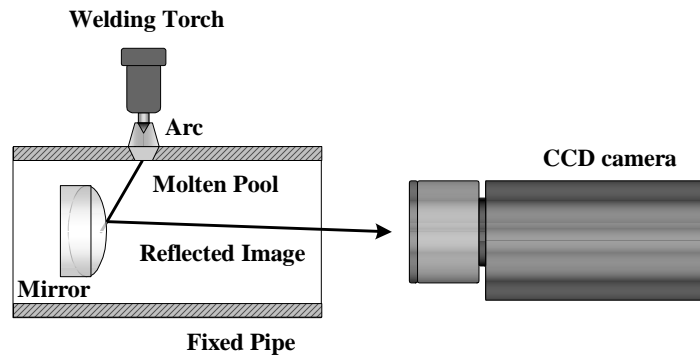
(a) Schematic of monitoring.
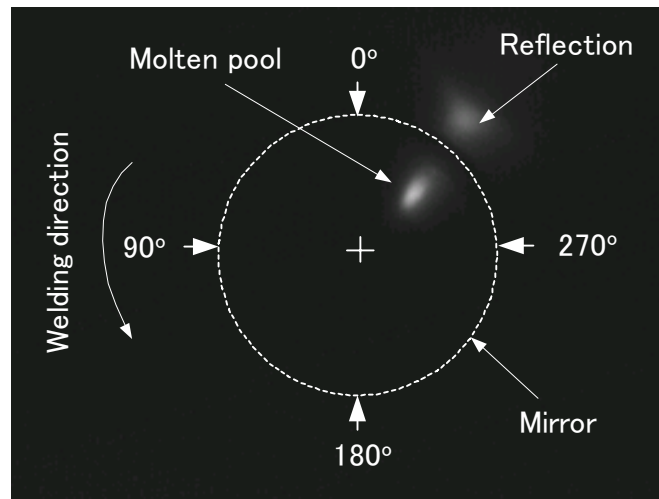
(b) Example of original image of molten pool.
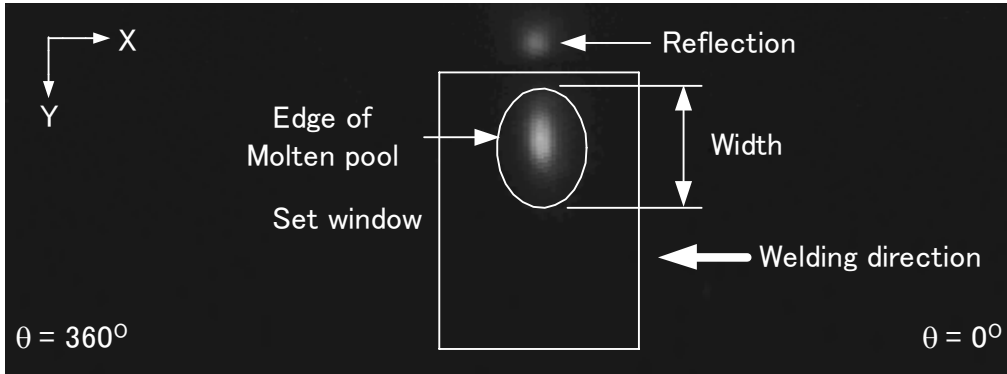
(c) Panorama image of molten pool.

Fig. 5.1 Monitoring of molten pool

Figure 5.2 (a) illustrates the image of molten pool. The edge of molten pool aligns between the outer and inner brightness. The cumulative percentage of brightness frequency is shown in Fig. 5.2 (b). From Eq. (5.3) and (5.4), we can find the outer brightness (g_{out}) and inner brightness (g_{in}) as shown in Fig. 5.2 (c). The range between g_{out} and g_{in} defined as brightness range for determining edge of molten pool. To detect the edge of molten pool, the set window as shown in Fig. 5.1 (c) was constructed automatically. Then, vertical scanning in this set window was performed to find the edge. In this study, the values of p_{out} and p_{in} were optimized using PSO and GA to find the minimum error of detected width.

5.3 Particle Swarm Optimization

PSO was developed by Edward and Kennedy in 1995 [90]. The process behind the algorithm was inspired by the social behavior of animals, such as bird flocking or fish schooling. PSO is similar to the continuous GA in that it begins with a random population matrix. However, unlike the GA, PSO has no evolution operators such as crossover and mutation. The rows in the matrix are called particles that contain the variable values and are not binary encoded. Each particle moves about the cost surface with a velocity. The particles update their velocities and positions based on the local and global best solutions [94]:

$$v_{m,n}^{new} = \omega \times v_{m,n}^{old} + \Gamma_1 \times r_1 \times \left(p_{m,n}^{local\,best} - p_{m,n}^{old} \right) + \\ \Gamma_2 \times r_2 \times \left(p_{m,n}^{global\,best} - p_{m,n}^{old} \right) \tag{5.5}$$

$$p_{m,n}^{new} = p_{m,n}^{old} + v_{m,n}^{new} \tag{5.6}$$

where

$v_{m,n}$ = particle velocity

ω = inertia weight

$p_{m,n}$ = particle variables

r_1, r_2 = independent uniform random numbers

$\Gamma_1 = \Gamma_2$ = learning factors

$p_{m,n}^{local\,best}$ = best local solution

$p_{m,n}^{global\,best}$ = best global solution

The algorithm updates the velocity vector for each particle then adds that velocity to the particle position or values. Velocity updates are influenced by both the best global solution associated with the lowest cost ever found by a particle and the best local solution associated with the lowest cost in the present population. If the best local solution has a cost less than the cost of the current global solution, then the best local solution replaces the best global solution. The particle velocity is reminiscent of local minimizers that use derivative information, because velocity is the derivative of position. The constant Γ_1 and Γ_2 is called the cognitive parameter and the social parameter, respectively. The advantages of PSO are that it is easy to implement and there are few parameters to adjust [94].
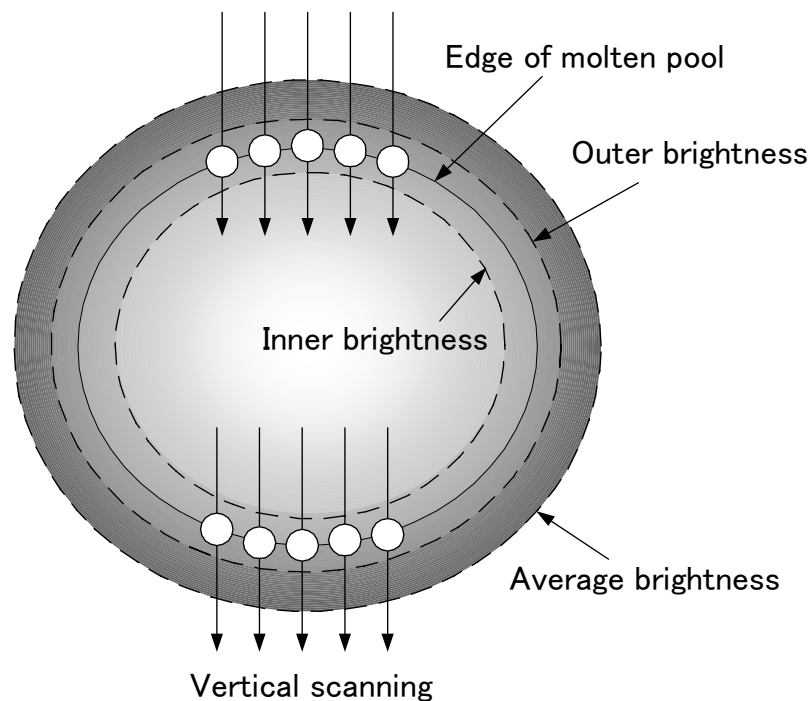
(a) Illustration image of molten pool
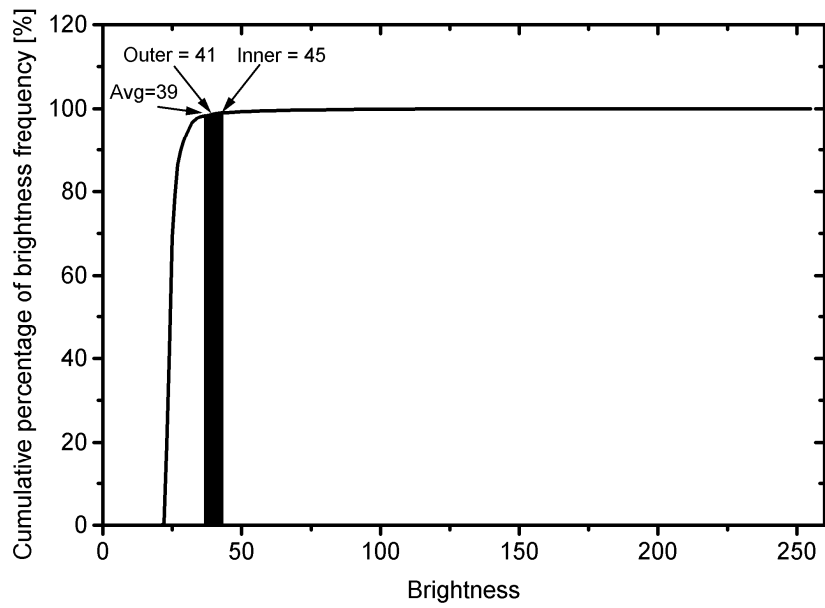
(b) Cumulative percentage of brightness frequency (θ=180°)
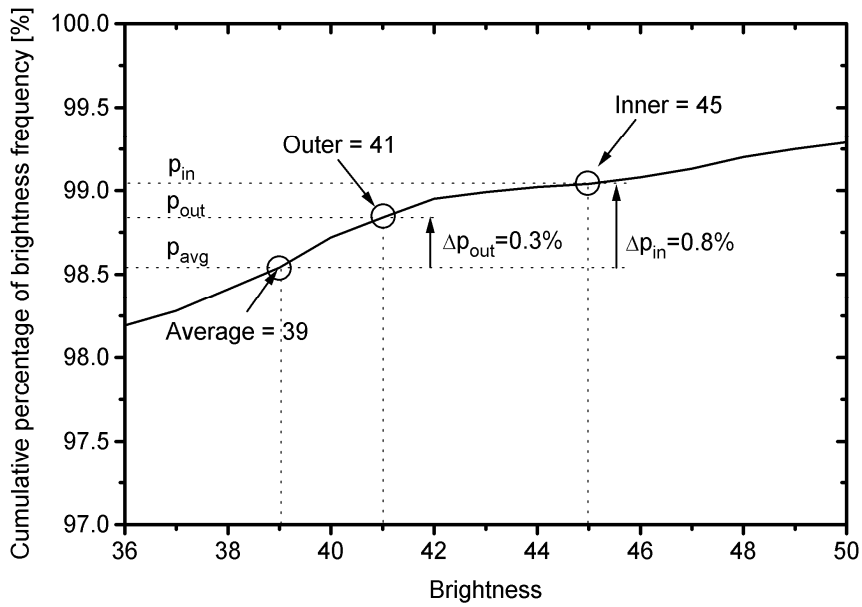
(c) Inner and outer brightness (θ=180°)

Fig. 5.2 Histogram analysis for edge detection

```
                    ┌─────────────────────────┐
                    │    Molten pool image     │
                    └─────────────────────────┘
                                 │
                                 ▼
                    ┌─────────────────────────┐
                    │    Histogram analysis    │
                    └─────────────────────────┘
                                 │
        ┌ ─ ─ ─ ─ ─ ─ ─ ─ ─ ─ ─ ┼ ─ ─ ─ ─ ─ ─ ─ ─ ─ ─ ┐
          PSO/GA                 ▼
        │           ┌─────────────────────────┐        │
                    │ Initialization of a      │
        │           │       population         │        │
                    └─────────────────────────┘
        │                        │                      │
                                 ▼
        │           ┌─────────────────────────┐        │
                    │     Fitness function     │
        │           └─────────────────────────┘        │
                                 │
        │                        ▼                      │
                    ┌─────────────────────────┐
        │           │ Updating new population  │        │
                    └─────────────────────────┘
        │                        │                      │
                                 ▼          No
        │                   ◇ Satisfy ◇ ──────────────►│
        │                        │                      │
                                 │ Yes
        └ ─ ─ ─ ─ ─ ─ ─ ─ ─ ─ ─ ┼ ─ ─ ─ ─ ─ ─ ─ ─ ─ ─ ┘
                                 ▼
                    ┌─────────────────────────┐
                    │    Find inner and outer  │
                    │        percentage        │
                    └─────────────────────────┘
                                 │
                                 ▼
                    ┌─────────────────────────┐
                    │      Edge detection      │
                    └─────────────────────────┘
```
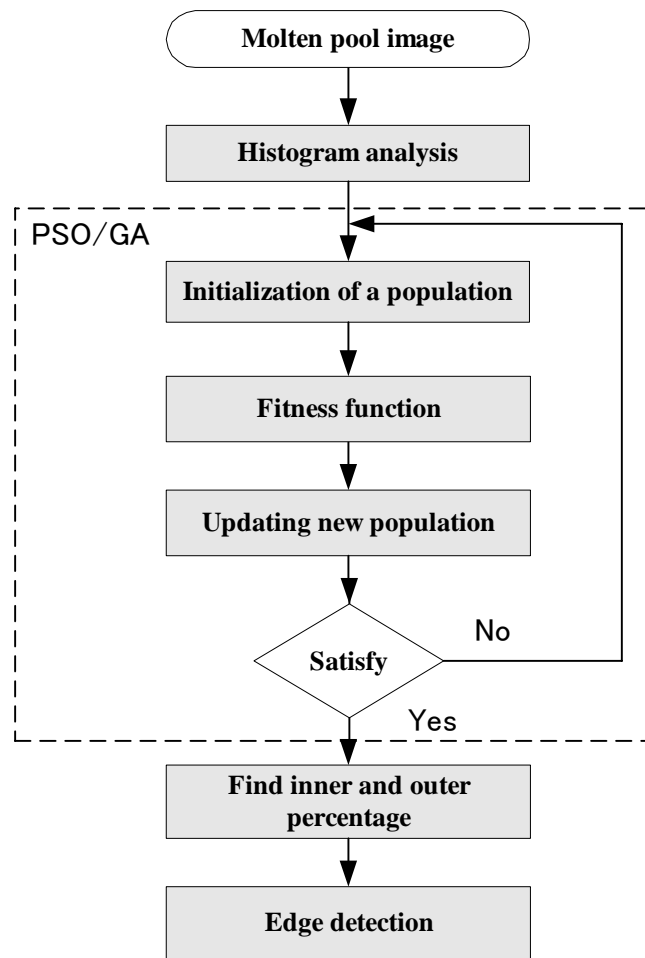
Fig. 5.3 Flowchart of edge detection of molten pool using PSO and GA

5.4 Genetic Algorithm

The genetic algorithm (GA) is an optimization and search technique based on the principles of genetics and natural selection. The method was developed by John Holland over the course of the 1960s and 1970s and finally popularized by one of his students, David Goldberg, who was able to solve a difficult problem involving the control of gas-pipeline transmission for his dissertation. GA encodes the decision variables (or input parameters) of the underlying problem into (solution) strings. Each string, called individual or chromosome, represents a candidate solution. Characters of the string are called genes. A fitness function is needed for differentiating between good and bad solutions. The fitness function of GA may be presented in a mathematical term, or as a complex computer simulation. Fitness generates a differential signal in accordance

which GA guides the evolution of solution to the problem. Three basic genetic operators, selection, crossover, and mutation, are applied to generate new individuals. The strength of GA is the exploration of different regions of the solution space simultaneously, which makes them perform well when considering large search spaces [94-95].

The GA simulates the continuous model of the generation, which eliminates and generates a few individuals in a generation (iteration). A candidate solution (individual) is composed of numerical parameters of the cumulative percentage of brightness frequency. In this study, we use the percentage outer brightness (p_{out}) and inner brightness (p_{in}).

5.5 Edge Detection

In order to apply PSO or GA for edge detection, each particle in PSO or GA represents the percentage outer (p_{out}) and inner brightness (p_{in}). The fitness function cost is defined as error of edge detection is calculated by the following equation,

$$f = \left\| \left(1 - \frac{w_c}{w_t}\right) \times 100\% \right\| \tag{5.7}$$

where w_c and w_t are the computed width and corresponding target of width, respectively. Therefore, the problem result is the minimization problem. The dimensional search space for PSO or GA was limited to the percentage of brightness from 90% to 100% which the value of brightness values of 25 – 255 were aligned. As shown in Fig. 5.3, based on their fitness, agents in population guided by position and speed of PSO or Eq. (5.5) and (5.6) and guided by genetic operators of GA. New p_{out} and p_{in} generated by PSO or GA. The algorithm was stopped when satisfied by two conditions: 1) Minimum error of edge detection – the detection value of the best agent was below the given threshold (1×10^{-3}%), or 2) the maximum iteration number was reached.

The experiment condition for optimization:

- Original image size is 256 x 220 pixels
- Panorama image size is 512 x 186 pixels
- Maximum set window size is150 x 100 pixels

PSO condition:

- $\Gamma_1 = \Gamma_2$ = learning factors = 2

GA condition:

- Crossover operator is single point crossover

- Mutation rate is 0.15

- Fraction of the population is 0.5

| Pop = 4, err = 6.69% | Pop = 8, err = 4.68% | Pop = 16, err = 3.38% |

(a) Particle swarm optimization

| Pop = 8, err = 6.69% | Pop = 16, err = 4.68% | Pop = 36, err = 3.38% |
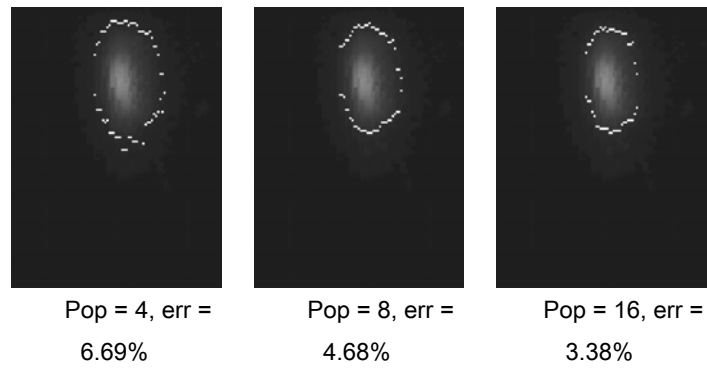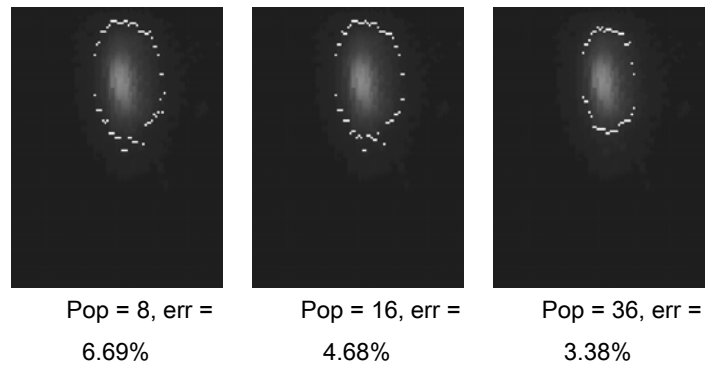
(b) Genetic algorithm

Fig. 5.4 Edge detection of molten pool in set window using PSO and GA at $\theta = 270^{o}$ and 10 iterations

Pop = 4, err = 4.33%	Pop = 12, err = 2.86%	Pop = 16, err = 0.74%

(a) Particle swarm optimization

Pop = 4, err = 16.92%	Pop = 12, err = 15.13%	Pop = 16, err = 7.93%
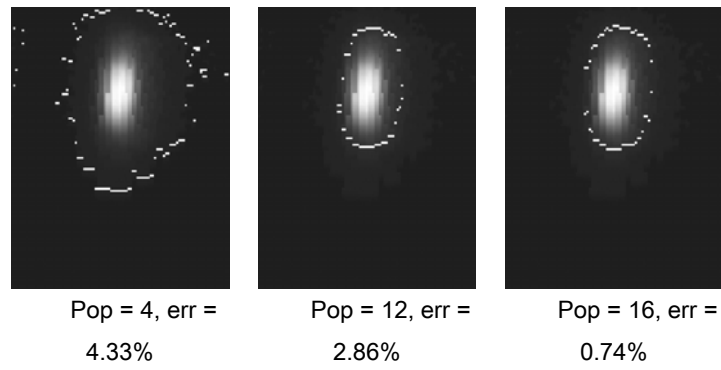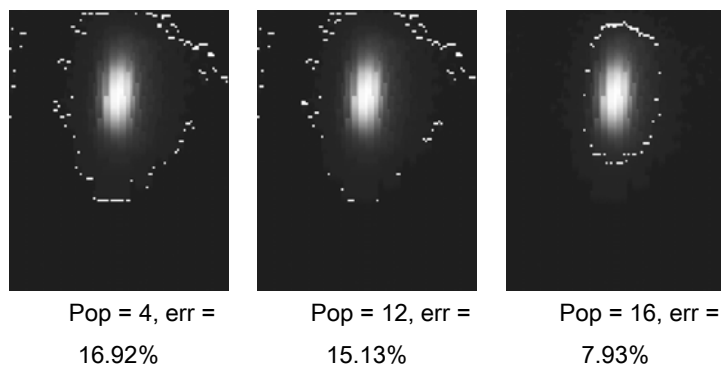
(b) Genetic algorithm

Fig. 5.5 Edge detection of molten pool in set window using PSO and GA at $\theta = 90^o$ and 20 iterations

Figure 5.4 shows the comparison of experiment results using PSO and GA at $\theta = 270^o$ and 10 iterations. Both PSO and GA can determine low error of detection. However, GA needs higher population to get the same error as in PSO. The same results also show the good detection of molten pool edge as shown in Fig. 5.5. The detection is conducted at $\theta = 90^o$ and 20 iterations. Both methods can detect the edge with low error of edge detection; however, the error of PSO is lower than GA.
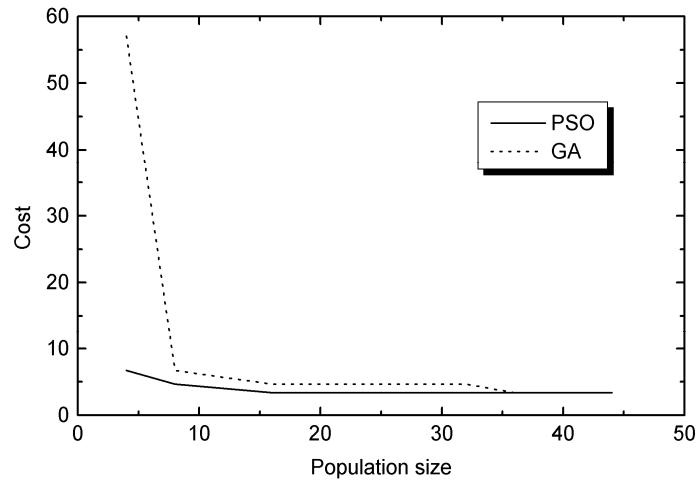
Fig. 5.6 The population size versus the fitness function cost in maximum iteration number is 10
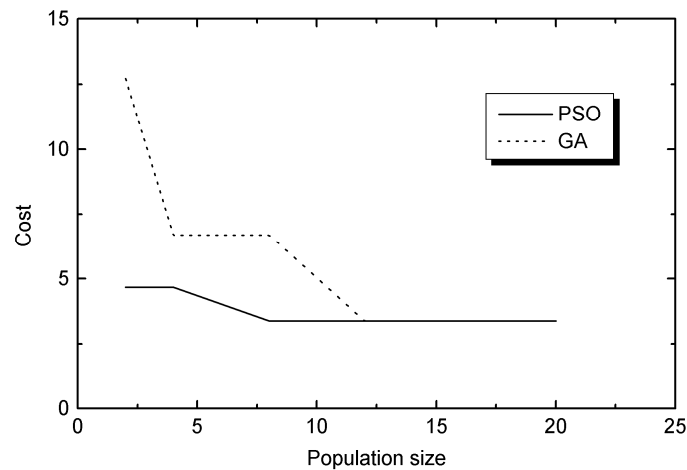
Fig. 5.7 The population size versus the fitness function cost in maximum iteration number is 20

Figure 5.6 shows the graphics of population size – cost of fitness function in maximum iteration is 10. The PSO achieves the lower cost at 3.38% faster than GA. PSO also reaches the minimum cost at the population size is 16, lower than GA which is 36.

Figure 5.7 shows the graphics of population size – cost of fitness function in maximum iteration is 20. It is shown that PSO can achieve the lower cost faster than GA. At minimum cost of 3.38%, PSO reaches faster at population size is 8 and GA is 12. However, by increasing the maximum iteration number, GA can obtain the minimum cost faster than in small iteration.
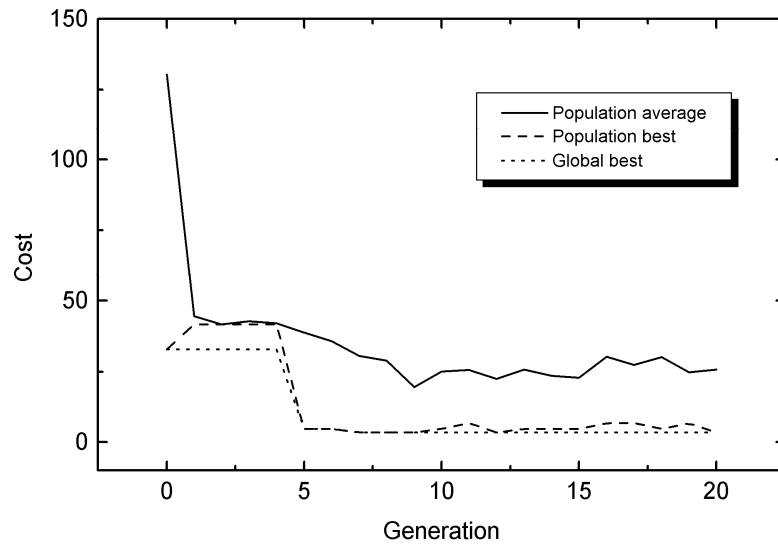
Fig. 5.8 The generation of population average, population best and global best at maximum iteration number is 20 and rotation angle is 270° in PSO
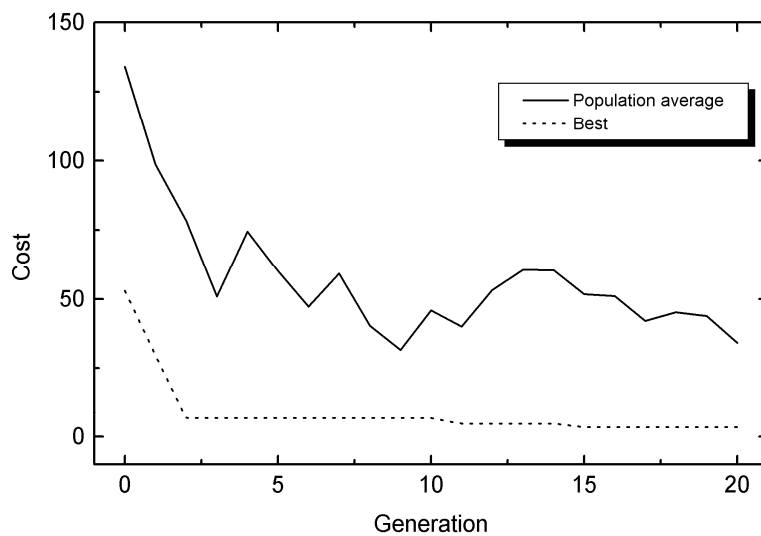
Fig. 5.9 The generation of population average and best at maximum iteration number is 20 and rotation angle is 270° in GA

From the optimization process, the result shows that PSO and GA can optimize the brightness range. The example of generation of population average, population best and global best at maximum iteration number is 20 and rotation angle is 270° in PSO is shown in Figure 5.8. Figure 5.9 shows the example result of generation of population average and best at maximum iteration number is 20 and rotation angle is 270°.

After optimizing 10 data of p_{out} and p_{in} generated by PSO and GA, the values of Δp_{out} and Δp_{in} calculated from Eq. (5.3) and (5.4) were averaged. The average values of Δp_{out} and Δp_{out} from PSO were 0.14% and 0.79%, respectively. And the average values of Δp_{out} and Δp_{out} from GA optimization were 0.04% and 0.69%, respectively. These values were used for the proposed image processing algorithm. Results of detected edge using PSO and GA optimization are shown in Fig. 5.10 and Fig 5.11, respectively. Figure 5.12 shows the relation between measured back bead width and detected molten pool width. Image resolution is 0.093 mm/pixel. It is clearly seen that image processing algorithm using both PSO and GA optimization could detect the molten pool width with good approximation. PSO achieved the lower RMSE of 1 mm and the standard deviation was 0.5 mm. And also GA had RMSE of 1 mm with the standard deviation was 0.5 mm. The cause of the errors might come from the detected threshold values as the brightness range for scanning the edge of molten pool. Very low brightness of molten pool also generated poor detection of threshold values; therefore the edge detection could be failed.

| $\theta = 90°$ | $\theta = 135°$ | $\theta = 180°$ |
| $\theta = 225°$ | $\theta = 270°$ | $\theta = 315°$ |
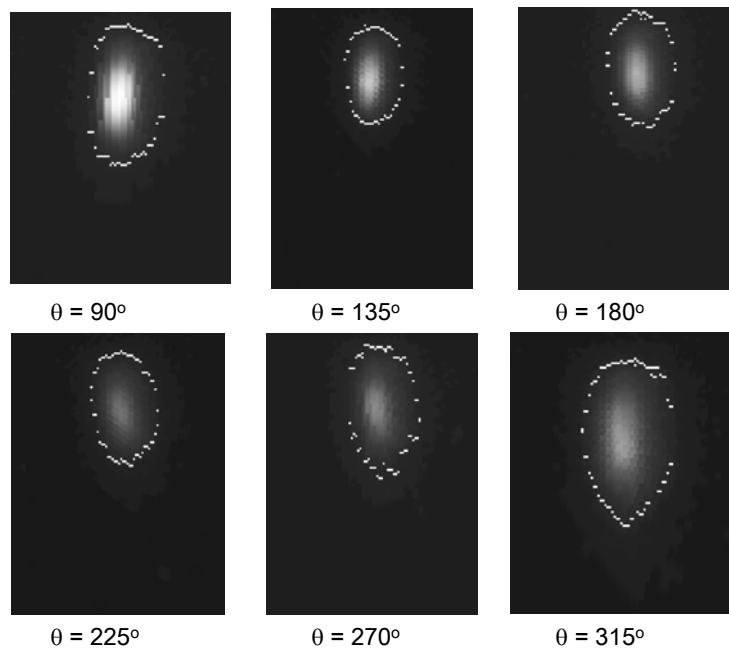
Fig. 5.10 Result of image processing using PSO with ΔP_{out} = 0.14% and ΔP_{in} = 0.79%

94

θ = 90°   θ = 135°   θ = 180°

θ = 225°   θ = 270°   θ = 315°
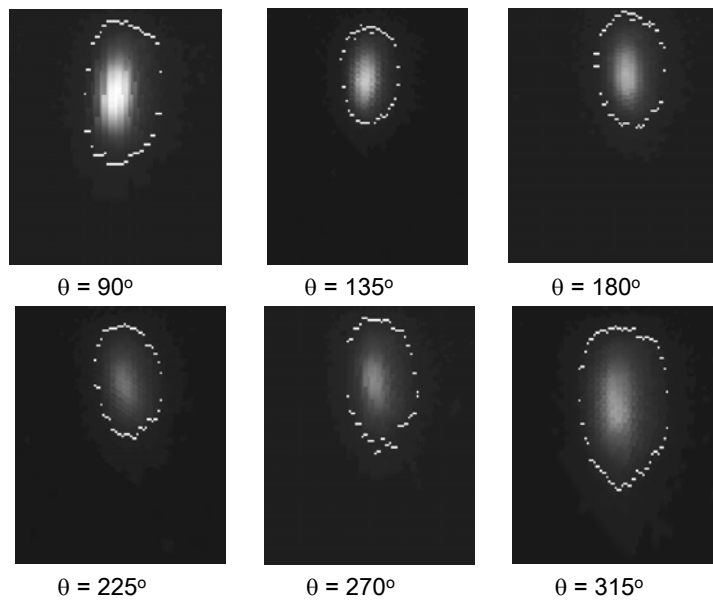
Fig. 5.11 Result of image processing using genetic algorithm with ΔP_{out} = 0.04% and ΔP_{in} = 0.69%
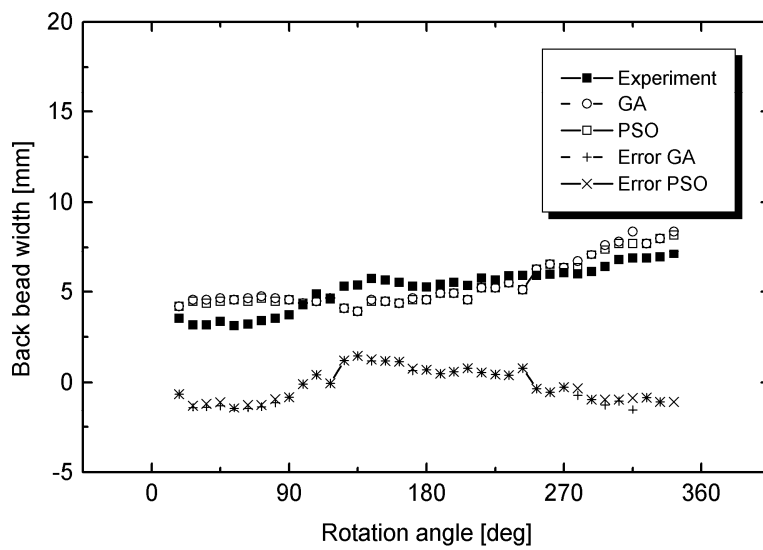
Fig. 5.12 The result of measured back bead width from experiment, GA and PSO approximation, and both errors of detection

(a) Manual, error = 13.33%   (b)PSO, error = 0.74%

(c) Manual, error = 3.38%   (d) GA, error = 1.13%
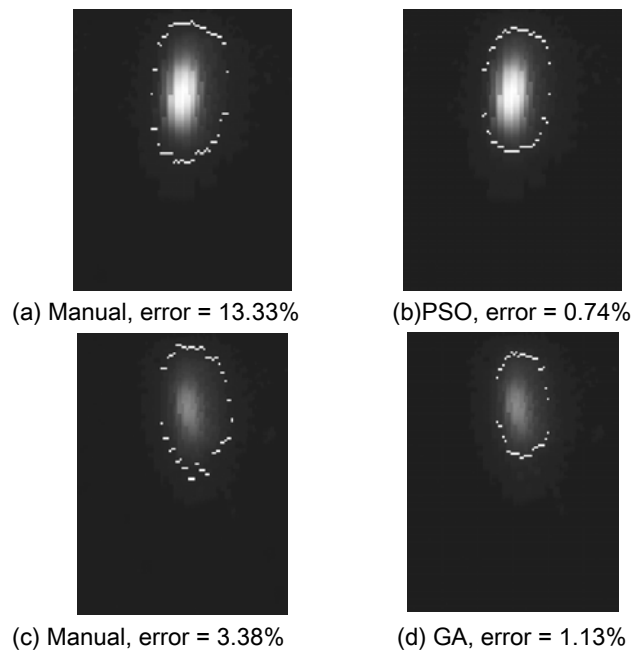
Fig. 5.13 Comparison results between manual judgment and optimization using PSO and GA

To compare the robustness of optimization results, the manual judgment of p_{out} and p_{in} was conducted by simply chose Δp_{out} = 0.3% and Δp_{in} = 0.8% and added into the Eq. (5.3) and (5.4). Then the edge detection results were compared to the optimized results using PSO and GA as shown in Fig. 5.13. It is shown that the optimization results using PSO and GA can perform the brightness range to detect of molten pool better than manual decision.

5.6 Experiment with Control

This section presents experiment with control using a fuzzy inference system. Welding process was conducted autogenously for 360° of circumference and in fixed position of pipe. In constant welding current of 60 A, the torch started to initiate the arc until the initial penetration was produced. The experiment with control was conducted using fuzzy inference system as control system [66-68]. The output of the image processing which is the width of molten pool, w will become the input of fuzzy control. The output of fuzzy control is the correction of welding speed.

(a) Input: back bead width
error, e [mm]

(b) Input: back bead width
error deviation, Δe [mm]

(c) Output: welding speed
correction, Δv [cm/min]
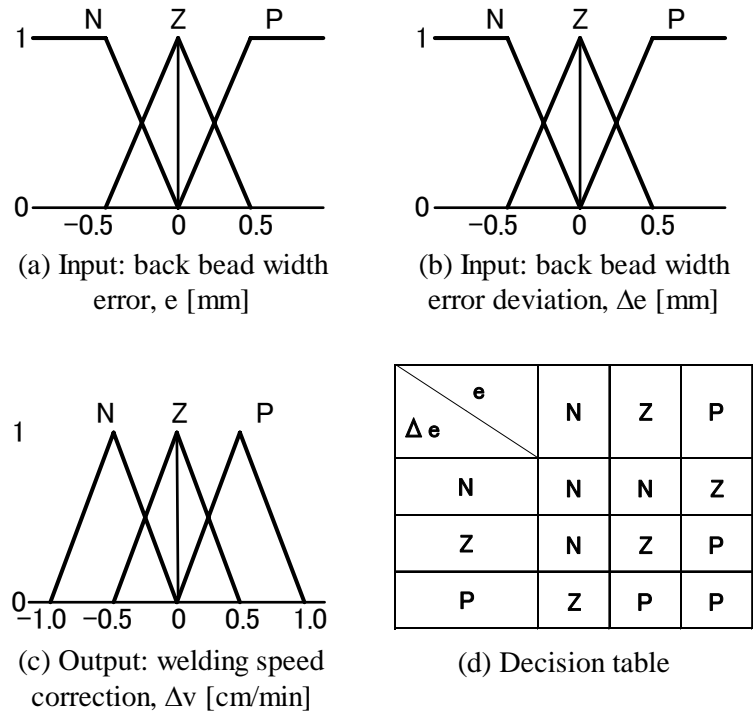
(d) Decision table

Fig. 5.14 Fuzzy sets and decision table for fuzzy control of welding speed

In this study, the proposed fuzzy control had two variables to be fuzzified. One was an error (e_n), which was the difference of back bead width (w_n) at the concerned time step (n) from the reference back bead width (w_r):

$$e_n = w_r - w_n \tag{5.8}$$

where w_r was set at 5 mm.

The other variable was the change of an error defined as:

$$\Delta e_{n+1} = w_{n+1} - w_n \tag{5.9}$$

Three kind of membership (N – Negative, Z – Zero, P – Positive) and triangular membership functions were used to fuzzify the inputs. Figure 5.14 (a), (b), (c) shows the membership functions and ranges for each fuzzy variable. Figure 5.14 (d) presents the decision table for the fuzzy control of welding speed.

5.7 Results and Discussion

In control experiment, to produce stable arc condition, the welding speed of 7 cm/min at θ = 0° – 45° was kept constant. Figure 5.15 and 5.16 show the experiment result using control with PSO and GA Optimization, respectively.

In PSO, result of back bead width and welding speed using fuzzy controller is shown in Fig. 5.15 (a). It is shown that fuzzy control could determine the correction of welding speed to keep the back bead width in the target range of 5±1 mm. The result of experiment with control has the average error is 0.3 mm and standard deviation of 0.4 mm. The back bead width increases slightly due to the starting speed. Back bead width is kept stable by maintaining the welding speed around 8 – 12.5 cm/min. Back bead appearance is shown in Fig. 5.15 (b).

In GA optimization, result of back bead width and welding speed is shown in Fig. 5.16 (a). It is also shown that the correction of welding speed has kept the back bead width in the target range of 5±1 mm. The result of experiment with control has the average error is 0.3 mm and standard deviation of 0.6 mm. At the beginning, the back bead width decreases due to the starting speed. But after $\theta = 45°$ the back bead width increases while the welding speed also increases. Back bead width is kept stable by maintaining the increased welding speed until 20 cm/min. Figure 5.16 (b) shows the back bead appearance.

Accordingly, by proper control of welding speed, it will produce excellent back bead width as shown in Fig. 5.15 (b) and 5.16 (b). The back bead width also aligned in the range target of 4 – 6 mm in width. In this study, the welding condition was change during the welding proceeded along the circumference of the pipe. However, the suitable welding condition for producing the good result was obtained at welding current, I = 60 A, pulsed current frequency, f = 50 Hz, minimum welding speed, v_{min} = 7 cm/min, and maximum welding speed, v_{max} = 20 cm/min. In general, the proposed automatic welding system produced sound weld of aluminum pipes by monitoring backside image of molten pool using omnidirectional camera.
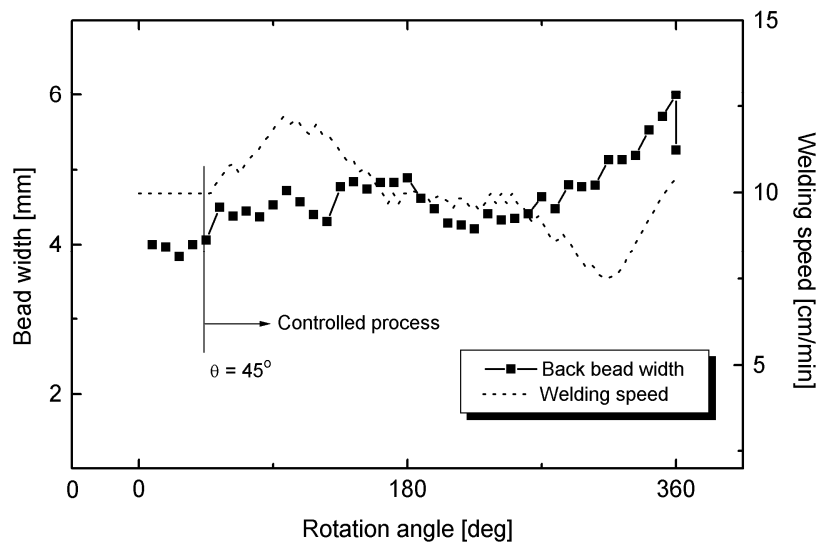
(a) Back bead width and welding speed
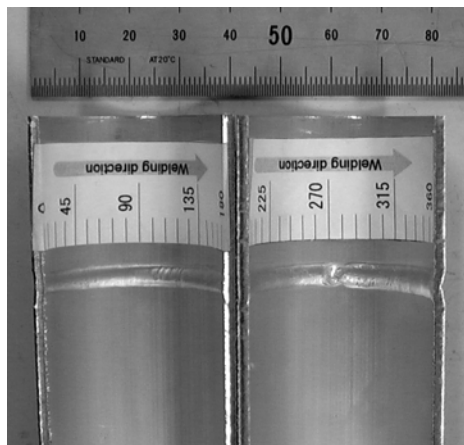
(b) Back bead appearance

Fig. 5.15 Result of experiment with control using PSO
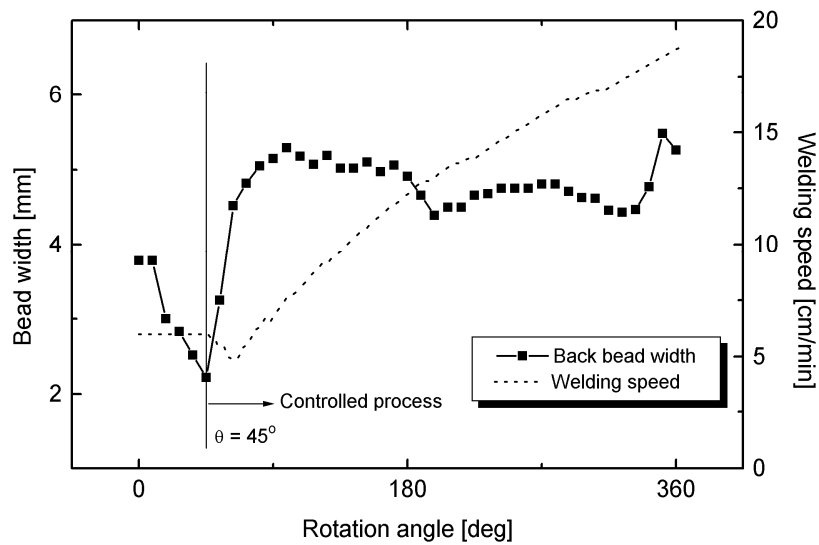
(a) Back bead width and welding speed
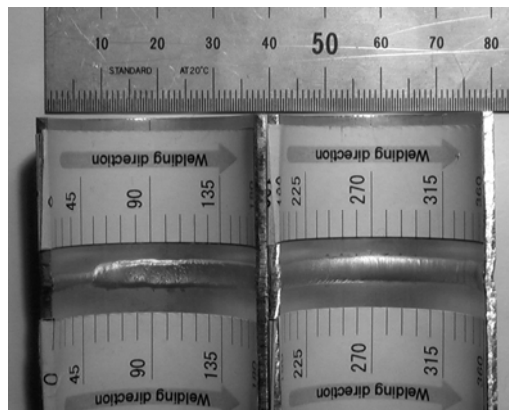
(b) Back bead appearance

Fig. 5.16 Result of experiment with control using GA optimization

5.8 Discussion of Monitoring and Control Methods Used in this Study

From the Chapter 2 – 5, the different monitoring and control methods have been presented. In the monitoring of backside image of molten pool using plain mirror, the system used two control methods which are neural network and fuzzy inference system. The new design of omnidirectional camera has been proposed to improve the previous monitoring method. And 3 methods of image processing optimization using manual/experience, PSO and GA have been described. The following discussion will summarize the characteristics of monitoring and control methods used in this study.

The summary of comparison results of back bead width using plain mirror in different control methods is shown in Table 5.2. It is shown that the experiment using fuzzy inference system produces lower error compared to neural network. Moreover, by using neural network, it is necessary to collect training data from experiment without control. It needs huge effort and number of pipes to be welded. By using fuzzy inference system, we can reduce training data 70% less than in neural network as shown in Section 3.3.2.

The summary of comparison results of image processing using different monitoring methods is shown in Table 5.3. It is shown that both monitoring methods provide almost same error in detection. However, in experiment using omnidirectional camera provides less error than using plain mirror. The modification of hyperboloidal mirror and proper magnification of lens will increase image resolution and reduce the error of detection.

Table 5.4 shows the comparison results of back bead width using omnidirectional camera in different optimization methods. It is shown that optimization method using PSO achieves lowest error compared to optimization method using manual/experience or GA, although all the results are still in the target range. Moreover, PSO and GA methods provide good approach in optimization to reduce time consumption.

The summary of control and optimization methods used in this study is shown in Table 5.5. All of the methods provide advantages and disadvantages. By appropriate design of the method and proper parameter setting, the process can achieve good welding products.

Table 5.2 Comparison results of back bead width using plain mirror in different control methods

No	Control Method	Average Error (mm)	Standard Deviation (mm)
1	Neural network	0.3	0.6
2	Fuzzy inference system	-0.1	0.4

Table 5.3 Comparison results of image processing using plain mirror and omnidirectional camera

No	Monitoring	Average Error (mm)	Standard Deviation (mm)
1	Plain mirror (Resolution = 0.06 mm/pixels)	0.3	0.6
2	Omnidirectional camera (Resolution = 0.093 mm/pixels)	0.0	0.4

Table 5.4 Comparison results of back bead width using omnidirectional camera in different optimization methods

No	Optimization Method	Average Error (mm)	Standard Deviation (mm)
1	Manual/experience	-0.3	0.5
2	PSO	0.3	0.4
3	GA	0.3	0.6

Table 5.5 Summary of control and optimization methods used in this study

No	Method	Advantages	Disadvantages
1	Neural network	- Neural networks are applicable to multivariate non-linear problems. - The process provides very fast performance in recall phase. - There is no need to assume an underlying data distribution such as usually is done in statistical modeling. - The individual relations between the input variables and the output variables are not developed by engineering judgment so that the model tends to be a black box or input/output table without analytical basis. - The experiment using neural network control model provides sound weld product.	- Training phase is very time consuming - The sample size has to be large. It is difficult to collect good training data from experiment without control. - The neural network construction (e.g. hidden layer number) and parameter setting for training phase have to be set for proper result and it needs experience.
2	Fuzzy inference system	- Fuzzy controllers are more robust than PID controllers because they can cover a much wider range of operating conditions than PID can, and can operate with noise and disturbances of different natures. - Developing a fuzzy controller is cheaper than developing a model-based or other controller to do the same thing. - Fuzzy controllers are customizable, since it is easier to understand and modify their rules, which not only use a human operator's strategy but also are expressed in natural linguistic terms. - It is easy to learn how fuzzy controllers operate and how to design and apply them to a concrete application. - From experiment using fuzzy inference system, it shows good result of back bead width and has lower error compared to control model using neural network.	- Since the rule set and membership functions are codependent, they should be defined simultaneously. This can lead to more optimal solutions. - Since the performance of a fuzzy system is more dependent on fuzzy rules rather than membership functions, fine tuning of the fuzzy system is better possible by tuning of membership functions. So it seems that it is better first to select the optimal rule set and then tune the membership functions.

No	Method	Advantages	Disadvantages
3	Particle swarm optimization (PSO)	- PSO is effective in nonlinear optimization problems and it is easy to implement. There are few parameters to adjust. Because the update process in PSO is based on simple equations, - Take real numbers as particles. - PSO can be efficiently used on large data sets. - The particle swarm operates through the cooperation of individuals. No particles are killed off; all members of the population survive throughout, participating as both learners and teachers in the social problem-solving endeavor. - In image processing optimization, it is shown that PSO can optimize the process and obtain low error of detection. Compared to GA, PSO can reach the minimum cost at lower population and same iteration. - From experiment using fuzzy inference system, it shows good result of back bead width.	- The appropriate fitness function can be obtained by using proper setting of PSO parameters. - If the swarm size is small, then PSO algorithm has a disadvantage of getting stuck at a position where velocity might approach to zero. It tends to be trapped in a local optimum under some initialization conditions.
4	Genetic algorithm (GA)	- GA efficiently search the large model space and work on a wide range of problems - GA can quickly scan a vast solution set. - The inductive nature of the GA means that it doesn't have to know any rules of the problem - it works by its own internal rules. This is very useful for complex or loosely defined problems. - In image processing optimization, it is shown that GA can optimize the process and obtain low error of detection. By increasing the maximum iteration number, GA can obtain the minimum cost faster than in small iteration. - From experiment using fuzzy inference system, it shows good result of back bead width.	- GA is slow, therefore it is not suitable for real time applications and take long to converge to the optimal solution - No guaranteed convergence even to local minimum. - The convergence of the process depends on proper setting of GA parameters. - In image processing optimization, at same iteration and same population, GA can achieve the lower cost but slower than PSO.

5.9 Conclusions

The conclusions of this chapter are summarized as follows:

1. This research proposes edge detection of molten pool in fixed pipe welding using PSO and GA. The brightness range for edge detection was constructed using the percentage of outer brightness (p_{out}) and inner brightness (p_{in}).

2. The experimental results shows that the both proposed method can detect edge of molten pool with minimum error. The method can perform the optimization of brightness range; reduce the computational cost and time consumption. Experiments on two different maximum iteration number show that PSO is more suitable for this problem than GA.

3. PSO and GA optimized image processing algorithm was applied into the real time process using omnidirectional vision-based monitoring of molten pool. From the experimental results using fuzzy inference system, it shows the effectiveness of the control system.

4. The monitoring and control methods used in this study have been discussed. Fuzzy inference system produces lower error compared to neural network. The experiment using omnidirectional camera provides less error than using plain mirror. The optimization method using PSO achieves lowest error compared to optimization method using manual/experience or GA, although all the results are still in the target range. By appropriate design of the monitoring and control method, the automatic welding process can achieve good welding products.

Chapter 6

Conclusions

In this thesis, we present automatic welding system for fixed aluminum pipes in TIG welding using vision sensors. Our main concern is to develop robust image processing algorithm, appropriate control system, new monitoring system using plain mirror and omnidirectional camera, and to optimize image processing algorithm using PSO and GA. This research constructed the intelligent welding process of aluminum alloy pipe 6063S-T5 in fixed position using the AC welding machine. The monitoring system used a charge-coupled device (CCD) camera to monitor backside image of molten pool. The captured image was processed to recognize the edge of molten pool by image processing algorithm.

The recognition of molten pool during aluminum pipe welding Al6063S-T5 to control welding penetration was performed. Owing to the low brightness of aluminum's molten pool, due to low melting point, the stable and robust image processing algorithm must be constructed. The image rotation was performed to make the image uniform. The histogram analysis and scan of brightness range were implemented to obtain top and bottom threshold used in edge detection. Error correction of maximum position was performed to eliminate the error. From the preliminary welding, the proposed image processing algorithm constructs good approximation of detection. Hence, the recognition of molten pool using vision sensors provides an effective method of monitoring process.

Neural network model for welding speed control was constructed to perform the process automatically. This experimental result shows a good agreement with previous experiment without control that the welding speed at $\theta = 90^o - 180^o$ was very important to affect next welding result. Accordingly, by proper control of welding speed, it will produce excellent back bead width.

Simulation of welding control using fuzzy inference system was constructed to simulate the welding control process. The simulation result shows that fuzzy controller was suitable for controlling the welding speed and appropriate to be implemented into the welding system. A series of experiments was conducted to evaluate the

performance of the fuzzy controller. From the experimental results it shows the effectiveness of the control system that is confirmed by sound weld of experimental results.

New method of welding penetration control for aluminum pipes in Tungsten Inert Gas (TIG) welding using omnidirectional vision-based monitoring of molten pool was proposed. This camera consists of a perspective camera and a hyperboidal mirror allowing a central projection by reflected rays. The detection of molten pool during aluminum pipe welding Al6063S-T5 to control welding penetration was performed. All of the image will be transformed into panorama extended image. After finding the center of gravity, set window was created automatically to locate the scanning area and reduce the time of edge detection. From the original image, the vertical scanning was performed to find top and bottom edge detection. In order to find the width of molten pool, the scanning of widest value of top and bottom edges was conducted. After implementing the image processing algorithm into the experimental without control, it is clearly seen that image processing algorithm could detect the molten pool width with good approximation.

Edge detection of molten pool in fixed pipe welding using PSO and GA was proposed. The brightness range for edge detection was constructed using the percentage of outer brightness (p_{out}) and inner brightness (p_{in}). The experimental results shows that the both proposed method can detect edge of molten pool with minimum error. The method can perform the optimization of brightness range; reduce the computational cost and time consumption. Experiments on two different maximum iteration number show that PSO is more suitable for this problem than GA. The faster results are obtained by using PSO, although GA can also reach the same minimum cost but in large number of population size. Therefore, PSO can achieve search performance more effective than GA. In large population size and iteration number, both PSO and GA work better than small population size and iteration number. PSO and GA optimized image processing algorithm was applied into the real time process using omnidirectional vision-based monitoring of molten pool. From the experimental results using fuzzy inference system, it shows the effectiveness of the control system.

The monitoring and control methods used in this study have been discussed. By appropriate design of the monitoring and control method, the automatic welding process can achieve good welding products.

As future work, it is necessary to develop new method to collect training data for control system by constructing the heat simulation model. The new design of omnidirectional mirror and new image processing algorithm are also necessary to make the monitoring system more robust. The application of new control model and optimization method will improve the capability of automatic welding system. The application of fuzzy inference system using an extended Support Vector Machine (SVM), an extended Feature Vector Selection (FVS) and an extended Relevance Vector Machine (RVM) will generate the number of fuzzy rules and the parameter values of membership function automatically. The optimization method using ant colony optimization (ACO) or hybrids with other computational intelligence techniques will provide different approaches to solve optimization problems.

References

[1] Saedi, H.R. and Unkel, W., Arc and Weld Pool Behavior for Pulsed Current GTAW, *Welding Journal,* vol. 67 no. 11 (1998), pp. 247-255.

[2] Andersen, K. and Cook, G.E., Artificial Neural Networks Applied to Arc Welding Process Modeling and Control, *IEEE transaction Industry Application,* vol. 26 no. 9 (1990), pp. 824-830.

[3] Lim, T.G. and Cho, H.S., Estimation of Weld Pool Sizes in GMA Welding Process Using Neural Networks, *Journal of Systems and Control Engineering,* vol. 207 no.1 (1993), pp. 15-26.

[4] Yang, S.M., Cho, M.H., Lee, H.Y. and Cho, T.D., Weld Line Detection and Process Control for Welding Automation, *Measurement Science and Technology*, vol. 18 (2007), pp. 819-826.

[5] Dutta, P. and Pratihar, D.K., Modeling of TIG Welding Process Using Conventional Regression Analysis and Neural Network-Based Approaches, *Journal of Material Processing*, vol. 184 (2007), pp. 56-68.

[6] Pal, S., Pal, S.K. and Samantaray, A.K., Artificial Neural Network Modeling of Weld Joint Strength Prediction of a Pulsed Metal Inert Gas Welding Process Using Arc Signals, *Journal of Material Processing*, vol. 202 (2008), pp. 464-474.

[7] Kanti, K.M. and Rao, P.S., Prediction of Bead Geometry in Pulsed GMA Welding Using Back Propagation Neural Network, *Journal of Materials Processing Technology*, vol. 200 (2008), pp. 300-305.

[8] Lee, C.Y., Tung, P.C. and Chu, W.H., Adaptive Fuzzy Sliding Mode Control for an Automatic Arc Welding System, *International Journal of Advanced Manufacturing Technology*, vol. 29 (2006), pp. 481-489.

[9] Tsai, C.H., Hou, K.H., Chuang, H.T., Fuzzy Control of Pulsed GTA Welds by Using Real-Time Root Bead Image Feedback, *Journal of Materials Processing Technology*, vol. 176 (2006), pp. 158 – 167.

[10] Huang, X. and Chen, S., SVM-Based Fuzzy Modeling for the Arc Welding Process, *Materials Science and Engineering A*, vol. 427 (2006), pp. 181-187.

[11] Carrino, L., Natale, U., Nele, L., Sabatini, M.L., Sorrentino, L, A Neuro-Fuzzy Approach for Increasing Productivity in Gas Metal Arc Welding Processes,

International Journal of Advanced Manufacturing Technology, vol. 32 (2007), pp. 459-467.

[12] Fennander, H., Kyrki, V., Fellman, A., Salminen, A. and Kalviainen, H., Visual Measurement and Tracking in Laser Hybrid Welding, *Machine Vision and Applications*, vol. 20 (2009), pp. 103-118.

[13] Brzakovic, D. and Khani, D.T., Weld Pool Edge Detection for Automated Control of Welding, *IEEE Transactions on Robotics and Automation,* vol. 7 no. 3 (1991), pp. 397-403.

[14] Lu, W. and Zhang, Y.M., Robust Sensing and Control of the Weld Pool Surface, *Measurement Science and Technology*, vol. 17 (2006), pp. 2437-2446.

[15] Lee, C.W. and Na, S.J., A Study on the Influence of Reflected Arc Light on Vision Sensors for Welding Automation, *Welding Journal,* vol. 75 no. 12 (1996), pp. 379-387.

[16] Richardson, R.W. and Gutow, D.A., Coaxial Arc Weld Pool Viewing for Process Monitoring and Control, *Welding Journal,* vol. 63 no. 3 (1984), pp. 43-50.

[17] Far, I.S. and Javadi, Y., Influence of Welding Sequence on Welding Distortions in Pipes, *International Journal of Pressure Vessels and Piping*, vol. 85 (2008), pp. 265-274.

[18] Kou, S., Le, Y., Heat Flow During the Autogeneous GTA Welding of Pipes, *Metallurgical Transactions A*, vol. 15A (1984), pp. 1165–1171.

[19] Lho, T.J., Na, S.J., A Study on Parameter Optimization with Numerical Heat Conduction Model for Circumferential Gas Tungsten Arc (GTA) Welding of Thin Pipes, *Proc. Inst Mechanical Engineers*, *Part B*, vol. 206 (1992), pp. 101–111.

[20] Na, S.J., Lee, H.J., A Study on Parameter Optimization in the Circumferential GTA Welding of Aluminum Pipes Using a Semi-Analytical Finite-Element Method, *Journal of Material Processing Technology,* vol. 57 (1996), pp. 95–102.

[21] Kondoh, K., Ohji, T., and Ueda, K., Optimum Heat Input Control in Arc Welding of Steel and Aluminum Pipe, *Material Transaction*, *JIM*, vol. 39 no. 3 (1998), pp. 413–419.

[22] Wang, J.J., Lin, T., and Chen, S.B, Obtaining Weld Pool Vision Information During Aluminum Alloy TIG Welding, *The International Journal of Advanced Manufacturing Technology*, vol. 26, no. 3 (2004), pp. 219-227.

[23] Laiping, L., Tao, L., Shanben, C., Light Intensity Analysis of a Passive Visual Sensing System in GTAW, *The International Journal of Advanced Manufacturing Technology* (2004), vol. 27, no. 1-2 (2004), pp. 106-111.

[24] Messler, R.W., Principles of Welding: Processes, Physics, Chemistry, and Metallurgy, Wiley-VCH Verlag GmbH & Co. KGaA, Weinheim, 2004.

[25] Khan, M.I., Welding Science and Technology, New Age International Limited, New Delhi, 2007.

[26] Hicks, J., Welded Design – Theory and Practice, Abington Publishing, Cambridge, England, 2000.

[27] Wikipedia, Gas Tungsten Arc Welding, http://en.wikipedia.org/wiki/Gas_tungsten_arc_welding

[28] Nayyar, M.L., Piping Handbook, McGraw-Hill, Seventh Edition, US, 2000.

[29] Brislow, R., Orbital Welding: a Status Report, *Welding Design and Fabrication*, December (1998), pp. 21-27.

[30] Emmerson, J.G., Multipass Orbital Welding Pipe: a Primer for the Prospective First-Time User, *The Tube and Pipe Journal,* vol. 10 no. 1, January-February (1999).

[31] Emmerson, J.G., FCAW Orbital Pipe Welding Technology Improves FAB Shop Productivty, *Welding Journal*, November (1999), pp. 1-4.

[32] ESAB AB, Welding Components for the Petrochemical Industry at Sirz Motaggi srl, Svetsaren, vol. 57 No. 1 (2002), pp. 13-15.

[33] ESAB AB, CIMTAS, An International Player in Power Generation and Energy Storage, vol. 57 No. 2 (2002), pp. 45-49.

[34] Kuvin, B.F., GTAW in the Round at Zurn Energy, Welding Design and Fabrication, December (1998), pp. 30-31.

[35] Butler, P., Emmerson, J.G., Berg, R.V.D., Welding the Maui A-B Pipeline, Welding Journal, November (1993), pp. 31-38.

[36] Arc Machines, Inc., http://www.arcmachines.com/

[37] Stava, E.K., Technology Gets to the Root of Pipe Welding, *Tube and Pipe Technology*, March/April (2000), pp.136-137.

[38] ASM Handbook, Volume 2: Properties and Selection, Nonferrous Alloys and Special Purpose, 9th Ed., Ohio, 1989.

[39] Mathers, G., The Welding of Aluminum and Its Alloys, *Woodhead Publishing Limited*, Cambridge, England, 2002.

[40] Chen, S.B, Qiu, T., Lin, T., Wu, L., Tian, J.S, Lv, W.X., Zhang, Y., Intelligent Technologies for Robotic Welding, *Robotic Welding, Intelligence and Automation, LNCIS 299* (2004), pp. 123-143.

[41] Pires, J.N., Loureiro, A., Godinho, T., Ferreira, P., Fernando, B., Morgado, J., Welding Robots, *IEEE Robotics and Automation Magazine*, June (2003), pp. 45-55.

[42] Sicard, P. and Levine, M.D., An Approach to an Expert Robot Welding System, *IEEE Transactions on System, Man, And Cybernetics*, vol. 18 no. 2 (1988), pp. 204-222.

[43] Vilkas, E.P., Automation of the Gas Tungsten Arc Welding, *Welding Journal*, vol. 45 no. 5, (1966), pp. 410 - 416.

[44] Cook, G.E., Barnett, R.J., Andersen, K., Strauss, A.M., Weld Modeling and Control Using Artificial Neural Networks, *IEEE Transactions on Industry Applications*, vol. 31 no. 6 (1995), pp. 1484-1491.

[45] Muramatsu, M., Suga, Y., Mori, K., Autonomous Mobile Robot System for Monitoring and Control of Penetration during Fixed Pipes Welding, *JSME International Journal Series A*, vol. 46 no.3 (2003), pp. 391-397.

[46] Bingul, Z., Cook, G.E, and Strauss, A.M., Application of Fuzzy Logic to Spatial Thermal Control in Fusion Welding, *IEE Transaction on Industry Applications*, vol. 36 no. 6 (2000), pp. 1523-1530.

[47] Bae, K.Y., Lee, T.H., Ahn, K.C., An Optical Sensing System for Seam Tracking and Weld Pool Control in Gas Metal Arc Welding of Steel Pipe, *Journal of Materials Processing Technology*, vol. 120, issues 1-3 (2003), pp. 458-465.

[48] Di,L., Srikanthan, T., Chandel, R.S., Katsunori, I., Neural-Network-Based Self-Organized Fuzzy Logic Control for Arc Welding, *Engineering Applications of Artificial Intelligence* 14 (2001), pp. 115-124.

[49] Zhang, Y.M. and Kovacevic, R., Neurofuzzy Model-Based Predictive Control of Weld Fusion Zone Geometry, *IEEE Transactions on Fuzzy Systems*, vol. 6 no. 3 (1998), pp. 389-401.

[50] Brzakovic, D., Khani, D.T., Awad, B., A Vision System for Monitoring Weld Pool, *Proceeding for the 1992 IEEE International Conference on Robotics and Automation*, Nice, Frace-May (1992), pp. 1609-1614.

[51] Chen, S.B, Zhao, D.B., Lou, Y.J., and Wu, L., Computer Vision Sensing and Intelligent Control of Welding Pool Dynamics, *Robotic Welding, Intelligence and Automation, LNCIS* 299 (2004), pp. 25-55.

[52] Wu, C.S, Gao, J.Q., Liu, X.F., Zhao, Y.H., Vision-Based Measurement of Weld Pool Geometry in Constant-Current Gas Tungsten Arc Welding, *Proc. Instn Mech. Engs Part B: J. Engineering Manufacture,* vol. 217 (2003), pp. 1-4.

[53] Zhao, D.B., Yi, J.Q., Chen, S.B., Wu, L., Chen, Q., Extraction of Three-Dimensional Parameters for Weld Pool Surface in Pulsed GTAW With Wire Filler, *Journal of Manufacturing Science and Engineering ASME*, vol. 124 (2003), pp. 493-503.

[54] Quanying, D., Shanben, C., Tao, L., Inspection of Weld Shape Based on The Shape From Shading, *International Journal of Advanced Manufacturing Technology*, vol. 27, no. 7-8 (2005), pp. 667-671.

[55] Engelbrecth, A.P., Computational Intelligence: An Introduction, *John Wiley & Sons, Ltd.*, England, 2002.

[56] Floreano, D., Bio-Inspired Artificial Intelligence: Theories, Methods, and Technologies, *MIT Press*, USA, 2008.

[57] Baskoro,A.S. and Suga,Y., Recognition of Molten Pool During Aluminum Pipe TIG Welding Using Vision Sensor, *Proceeding of The 9th International Conference on Quality in Research*, September 2006, Depok, Indonesia, pp. 1-5.

[58] Baskoro,A.S., Suga,Y., Circumferential TIG Welding of Aluminum Pipe Using Neural Network, *Proceeding of The 5th Annual National Conference of Mechanical Engineering* , November 2006, Depok, Indonesia, pp. 1-6.

[59] Baskoro, A., Suga, Y., Investigation of Welding Penetration Control in TIG Welding of an Aluminum Pipe using Vision Sensing, *Proceeding of The 14th Material and Processing 2006 (M&P 2006)*, Material and Process Engineering Lecture, JSME, November 2006, Chiba, Japan, pp. 131-132.

[60] Baskoro,A.S., Suga,Y., Monitoring of Backside Image of Molten Pool During Aluminum Pipe Welding Using Vision Sensor, *Abstract Book of International Welding/Joining Conference-Korea 2007*, May 2007, Seoul, Korea, pp. 356-357.

[61] Baskoro,A.S. Kabutomori,M., Suga,Y., Welding Penetration Control of Aluminum Pipe by Monitoring Backside Image of Molten Pool using Vision Sensor, *The 78th Research Meeting of Light Weight Structure Welding Division*, Japan Welding Society, July 2007, Osaka, Japan, pp. 1-9.

[62] Kabutomori, M., Baskoro, A.S., Suga, Y., The Welding Penetration Control of Aluminum Pipe Using Vision Sensor, *Proceeding of The 15th Material and Processing 2007 (M&P 2007)*, JSME, November 2007, Nagaoka, Japan, pp. 91-92.

[63] Baskoro,A.S. Kabutomori,M. Suga,Y., Penetration Control in Welding of Fixed Aluminum Pipes by Monitoring Backside Image of Molten Pool, *Proceeding of the International Conference of the 11th AUN/SEED.Net Field Wise Seminar*, December 2007, Kuala Lumpur, Malaysia, pp. 109-117.

[64] Baskoro, A.S., Kabutomori, M., Suga,Y., Monitoring of Backside Image of Molten Pool during Aluminum Pipe Welding Using Vision Sensor, *Material Science Forum*, vols. 580-582 (2008), pp. 379-382.

[65] Baskoro, A.S., Kabutomori, M., Suga.Y., Automatic Welding System of Aluminum Pipe by Monitoring Backside Image of Molten Pool Using Vision Sensor, *Journal of Solid Mechanics and Materials Engineering*, vol. 2 no. 5 (2008), pp.582-592.

[66] Baskoro, A.S., Kabutomori, M., Suga,Y., Welding Penetration Control of Aluminum Pipe Using Fuzzy Logic Control, *The 2008th Spring Round Precision Engineering Conference, The Japan Society for Precision Engineering*, March 2007, Kawasaki, Japan, pp. 703-704.

[67] Baskoro, A.S., Kabutomori, M., Suga,Y., Welding Penetration Control of Fixed Pipe in TIG Welding Using Fuzzy Inference System, *Proceeding of the International Conference on Material Processing (ICM&P) 2008*, October 2008, IL, USA, pp. 1-8.

[68] Baskoro, A.S., Kabutomori, M., Suga, Y., Welding Penetration Control of Fixed Pipe in TIG Welding Using Fuzzy Inference System, *Journal of Solid Mechanics and Materials Engineering*, vol. 3 no. 1 (2009), pp.38-48.

[69] Masuda, R., Kabutomori, M., Baskoro, A.S., Suga, Y., Welding Penetration Control of Aluminum Pipe Using Omni-directional Camera, *Proceeding of the Mechanical Engineering Congress, 2008 Japan (MECJ-08)*, August 2008, Yokohama, Japan.

[70] Baskoro, A.S., Kabutomori, M., Suga, Y., Welding Penetration Control for Aluminum Pipe Welding Using Omnidirectional Vision-based Monitoring of Molten Pool, *Proceeding of the 8th International Welding Symposium (8WS) 2008*, November 2008, Kyoto, Japan, p. 27.

[71] Baskoro, A.S., Masuda, R., Kabutomori, M., Suga, Y., Welding Penetration Control for Aluminum Pipe using Omnidirectional Camera, *Research Meeting of The 83rd Light Weight Structure Welding Division, Japan Welding Society*, November 2008, Osaka, Japan, pp. 1-6.

[72] Baskoro, A.S., Kabutomori, M., Suga, Y., Welding Penetration Control for Aluminum Pipe Welding Using Omnidirectional Vision-based Monitoring of Molten Pool, *Quarterly Journal of The Japan Welding Society*, (to appear).

[73] Baskoro, A.S., Masuda, R., Kabutomori, M., Suga, Y., A Comparison of Particle Swarm Optimization and Genetic Algorithm for Edge Detection of Molten Pool in Fixed Pipe Welding, *Proceeding of the Joint 4th International Conference on Soft Computing and Intelligent System and 9th International Symposium on Advanced Intelligent System (SCIS & ISIS 2008)*, September 2008, Nagoya, Japan, pp. 1743-1748.

[74] Baskoro, A.S., Masuda, R., Kabutomori, M., Suga, Y., An Application of Genetic Algorithm for Edge Detection of Molten Pool in Fixed Pipe Welding, *International Journal of Advanced Manufacturing Technology*, DOI 10.1007/s00170-009-2048-1 (published online: 29 April 2009).

[75] Heinz, A., Haszler, A., Keidel, C., Moldenhauer, S., Benedictus, R., Miller, W.S., Recent Development in Aluminum Alloys for Aerospace Applications, *Material Science and Engineering A280* (2000), pp. 102-107.

[76] Barnes, T.A., Pashby, I.R., Joining Techniques for Aluminum Spaceframes Used in Automobiles Part I – Solid and Liquid Phase Welding, *Journal of Materials Processing Technology 99* (2000), pp. 62-71.

[77] Kasabov, N.K., Foundations of Neural Networks, Fuzzy Systems, and Knowledge Engineering, *The MIT Press*, USA, 1998.

[78] King, P.J., Mamdani, E.H., The Application of Fuzzy Control System to Industrial Processes, *Automatica*, vol. 13 (1977), pp. 235-242.

[79] Zadeh, L.A., Fuzzy Sets, *Information and Control* 8 (1965), pp. 338-353.

[80] Zadeh, L.A., A Fuzzy-Algorithmic Approach to the Definition of Complex or Imprecise Concepts, *International Journal of Man-Machine Studies* (1976) 8, pp. 249-291.

[81] Zadeh, L.A., Outline of a New Approach to the Analysis of Complex System and Decision Processes, *IEEE Transactions on Systems, Man, And Cybernetics*, vol. SMC-3, no. 1, pp. 28-44.

[82] Nedjah, N., Mourelle, L.M., Introducing You to Fuzziness, *StudFuzz* 181 (2005), pp. 3-21.

[83] Reznik, L., Fuzzy Controllers, *Butterworth-Heinemann*, Oxford, 1997.

[84] Svoboda, T., Pajdla, T., Hlavac, V., Central panoramic cameras: geometry and design, *Research Report K335/97/147*, Center for Machine Perception, Czech Technical University (1997).

[85] Kang, S.B. and Szeliski, R., 3-D scene data recovery using omnidirectional multibaseline stereo, *International Journal of Computer Vision* 25 (1997), pp. 167–183.

[86] Svoboda, T. and Pajdla, T., Epipolar geometry for central catadioptric cameras, *International Journal of Computer Vision* 49 (2002), pp. 23–37.

[87] Gluckman, J., and Nayer, S.K., Ego-motion and omnidirectional camera, *Proceedings of International Conference on Computer Vision* (1998), pp. 999–1005.

[88] Vassallo, R., Santos-Victor, J., Schneebeli, J., A general approach for egomotion estimation with omnidirectional images, *Proceedings of IEEE Workshop on Omnidirectional Vision* (2002), pp. 97–103.

[89] Kim, J., Muramatsu, M., Murata, Y., Suga, Y., Omnidirectional Vision-Based Ego-Pose Estimation for an Autonomous In-pipe Mobile Robot, *Advanced Robotics*, vol.21 no.3-4, (2007), pp.441-460.

[90] Kennedy, J. and Eberhart, R., Particle Swarm Optimization, *Proceedings of IEEE International Conference on Neural Networks* (1995), p. 1942-1948.

[91] Shi, Y. and Eberhart, R., A Modified Particle Swarm Optimizer, *Proceedings of the IEEE World Congress on Computational Intelligence* (1998), p.69-73.

[92] Clerc, M. and Kennedy, J., The Particle Swarm-Explosion, Stability, and Convergence in a Multidimensional Complex Space, *Proceedings of the IEEE Transactions on Evolutionary Computation*, vol. 6 (2002), p.58-73.

[93] Kennedy, J., Eberhart, R.C., Shi, Y., Swarm Intelligence, *Morgan Kaufmann Publisher*, USA, 2001.

[94] Haupt, R.L. and Haupt, S.E., Practical Genetic Algorithms, *A Wiley-Interscience Publication*, 1998.

[95] Ahn, C.W., Advances in Evolutionary Algorithms: Theory, Design and Practice, *Springer*, 2006.

[96] Mishra, S. and DebRoy, T., Tailoring Gas Tungsten Arc Weld Geometry Using a Genetic Algorithm and a Neural Network Trained with Convective Heat Flow Calculations, *Material Science and Engineering A* 454-455 (2007), pp. 477-486.

[97] Tseng, H.Y., Welding Parameters Optimization for Economic Design Using Neural Approximation and Genetic Algorithm, *International Journal of Advanced Manufacturing Technology* 27 (2006), pp. 897-901.

Curriculum Vitae

Personal

Name   : Ario Sunar Baskoro

Office Address : Mechanical Engineering Department, Faculty of Engineering,

        University of Indonesia, Kampus Baru UI Depok, Indonesia

School Address : School of Integrated Design Engineering

        Faculty of Science and Technology, Keio University,

        3-14-1 Hiyoshi, Kohoku-ku, Yokohama, Kanagawa, Japan

Education

2006.09 – 2009.09   Ph.D in School of Integrated Design Engineering,

           Keio University, Yokohama, Japan.

           Major: Material Processing Technology

           Thesis Topic: A Study on Intelligent Welding System of Fixed Aluminum Pipes Using Vision Sensors

           Advisor: Prof. Yasuo Suga, Ph.D

2004.09 – 2006.09   M.Eng in School of Integrated Design Engineering,

           Keio University, Yokohama, Japan.

           Major: Material Processing Technology

           Thesis Topic: The Welding Penetration Control of Aluminum Pipe in TIG Welding Using Vision Sensing

           Advisor: Prof. Yasuo Suga, Ph.D

2002.07 – 2004.01   M.Eng in Mechanical Engineering,

           University of Indonesia, Depok, Indonesia.

           Major: Manufacturing Engineering

           Thesis Topic: The Design of Web-based Milling System for Laboratory Scale

           Advisor: Dr.Ing. Budi Ibrahim

| 1994.08 – 1998.08 | B.Eng in Mechanical Engineering, University of Indonesia, Depok, Indonesia. |

1994.08 – 1998.08   B.Eng in Mechanical Engineering,
University of Indonesia, Depok, Indonesia.
Major: Mechanical Engineering
Thesis Topic: Effects of The Distance Between Driving Nozzle and Mixing Tube on Jet Pump System
Advisor: Ahmad Indra Siswantara, Ph.D

Research Experience

- "Prototyping Electric Vehicle 'Bajaj Langit Biru' - BALABI", (University of Indonesia: 1999.8 – 2000.7)
- "Kinematics Analysis of Articulated Robot with Six Degrees of Freedom in Welding Process", (University of Indonesia: 2000.7 – 2001.8)
- "Optical and Electronic Device Technology for Access Network", (The 21st century COE Program, Keio University, Graduate School Information, Electrical Engineering, Electronics, Japan), (Keio University: 2006.10 – 2007.3)

Activities

1999.03 – recent   Lecturer in Mechanical Engineering Department, Faculty of Engineering University of Indonesia
2006.10 – 2007.03   Research Assistant in Keio University

Awards and Honors

2007.03 – 2009.09   Monbukagakusho Scholarship supported by Ministry of Education, Culture, Sports, Science and Technology, Japan
2008.11   Best Poster OTC Daihen Award in The 8th International Welding Symposium Kyoto, Japan
2008.10   Incentive Award for Presentation in International Conference supported by Graduate School of Keio University
2004.03 – 2006.09   Keio Graduate Scholarship Program supported by Keio University
2004.1   Cumlaude Award and Fastest Graduation for Master Program, University of Indonesia

Publications

- ### Accepted Paper for Publication in International Journal

1. Baskoro, A.S., Kabutomori, M. and Suga, Y., "Monitoring of Backside Image of Molten Pool during Aluminum Pipe Welding Using Vision Sensor", Material Science Forum, Vol. 580-582 (2008), pp. 379-382 .

2. Baskoro,A.S., Kabutomori, M. and Suga, Y., "Automatic Welding System of Aluminum Pipe by Monitoring Backside Image of Molten Pool Using Vision Sensor", Journal of Solid Mechanics and Materials Engineering, Vol. 2, No. 5 (2008), pp. 582-592.

3. Baskoro, A.S., Kabutomori, M. and Suga, Y., "Automatic Welding Penetration Control of Fixed Pipe in TIG Welding Using Fuzzy Inference System", Journal of Solid Mechanics and Materials Engineering, Vol. 3, No. 1 (2009), pp. 38-48.

4. Baskoro, A.S., Masuda, R., Kabutomori, M. and Suga, Y., "Welding Penetration Control for Aluminum Pipe Welding Using Omnidirectional Vision-based Monitoring of Molten Pool", Quarterly Journal of The Japan Welding Society, (to appear).

5. Baskoro, A.S., Masuda, R., Kabutomori, M. and Suga, Y., "An Application of Genetic Algorithm for Edge Detection of Molten Pool in Fixed Pipe Welding", International Journal of Advanced Manufacturing Technology, DOI 10.1007/s00170-009-2048-1 (published online: 29 April 2009)

- ### International Conference Paper

1. Baskoro, A.S. and Suga, Y., "Recognition of Molten Pool During Aluminum Pipe TIG Welding Using Vision Sensor", Proceeding of The 9th International Conference on Quality in Research, September 2006, pp. 1-5, Depok, Indonesia.

2. Baskoro, A.S. and Suga,Y., "Monitoring of Backside Image of Molten Pool During Aluminum Pipe Welding Using Vision Sensor", Abstract Book of International Welding/Joining Conference-Korea 2007, May 2007, pp. 356-357, Seoul, Korea.

3. Baskoro,A.S., Kabutomori,M. and Suga,Y., "Penetration Control in Welding of Fixed Aluminum Pipes by Monitoring Backside Image of Molten Pool", Proceeding of the International Conference of the 11th AUN/SEED.Net Field Wise Seminar, December 2007 , pp. 109-117, Kuala Lumpur, Malaysia.

4. Baskoro, A.S., Masuda, R., Kabutomori, M. and Suga, Y., "A Comparison of Particle Swarm Optimization and Genetic Algorithm for Edge Detection of Molten

Pool in Fixed Pipe Welding", Proceeding of the Joint 4th International Conference on Soft Computing and Intelligent System and 9th International Symposium on Advanced Intelligent System (SCIS & ISIS 2008), September 2008, pp. 1743-1748, Nagoya, Japan.

5. Baskoro, A.S., Kabutomori, M. and Suga,Y., "Welding Penetration Control of Fixed Pipe in TIG Welding Using Fuzzy Inference System", Proceeding of the International Conference on Material Processing 2008 (ICM&P), October 2008, pp. 1-8, IL, USA,.

6. Baskoro, A.S., Kabutomori, M. and Suga, Y., "Welding Penetration Control for Aluminum Pipe Welding Using Omnidirectional Vision-based Monitoring of Molten Pool", Proceeding of the 8th International Welding Symposium (8WS) 2008, November 2008, p. 27, Kyoto, Japan.

- **Domestic Conference Paper**

1. Baskoro, A.S. and Suga,Y., "Circumferential TIG Welding of Aluminum Pipe Using Neural Network", Proceeding of The 5th Annual National Conference of Mechanical Engineering , November 2006, pp. 1-6, Depok, Indonesia.

2. Baskoro, A.S. and Suga, Y., "Investigation of Welding Penetration Control in TIG Welding of an Aluminum Pipe using Vision Sensing", Proceeding of The 14th Material and Processing 2006 (M&P2006) JSME, November 2006, pp. 131-132, Chiba, Japan.

3. Baskoro, A.S., Kabutomori, M. and Suga, Y., "Effects of Welding Speed Variation of Aluminum Pipe in Circumferential TIG Welding", Proceeding of The 16th Indonesian Scientific Conference (TI-2007), August 2007, pp. 218-220, Kyoto, Japan.

4. Baskoro, A.S., Kabutomori, M. and Suga,Y., "Welding Penetration Control of Aluminum Pipe by Monitoring Backside Image of Molten Pool using Vision Sensor", The 78th Research Meeting of Light Weight Structure Welding Division Japan Welding Society, July 2007, pp. 1-9, Osaka, Japan.

5. Kabutomori, M., Baskoro, A.S. and Suga, Y., "The Welding Penetration Control of Aluminum Pipe Using Vision Sensor", Proceeding of The 15th Material and Processing 2007 (M&P 2007) JSME, November 2007, pp. 91-92, Nagaoka, Japan.

6. Baskoro, A.S., Kabutomori, M. and Suga,Y., "Welding Penetration Control of Aluminum Pipe Using Fuzzy Logic Control", The 2008th Spring Round Precision Engineering Conference, The Japan Society for Precision Engineering, March 2007, pp. 703-704, Kawasaki, Japan.

7. Masuda, R., Kabutomori, M., Baskoro, A.S. and Suga, Y., "Welding Penetration Control of Aluminum Pipe Using Omni-directional Camera", Proceeding of the Mechanical Engineering Congress, 2008 Japan (MECJ-08), August 2008, pp. 399-400, Yokohama, Japan.

8. Baskoro, A.S., Nakamura, S., Hayashi, T. and Suga., Y., "Welding Penetration Control in Underwater Welding Using Molten Pool Oscillation Model", Proceeding of the Mechanical Engineering Congress Japan 2008 (MECJ-08), August 2008, pp. 401-402, Yokohama, Japan.

9. Baskoro, A.S., Masuda, R., Kabutomori, M. and Suga,Y., "Application of Omnidirectional Camera for Molten Pool Monitoring During Aluminum Pipe Welding", Abstract Book of The 17th Indonesian Scientific Meeting in Japan, August 2008, p. 3, Tokyo, Japan.

10. Baskoro, A.S., Masuda, R., Kabutomori, M. and Suga, Y., "Welding Penetration Control for Aluminum Pipe using Omnidirectional Camera", Research Meeting of The 83rd Light Weight Structure Welding Division Japan Welding Society, November 2008, pp. 1-6, Osaka, Japan.

11. Baskoro, A.S. and Ibrahim, B., "The Design of Web-based Milling System for Laboratory Scale", The 7th International Conference on Quality in Research, Depok, Indonesia, 2004.

12. Baskoro, A.S., "The Proposed Design of Web-based Milling System", The 2nd Annual National Conference of Mechanical Engineering, Padang, Indonesia, 2003. (in Indonesian)

13. Baskoro, A.S., Mint, M.A. and Nugroho, H.S., "Kinematics Analysis of Articulated Robot with Six Degrees of Freedom in Welding Process", The 4th Conference on Quality in Research, Depok, Indonesia, August, 2001. (in Indonesian)

14. Baskoro, A.S. and Soemarsono, D.A., "Design of Intermediate Shaft in Electric Vehicle Transmission System 'Bajaj Langit Biru' - BALABI", The 3rd Conference on Quality in Research, Depok, Indonesia, August, 2000. (in Indonesian)

15. Baskoro,A.S. and Soemarsono, D.A., "Prototyping Electric Vehicle 'Bajaj Langit Biru' - BALABI", The 3rd Conference on Quality in Research, Depok, Indonesia, August, 2000. (in Indonesian)

16. Baskoro, A.S. and Siswantara, A.I., "Effects of The Distance between Driving Nozzle and Mixing Tube on Jet Pump System", The 1st Conference on Quality in Research, Depok, Indonesia, August, 1998. (in Indonesian)